Ceramics International 48 (2022) 5845–5875

Contents lists available at ScienceDirect

Ceramics International

journal homepage: www.elsevier.com/locate/ceramint

WO_3–based photocatalysts: A review on synthesis, performance enhancement and photocatalytic memory for environmental applications

Ojo Samuel [a,b], Mohd Hafiz Dzarfan Othman [a,*], Roziana Kamaludin [a], Oulavanh Sinsamphanh [c], Huda Abdullah [d], Mohd Hafiz Puteh [e], Tonni Agustiono Kurniawan [f]

[a] Advanced Membrane Technology Research Centre (AMTEC), School of Chemical and Energy Engineering, Universiti Teknologi Malaysia, 81310, UTM JB, Skudai, Johor, Malaysia
[b] Department of Chemical Engineering, Federal Polytechnic, Mubi, P.M.B 35, Mubi, Adamawa State, Nigeria
[c] Faculty of Environmental Science, National University of Laos, Dongdok, Campus, Xaythany District, Vientiane Capital, Lao Democratic People's Republic
[d] Department of Electrical, Electronic & Systems Engineering, Faculty of Engineering & Built Environment, The National University of Malaysia, Malaysia
[e] School of Civil Engineering, Faculty of Engineering, Universiti Teknologi Malaysia, 81310, Skudai, Johor, Malaysia
[f] College of the Environment and Ecology, Xiamen University, Xiamen, 361102, Fujian, PR China

ARTICLE INFO

Keywords:
Functional photocatalyst
Round-the-clock
Electron storage
Visible light
Memory catalysis
Tuugsten oxide

ABSTRACT

A significant drawback of the traditional photocatalysts such as titanium dioxide (TiO_2) is their inability to absorb visible light from the solar spectrum due to their wide band gap energy. They are only photoactive in the ultraviolet (UV) region which is just a little fraction of the solar spectrum and could be harmful with much exposure to it. Due to its abundance in the solar spectrum, visible light needs to be harnessed for environmental applications. However, we lack visible light driven photocatalysts with long-lasting energy storage capacity for "round-the-clock photocatalytic" (RTCP) applications. For this reason, there is a growing need to find new photocatalysts that can mitigate these bottlenecks. It is evident from some carefully selected published articles (1976–2021) that tungsten oxide (WO_3) and its composites have attracted popularity in recent years because of its outstanding properties and particularly its smaller band gap energy of 2.8 eV. However, pristine WO_3 is limited due to relatively low energy density and smaller specific surface area. These drawbacks can be addressed by developing various WO_3 – based materials to improve their performance. This paper reviews and discusses their recent development in surface advancement, morphology control, modification of nanostructured WO_3 and its composites, and their RTCP energy storage for photocatalytic activities in visible light and the dark for environmental applications. Specific aspects focused on its nature, structure, properties, synthesis, coatings, deposition, approaches at modifying and enhancing its visible light photoactivity for enhanced performance and energy storage potential.

1. Introduction

The ever-increasing global population has brought about a corresponding increase in environmental pollution and energy demand. This has become a serious problem globally due to the negative health implications the presence of pollutants in the environment poses to humans, animals, and aquatic lives. Emphasis is on the organic pollutants which have been reported to be detected in significant quantities in drinking water obtained as either underground or surface water. These organic pollutants include pesticides, industrial chemicals, pharmaceuticals wastes, and personal care products [1–4].

Some of these pollutants are not biodegradable and thus pose serious health concerns. Some of these contaminants such as pesticides and herbicides have been reported to have had adverse health and biological effect on aquatic life among which involves inducing toxicity and estrogenicity into these aquatic habitats [5]. Apart from aquatic habitats, various studies have also reported the adverse health implication of these pollutants from sources such steroids hormones, personal care products, pesticides, flame retarders, etc to humans ranging from endocrine disruption, oxidative stress, cancer, reproductive problem among several others [6–10]. However, with the increasing human population ever-expanding industrialization, it is expected that the generation of these pollutants will continue to increase and find a way into the environment and consequently the water body.

* Corresponding author.
E-mail address: hafiz@petroleum.utm.my (M.H.D. Othman).

https://doi.org/10.1016/j.ceramint.2021.11.158
Received 12 October 2021; Received in revised form 12 November 2021; Accepted 16 November 2021
Available online 27 November 2021

Because of this fact, tremendous research has been carried out in the field of purification studies in the case of water treatment to come up with suitable and appropriate treatment technologies to remove these pollutants from the environment and the water body. Although a variety of physical treatment technologies such as adsorption, coagulation, flocculation, reverse osmosis has been proposed for the removal of these pollutants. These treatment technologies have encountered peculiar challenges, which make them inefficient to remove target contaminants from the aquatic environment [11]. This can be attested to by the fact that most of these pollutants are still found in some reasonable quantities in treated effluents via the use of these treatment methods [12]. Other treatment technologies that have been developed for this purpose and have witnessed tremendous progress include advanced oxidation processes such as advanced electrochemical oxidation, homogenous and heterogenous photocatalysis, photoelectrocatalytic oxidation, and Fenton reaction [13–16].

Over the years, particular interest has been focused on heterogenous photocatalysis and tremendous research has been conducted in this area with specific interest on TiO_2 as the main semiconductor or photocatalyst. Heterogenous photocatalysis has been at the center of research for the removal of organic pollutants and other contaminants including oil-water emulsion which is known to be difficult to separate. This technology is considered promising since it can completely oxidize and mineralize a wide range of these organic pollutants into CO_2 and water as well as degrade oil droplets and emulsion.

Titanium dioxide (TiO_2) as a semiconductor photocatalyst have been shown in the early 20th century to exhibit the ability to absorb ultraviolet (UV) light for photocatalytic activity. However, its applications for pollutant removal were only reported in the late 1970s and 1980s [17–22]. TiO_2 has gained enormous attention over the years because of its outstanding properties such as being chemically stable, non-toxic, low-cost, and highly photoactive [23–27].

However, its major setback includes its inability to harness visible light. Due to its large band gap (3.2 eV), TiO_2 has a low visible spectrum utilization efficiency (only 4%) [28,29] As a result, it has low photocatalytic efficiency due to quick recombination of photo-reacted electron-hole pairs and poor photo-induced reaction performance. It also lacks the energy storage capacity to convert and store the photoelectron generated into useful energy in the absence of light irradiation. As a result, many UV lamps are required to maximize the elimination of target pollutants during treatment, raising the cost of operation. An ideal photocatalyst should work within the visible light range and have a band-gap of less than 3.0 eV to maximize the use of visible light. Various attempts and different novel methods have been proposed to address the setback experience by TiO_2 and these novel methods included the introduction of elemental doping, morphology engineering, co-catalyst hybridization, heterojunction formation, etc [30–34].

In addition, semiconductors with smaller band gap energy are still been investigated. Some of these semiconductors been considered as promising include g-C_3N_4 [35,36], BiOI [37,38], $ZnFe_2O_4$ [39–41], $BiVO_4$ [42,43], $_{\beta}$-Bi_2O_3 [44,45], BiOCl [46,47], Cu_2O [48,49], BiOBr [50,51], and WO_3 [52,53]. Other materials or composites being explored that can efficiently harness visible light from the solar spectrum include heterostructured $WO_{18}O_{49}$ [54], $ZnTiO_3$ [55,56], and doped Sn_3O_4 [57]. For practical usage, the ideal photocatalyst should be visible-light active and have a long lifetime. The use of the WO_3- based photocatalysts not only provides an environmentally responsible way to remove organic pollutants especially from wastewater, but it also optimizes the benefits of combining with other semiconductor photocatalysts as a composite, while also resolving TiO_2's limitation [29].

Tungsten trioxide (WO_3) has been one of the most important metal oxides and as a visible light active semiconductor has gained tremendous attention over the years which can be seen from the number of publications on WO_3 (Fig. 1) which is as a result of its outstanding chemical and physical properties, its small band gap energy, exceptional optical properties, resistance to photocorrosion effect, large surface

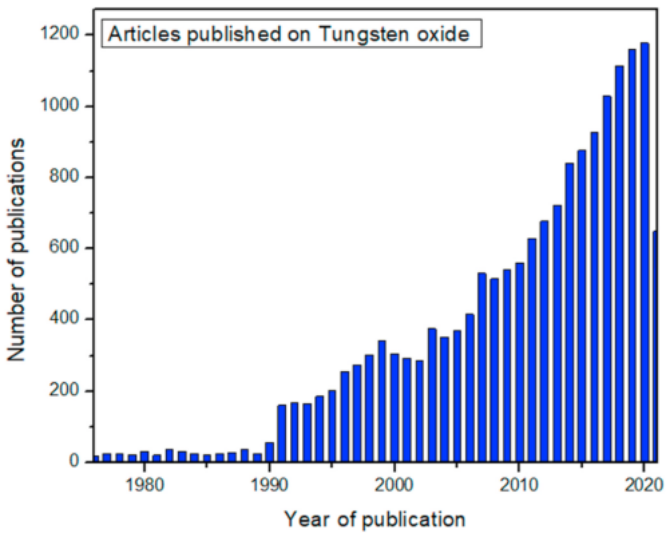

Fig. 1. Statistical publications indexed in the Web of Science (ISI) by using the term "tungsten oxide". The number of publications from 1976 to 2021. (Assessed in August 2021).

area, energy storage potential and its stable physiochemical properties [58–60].

WO_3 is considered a unique material because of its optical, chemical, and electrochemical properties. In comparison to TiO_2, WO_3 has a relatively smaller band gap energy (2.8eV) as well as the capacity to absorb a large range of the visible spectrum. Furthermore, its outstanding photo-corrosion resistance and chemical stability in sustained contact with solar light irradiation and its "round the clock photocatalytic" energy storage ability sometimes referred to as "Memory catalysis" for various photocatalytic applications makes it a unique material. WO_3 has attracted a lot of interest. Because of its greater surface area, particle size, and visible light use efficiency, a stable WO_3-based composite photocatalysts may have a favorable photocatalytic activity from a practical standpoint.

WO_3 semiconductor is one of the promising semiconductors for use in photocatalytic applications. WO_3 is inexpensive, has low toxicity, and high oxidizing ability of the holes in the valence band, stable physiochemical properties, good response to solar light, has highly tunable structures and stoichiometries, a narrow band gap of between 2.5 and 3.0 eV, and is readily available [61–63]. Apart from its application in photocatalysis, WO_3 has broad applications in sensors, high-temperature superconductivity, dye-sensitized solar cells (DSSCs), photoelectrochemical water splitting [61,62,64,65].

Owing to global challenges of climate change and global warming, cleaner energy sources have recently been explored to reduce the damage done to the environment due to variables such as greenhouse gas emissions and pollution, that result in global warming and climate change. This needs requires the creation of new and more efficient energy storage devices.WO_3- based photocatalysts have shown to be promising in the development of energy storage devices from semiconductor photocatalyst having long-lasting energy storage effect for climate change mitigation through energy storage for electrochemical, electrocatalysis, and photoreduction as can be seen in the development of Pd–Au/TiO_2-WO_3- based photocatalyst for photoreduction of carbon dioxide (CO_2) into methane (CH_4) and carbon monoxide (CO_2) [66,67]. WO_3-based semiconductor photocatalyst has also shown application for high energy storage devices for electrocatalytic conversion of CO_2 where the photocatalyst is prepared to inform of ultracapacitors or supercapacitors to withstand higher power requirement than battery without damage to itself for the electro-reduction process as can be seen in the preparation of WO_3-based polymorphs [68].

However, like many other metal oxide semiconductors, WO_3 has its

limitations such as rapid and fast recombination of photogenerated charge carriers and having a relatively lower conduction band (CB) level laying or existing above the reduction potential of O_2/O^{2-} which leads to less O_2 molecule reduction during degradation of pollutants by the photocatalytic process. This setback has led to much research in finding suitable methods that could address these setbacks by possibly modifying and adjusting the structure and reducing the band gap energy of the semiconductor for enhanced photocatalytic performance through its synthesis route and other enhancement strategies.

It is important to note that with a properly selected method of improving the visible light absorption capacity of WO_3, WO_3-based photocatalysts can absorb light energy and store this energy to be used in the absence of light source or the dark for photocatalytic degradation and mineralization of pollutants. Various research has reported the use of WO_3-based photocatalysts for pollutant degradation and mineralization but only a handful of researchers have reported on the ability of WO_3 to store energy after light absorption and utilize it even in absence of light or in the dark for photocatalytic activity which is referred to as "round the clock photocatalytic (RTCP) energy storage ability.

Generally, most reviews on WO_3 have not reported or considered the RTCP energy storage capacity of WO_3. This review work aims to highlight the RTCP energy storage ability of WO_3-based photocatalyst for pollutant degradation and other environmental applications which is one important property of WO_3 and an area of study that has been neglected by a lot of research on WO_3-based photocatalytic ability. In summary, this review discussed the main properties, synthesis route, morphology, visible light enhancement strategies, RTCP mechanism of WO_3, and its RTCP energy storage for environmental applications.

2. Main properties of WO_3

2.1. Nature of WO_3

WO_3 is an n-type semiconductor that has its lattice structure dependent on temperature [69]. It exists in the following crystal phases ranging between −180 and 900 °C thus; exist at a temperature of between 17 and 330 °C for the monoclinic I (γ-WO_3) phase, < −43 °C for the monoclinic II (ε-WO_3), between -43 and 17 °C for the triclinic (δ-WO_3), between 330 and 740 °C for the orthorhombic (β-WO_3) and >740 °C for the tetragonal (α-WO_3) [70] (Fig. 2). The monoclinic I (γ-WO_3) phase has a band gap energy ranging between 2.4 and 2.8 eV and the most investigated among the five phases which could be attributed to its show of greater stability at room temperature [71,72]. As a result, the monoclinic I (γ-WO_3) phase shows appreciably good optical absorption characteristics for harnessing visible light. The band gap energy value of the bulk semiconductor depends on its composition, while it depends on its size in the case of the nanocrystalline structure.

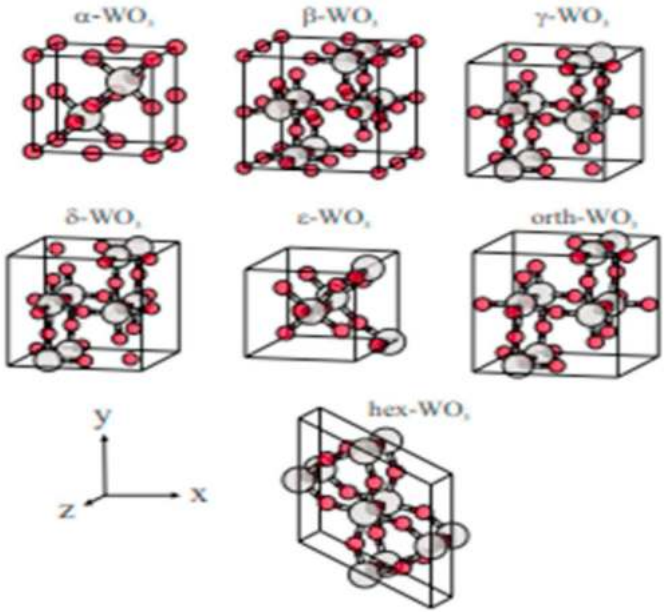

Fig. 2. Temperature-dependent crystalline phases of WO_3 [83].

For semiconductors of the nanocrystalline structure smaller in dimensions in comparison to the exciton size which is also known as the electrostatically bound electron-hole pair, normally shows the band to be wider and exhibit the quantum confinement effect [73,74]. The conditions and route of synthesis of WO_3 have a significant effect on its size and structure and invariably on its electronic and optical properties. The monoclinic I (γ-WO_3) phase is normally considered in the synthesis of electrochromic devices due to its excellent efficient coloration properties [75]. The γ-WO_3 is widely used in other areas including water splitting [76], perovskite solar cell [77], photocatalytic disinfection [78], gas sensing [79], hydrogen evolution reactions [80], organic contaminant degradation in water by photocatalysis and photoelectrocatalysis [52,53,81] and energy storage [82].

2.2. Electronic structure of WO_3

As stated earlier, at room temperature (RT), which is considered its most stable phase, WO_3 exhibits a simple monoclinic I (γ-WO_3) structure having space group $P2_1/n$. Fig. 3a shows the supercell structure (2 × 2 × 2) of WO_3 [84]. A unit cell structure of WO_3 at RT contains eight (8) tungsten (W) and twenty-four (24) oxygen (O) atoms having eight (8) sharing oxygen (O) atoms at the edges together with octahedral in a barely sufficient disfigured cubic arrangement. The structure is sometimes referred to as perovskite ABO_3 where A ions are lost hence suitable form for doping interstitially. Fig. 3b shows the WO_3's simple cubic supercell (4 × 4 × 4) structure comprising the same number of atoms as in the case of its monoclinic structure at room temperature. The tetragonal structure of WO_3 having a form of deformation from a simple cubic structure to some extent consist of two (2) formula units in its unit cell which has 8 atoms exhibiting a space group of P4/nmm. Fig. 3c shows a (4 × 4 × 2) WO_3 tetragonal supercell structure having four (4) equatorial (containing duo sets of an unequal oxygen atom) and two (2) axial oxygen atoms existing in a deformed octahedron WO_3 structure. The tetragonal structure of WO_3 has a bandgap of about 1.5–1.85 eV which is almost the same as the simple cubic structure due to little deformation in its structure from the normal to the tetragonal. With the variation in WO_3 structure due to temperature change, WO_3 has a monoclinic structure of very low temperature with space group *Pc* having four (4) formula units in its unit cell having twelve (12) oxygen with four (4) tungsten atoms as shown in Fig. 3d.

To compare this with other structures like the tetragonal structure, the oxygen is more distorted in the octahedron with mobile off-center tungsten atoms. Fig. 3f shows the orthorhombic structure of WO_3 with a *Pmnb* space group where the oxygen octahedron arrangement is distorted. It consists of eight (8) tungsten and twenty-four (24) oxygen atoms in the unit cell. Contrary to the structure of the triclinic phase of WO_3, it can be seen from Fig. 3e that the W–O bond having long-short lengths could be altered in the y and z directions due to the movement abroad of the W atoms from its equilibrium point [84]. The small red and wide green sphere in Fig. 3 denote oxygen (O) and tungsten (W) atoms individually and entirely denotes a 250-atom enclosed model.

2.3. Other properties of WO_3

Some of the properties exhibited by WO_3 that make it an attractive and promising candidate for energy storage and environmental pollutant removal via photocatalysis include its deep valence band, excellent optical absorption capacity in the visible light region, the relatively high electron mobility of about 6.5 cm^2/V.s, less vulnerability

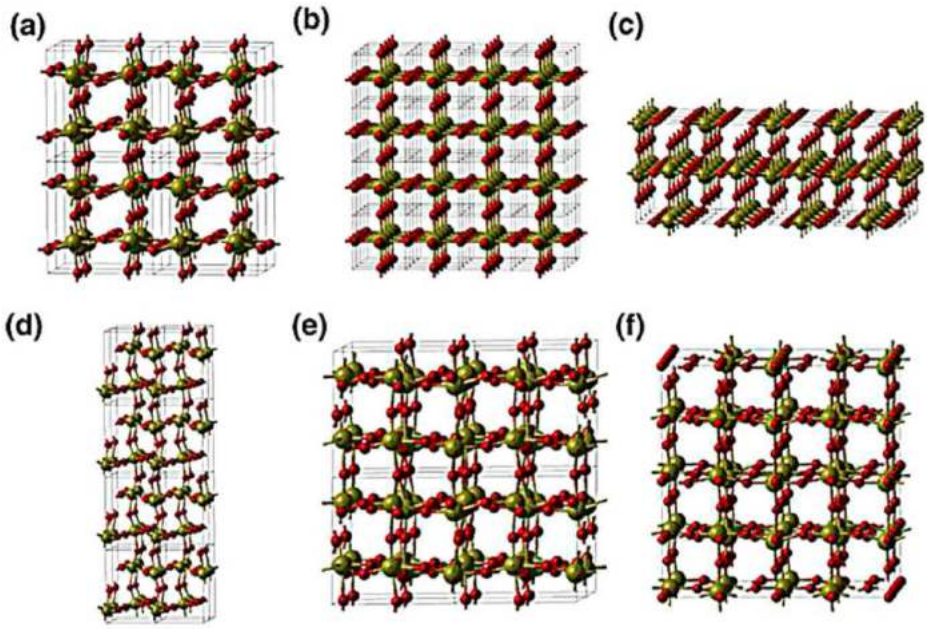

Fig. 3. The different configurations of WO_3 (a) at room temperature; monoclinic (b) cubic (c) tetragonal (d) at low temperature; monoclinic (e) triclinic (f) orthorhombic organizations (green spheres represent W, and red spheres denote O atoms) [85]. (For interpretation of the references to color in this figure legend, the reader is referred to the Web version of this article.)

to photocorrosion, non-toxicity, stability in acidic aqueous solution, low cost, and relatively low energy bandgap (Table 1) [86–88]. Hunge [89], and Riboni et al. [90] in their separate studies, found out that combining TiO_2 and WO_3 improved photocatalytic reactions and stability, implying that incorporating them into a semiconductor composite could improve charge separation by trapping photo-generated electrons. WO_3 displays varying oxidation state with high–power holes considered important for visible light applications in organic pollutant removal from the water via photocatalysis. However, its low conduction band level translating to reduced potential makes it less efficient for light energy conversion [91, 92].

In addition, like other metal oxides semiconductors, the photocatalytic activity of WO_3 is limited due to the rapid recombination of holes and photogenerated electrons. Because of this, various methods that have been adopted to minimize this limitation and enhance the photocatalytic activity of other photocatalyst has also been considered for WO_3. This involved morphology engineering for enhanced performance, metal doping, composite formation in combination with carbon materials, heterojunction formation with another semiconductor, etc. Table 1, summarizes the bandgap of WO_3-based photocatalyst.

Table 1
Bandgap of WO_3-based photocatalyst.

WO_3-based photocatalyst	Bandgap (eV)	References
WO_3 Monoclinic	2.57-2.58	[93]
WO_3 nanowires	3.17	[94]
$W_{18}O_{49}$	2.42	[95]
{100} faced WO_3	2.84	[96]
WO_3 films	3.30	[97]
WO_3 hexagonal	3.47-3.65	[98]
WO_3 orthorhombic	2.63	[99]
WO_3	2.6	[100]
	2.7	[101]
	2.63	[102]
	2.75	[103]
	2.47	[104]
	2.5-2.8	[105]
	Pristine: 2.53	[106]
	2.78	[107]
	Nanosheet: 2.61	[106]
	Monoclinic:2.53	[65]
	Orthorhombic: 2.73	[65]

3. Synthesis route for WO_3-based photocatalysts

The synthesis method plays a significant part in the preparation of a photocatalyst. Various synthesis approaches can be adopted for the synthesis of a photocatalyst having exciting and interesting morphologies, properties, shapes, structures, and sizes which are to a large extent responsible for enhanced photocatalytic performance [108,109]. Several synthesis methods have been reported for WO_3 and WO_3 grounded photocatalysts which are less expensive and environmentally friendly in a bit to synthesize a photocatalyst with a functional structure having an excellent and efficient performance for photocatalytic purposes [58,110]. In this review, some common synthesis routes are highlighted which include, hydrothermal techniques, co-precipitation, sol-gel, solvothermal methods, calcination method, etc. Another method considered to be a new and promising method referred to as "green synthesis" is also briefly discussed.

3.1. Hydrothermal method

The hydrothermal method is broadly considered as the most versatile technique in the synthesis of inorganic nanomaterials from aqueous solutions which takes place under temperature above ambient temperature and pressure conditions leading to chemical reaction [111]. Insoluble substances can be dissolved using this technique. The dissolved substance can equally be prepared from substances present in the aqueous solution using the hydrothermal method [110,112]. Some important parameters that need to be monitored and adjusted to the characteristics of the nanomaterials when using this method include temperature, precursor concentration, and pressure. In this method, water is commonly used as the solvent.

In this technique, the temperature and pressure are very vital because the water density and the dielectric constants are dependent on these parameters. A decrease in the dielectric constant of water is closely related to a reduction in pressure and an increase in temperature. The reaction rate is enhanced significantly as the dielectric constant of water

decreases which promotes the nucleation growth of crystals [113]. The hydrothermal method offer some advantages which include environmentally friendly, mild operating conditions, low-cost, good dispersion in solution, one-step synthesis, production feasibility, inexpensive instrumentation, and facile synthesis [114–116]. Another advantage of this method is that it may avoid the use of H_2 which significantly enhances safety. Because of its environmental friendliness and is a cheap method for preparing WO_3 and its composite-based photocatalysts, it has been reported that most WO_3 prepared using this method have shown some high degree of particle purity, good dispersion in solvent, and high crystallinity.

There have been studies that reported the preparation of tungsten bronze such as $K_{0.26}WO_3$ and $Cs_{0.33}WO_3$ nanorods by the hydrothermal method. $K_{0.26}WO_3$ nanorods were synthesis with K_2WO_4, K_2SO_4, and distilled water at 200 °C for 24hr under an atmosphere of H_2 (5 vol %)/N_2 [117]. Distilled water mixed with Cs_2WO_4, WO_2, WO_3 as the precursor was heated at 800 °C for 24hr in the preparation of $Cs_{0.33}WO_3$ [118]. The preparation of graphene-bridge Z-scheme WO_3/MoS_2-rGO composite for rhodamine B (RhB) degradation by the hydrothermal techniques shows an enhanced performance of the photocatalyst under visible light. The hydrothermal reaction was used to prepare the nanocomposite by reacting the thiourea, sodium molybdate dehydrate, and graphene oxide together [119].

The result of the scanning electron microscopy (SEM) from Fig. 4a reveals a micro-flower-shaped WO_3 composed of plenty WO_3 sheets of 2 μm in size. Fig. 4b displayed the morphology of MoS_2-rGO composing several MoS_2 curved nanosheets braided or interwoven together. It can be seen that WO_3/MoS_2-rGO composite displayed interaction of three (3) components in which the sphere-like MoS_2-rGO and flower-like WO_3 can be seen (Fig. 4c). Images from transmission electron microscopy (TEM) as seen from Fig. 5(d-h) show that the MoS_2-rGO composite was attached with WO_3. The dark WO_3 and light MoS_2-rGO can be differentiated by a high magnification TEM image. Photoelectron spectroscopy (XPS) and X-ray images analysis shows the presence of W, C, S, Mo, and O, in the WO_3/MoS_2-rGO composite. The binding energy peak of 38.12 and 35.92 eV from the XPS spectrum of W were designated to W $4f_{7/2}$ and $4f_{5/2}$ independently. The XPS spectrum value of 530.4 eV for O 1 s spectra was designated to oxygen O^{2-} lattice of WO_3 and rGO while the peak values at 286.6, 288.7, and 284.6 eV for C 1 s were assigned to C–O, C═O, and C–C, respectively.

WO_3/Ag_2CO_3 fabrication by hydrothermal method without the use of template or surfactant in the removal of RhB under visible light irradiation was also reported [120]. It can be seen from Fig. 5a that a rod shape plus an identical size shape of $AgCO_3$ was form having a constructive dispersion with a radial and axial length of between 1.7 and 2.0 μm and 400 nm, respectively. In the meantime, it was observed that several n-type WO_3 nanoparticles (polyhedron-like) were combined forming a hierarchical ordered arrangement of WO_3 nano-flowers as seen from the SEM images in Fig. 5b-e. In addition, it was also seen that the surfaces of individual WO_3 contained several important crystals facet which consequently provided more reaction sites for the catalytic degradation. In the case of AWp-20 samples, it was observed that rod-shaped Ag_2CO_3 and polyhedron-shaped WO_3 nanoparticles were chiefly present in the composites and little WO_3 nanoparticles were attached on Ag_2CO_3 surface. As can be seen from the XRD patterns (Fig. 5f) for the synthesized photocatalyst, all the diffraction peaks of the pure p-type Ag_2CO_3 can be well indexed with monoclinic phase Ag_2CO_3 without detecting peaks of other impurities like silver oxide and metallic silver [121,122]. Furthermore, it was observed that there was a good correlation between the monoclinic phase WO_3 with the n-type WO_3 (polyhedron-like WO_3) nanoparticles [123]. Fig. 5g also shows the X-ray diffraction (XRD) result of the polyhedron-like WO_3/Ag_2CO_3 p-n heterojunction having distinctive Ag_2CO_3 mass ratios indicating that by combining it with p-type Ag_2CO_3 nanoparticles, the respective diffraction peaks due to AWp-10, AWp-20, AWp-30, and AWp-40 composite were obtained for WO_3 and Ag_2CO_3 phases signifying the presence of n and p-type WO_3 and Ag_2CO_3 respectively [124]. Furthermore, the amount of Ag_2CO_3 doping correlates with the intensity of {2 1 0} facet indicating that the {2 1 0} facet diffraction peak gradually increases as the doping amount of Ag_2CO_3 increases.

It is worthy of note that the hydrothermal method is less energy consuming, controllable and convenient to adopt [125]. However, it is also significant to note that in the various preparations highlighted above, the different nanoparticles have varying reaction paths and processing conditions. Therefore, it is important to determine the most suitable chemical reactions with appropriate conditions for the various nanoparticles for optimal results. The hydrothermal method has also been reported to help in tailoring the morphologies and size of the synthesized nanomaterials to a suitable range of between 10 and 100 nm which is also applicable for the case of the WO_3 [126].

3.2. Solvothermal method

The solvothermal method involves the use of ethylene glycol and

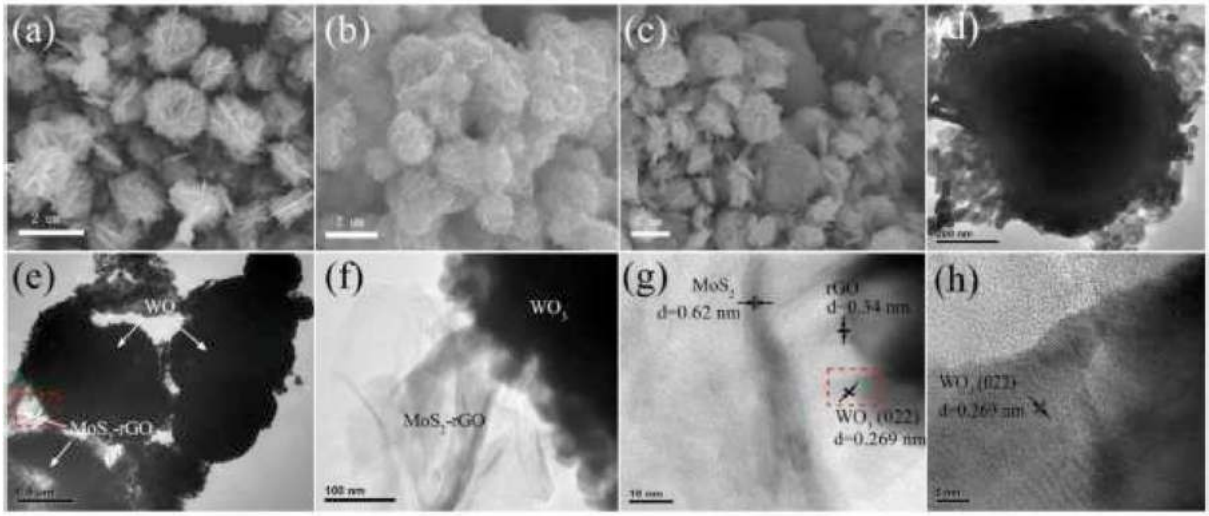

Fig. 4. SEM images of (a) WO_3, (b) MoS_2-rGO and (c) WO_3/MoS_2-rGO (mass fraction 10%); TEM images of (d) WO_3, (e) WO_3/MoS_2-rGO (mass fraction 10%), (f) high magnification graph of red box section in Fig. 4e, (g) HRTEM of WO_3/MoS_2-rGO (mass fraction 10%), (h) high magnification graph of red box section in Fig. 4g [120]. (For interpretation of the references to color in this figure legend, the reader is referred to the Web version of this article.)

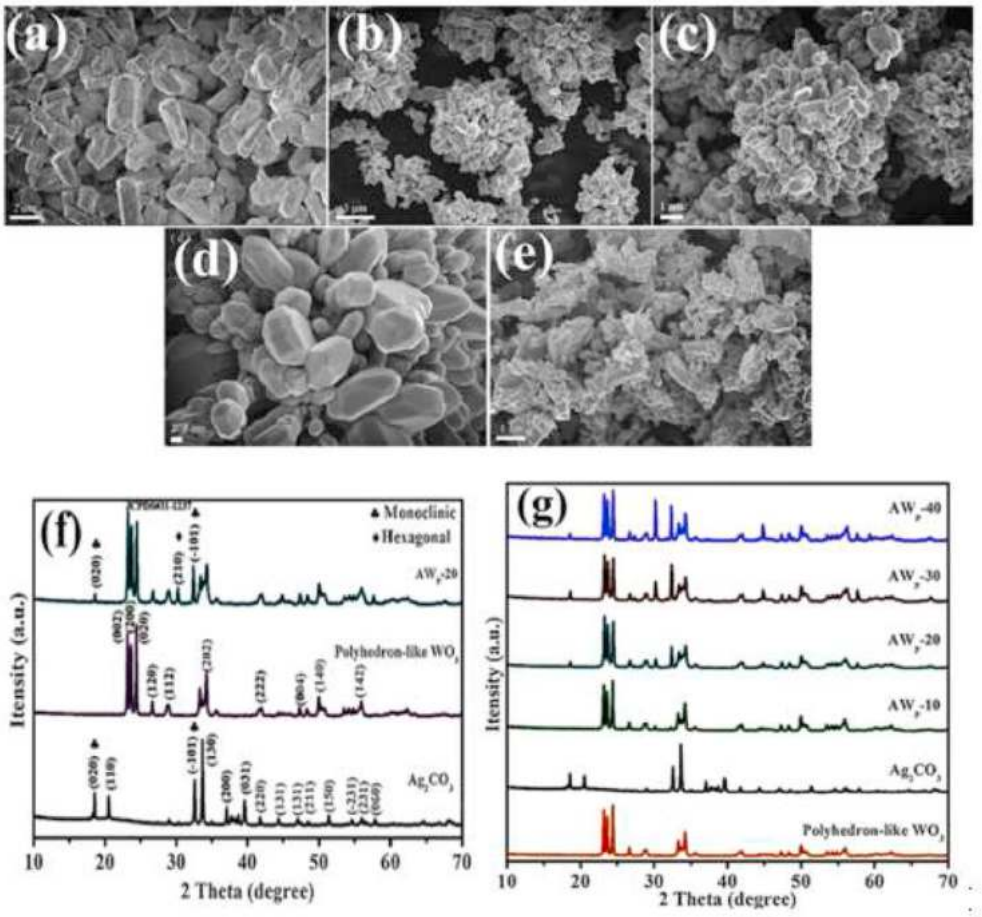

Fig. 5. SEM images of fabricated (a) Ag_2CO_3, (b), (c), and (d) polyhedron WO_3, (e) AWP-20, (f) XRD patterns of fabricated Polyhedron-like WO_3 and AWP-20. (inset figure, ♣ symbolizes crystal faces of a monoclinic phase of Ag_2CO_3 and ◆ denotes crystal faces of the hexagonal phase of Ag_2CO_3), (g) XRD patterns of Ag_2CO_3, WO_3, AWP-40, AWP-30, AWP-20, AWP-10 [124].

ethanol as the solvent instead of water as it is mostly in the case of the hydrothermal method. Ethylene glycol and ethanol are used to achieve the dual purpose of solvent and reducing agent. It is possible in this method to control the various variables by adjusting the pH, type of solvent, use of various surfactants, filled volume of autoclave, changing the reaction environment and reactant concentration to obtain a product having high crystallinity, purity, varying crystal structures, and phases, increased specific surface area, reduced size of particle and prevention of particle agglomeration [127,128]. The Teflon-lined autoclave is normally used for the solvothermal reaction of the precursor at the desired temperature of 150 °C and for a duration of normally 6hrs after which the obtained product will be centrifuged, washed with ethanol and water several times then vacuum dried [129]. The solvothermal method is commonly adopted for the fabrication of WO_3-based photocatalysts which has been seen to improve and significantly enhance the photoactivity and properties of the obtained photocatalyst. For the synthesis of WO_3- based photocatalysts using this method, tungsten chloride (Cl_6W), tungstic acid (H_2WO_4), and sodium tungstate dihydrate ($Na_2WO_3.2H_2O$) are mostly used as precursors. The solvothermal method has the advantage of ease of use, low cost, products are free from impurities (pure products are obtained), cyclic stability, excellent adhesion, stable synthesis, simplicity of the process, and easy scalability for applications industrially [130,131].

In the preparation of $WO_3/BiVO_4/BiOCl$ porous nanosheet composite ternary heterojunction photocatalyst by solvothermal method for visible light degradation of RhB, porous $BiVO_4$ nanosheets were firstly synthesized via an immersion – calcination method which uses biomass broomcorn core as a template. WCl_6 was then used to react with the prepared porous reticulated $BiVO_4$ nanosheets which provide chlorine (Cl) and the tungsten (W) sources to fabricate the $WO_3/BiVO_4/BiOCl$ ternary heterojunction in a one-step solvothermal method. The fabricated $WO_3/BiVO_4/BiOCl$ photocatalyst (Fig. 6 (A-G)) was reported to exhibit better energy level matching and created a gradient for charge transfer and migration which effectively reduced the recombination rate of photogenerated carriers, enhanced the electron separation process, improve visible light harvesting and increasing number of active site on the photocatalyst which consequently led to a considerable improvement in the photodegradation of RhB under visible and simulated solar light by approximately 2 and 1.5 times higher in comparison to $BiVO_4$ and binary $BiVO_4/BiOCl$ respectively and this was attributed to the synthesize method [132].

In a study for the preparation of immobilized nanostructured WO_3 photocatalyst from Na_2WO_4 via the solvothermal method for visible light degradation of methylene blue (MB), the result of the degradation process as can be seen from Fig. 7a-b, indicated that WO_3(EtOH) exhibited high adsorption capacity of 14.1% and MB degradation rate of 90% after an hour. This photocatalyst also demonstrated the highest photocatalytic efficiency for MB degradation under visible light of above 85% after three cycles. This superior photocatalytic performance was attributed to have originated due to the strong photocurrent, high crystallinity, and maturity of WO_3 nanostructures because of continuous conversion of the tungsten acid to WO_3 consequently providing more active sites for the photodegradation process. This also assisted in the separation and transfer of photogenerated electrons and holes. The ethanol solvent had a significant influence on the morphology, growth mode, structure, and photocatalytic effect of WO_3 filmed products in

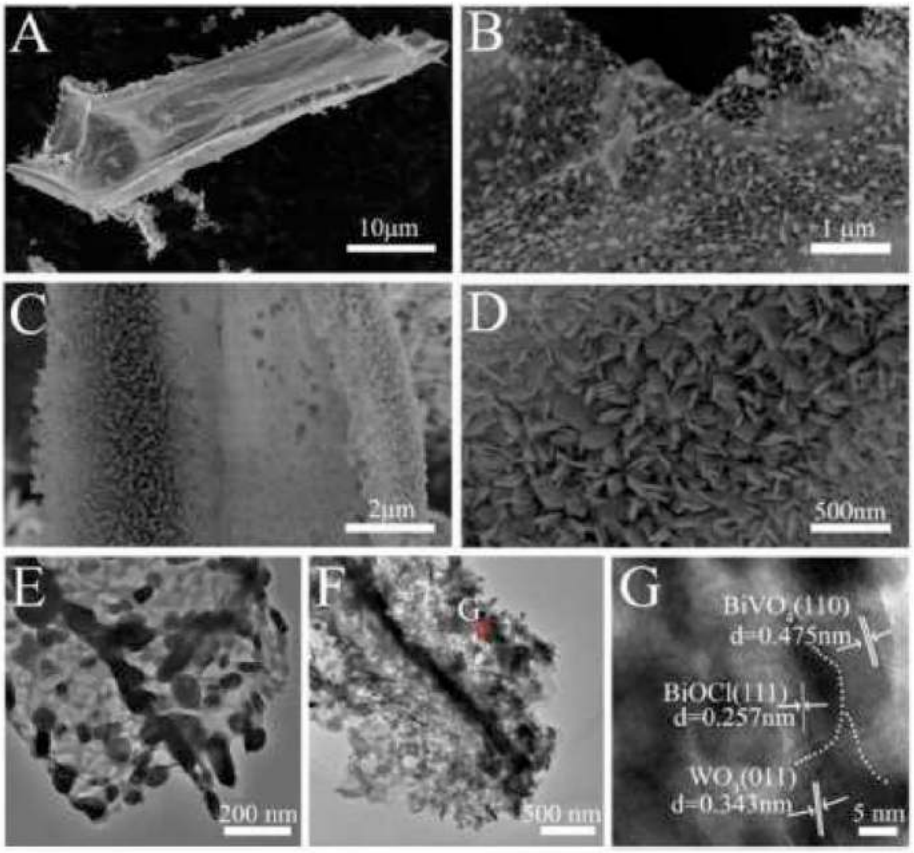

Fig. 6. (A, B) and (E) are SEM and TEM images of $BiVO_4$, respectively; (C, D), (F), and (G) are SEM, TEM, and HRTEM images of $WO_3/BiVO_4/BiOCl$ (12.5 wt%), respectively [132].

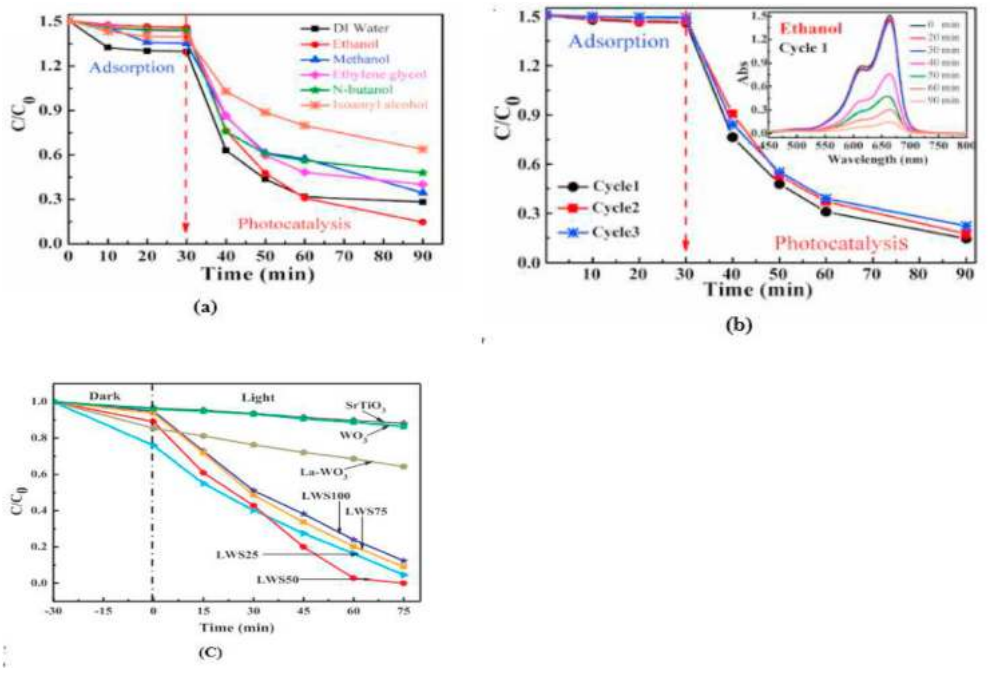

Fig. 7. (a) Degradation efficiency of MB at different immobilized WO_3 nanostructures; (b) Cyclic properties of WO_3(EtOH) [133], (c) Photocatalytic degradation of MO using pure $SrTiO_3$, La-WO_3, and various molar ratio La-WO_3/$SrTiO_3$ under visible light [135].

comparison with other solvents which is of considerable importance for the controllability of immobilized semiconductor materials [133]. WO_3/BiOCl heterostructure photocatalyst was fabricated through the electrospinning method then the solvothermal synthesis for degradation of RhB and Phenol in water. The photocatalyst demonstrated a high capacity for photogenerated charge carrier separation. The

photocatalyst also demonstrated enhanced photocatalytic efficiency for degradation of RhB and phenol by around 2.3 times in comparison with BiOCl (0.113 min^{-1}) having a rate constant of 0.259 min-^{1} for RhB degradation. Its improved photocatalytic performance was attributed to WO_3 nanofiber's anti-agglomeration ability, its well-arranged band structures for charge separation, high activity of BiOCl nanosheet, and synthesis method [134].

In a related study as shown in Fig. 7c, La-WO_3/$SrTiO_3$ photocatalyst was fabricated by the solvothermal method for visible light degradation of methyl orange (MO). The La-WO_3/$SrTiO_3$ photocatalyst ability to degrade MO was compared with pure WO_3 and $SrTiO_3$, in which the La-WO_3/$SrTiO_3$ demonstrated an excellent photodegradation ability of 100% decomposition of MO under visible light irradiation in 75 min and still showed good stability and maintained high photoactivity after five cycles of degradation. The improved photoactivity was attributed to effective electron-hole separation, accelerated transfer of photo-generated electron-hole pairs, and upon the three-dimensional hierarchical structure arrangement in the La– WO_3/$SrTiO_3$ heterojunctions [135]. However, the solvothermal method has the disadvantage of safety issues during the reaction process which is process monitoring challenges been that the reaction cannot be seen physically to access some important parameters such as temperature, pressure, and solvent. High equipment (autoclave) cost is also a disadvantage [136,137].

3.3. Co-precipitation method

The co-precipitation technique sometimes referred to as chemical precipitation is a process whereby a solution is altered by converting it into solid through transforming or converting the substance into a form that is an insoluble or supersaturated solution. This method is mostly employed in the preparation of Layered Double Hydroxides (LDHs), and this can be done at a constant or varying value of pH. However, the pH value of the co-precipitation mixture has a significant effect on the structural, chemical, and textural properties of the final product [138]. Several researchers have used the co-precipitation techniques to fabricate WO_3-based photocatalysts because of the simplicity of the process, cost-effectiveness, enhanced visible-light photocatalytic activity of fabricated photocatalyst for mineralization of various organic pollutants, easy scalability, environmentally friendly, ease of operation control, and continues reproducibility [139–141].

In a study a novel WO_3/Fe_3O_4 catalysts was fabricated via chemical co-precipitation method using Na_2WO_4 as a precursor to study their photocatalytic decomposition of thiacloprid under both simulated and UV sunlight radiation [142]. In this study, four nanopowder samples of WO_3/Fe_3O_4 with varying quantities of WO_3 were prepared via chemical co-precipitation method. The result of the photocatalytic performance showed that the 6.1WO_3/Fe_3O_4/H_2O_2 photocatalyst had a good degradation efficiency for thiacloprid decomposition than other synthesized catalysts with a decomposition rate of 2.2 times higher in comparison to bare Fe_3O_4. This was attributed to the existence of magnetite and hematite nano-dimensional Fe_3O_4 in the photocatalyst as shown from the XRD analysis result (Fig. 8a) which shows increasing WO_3 content as the magnetite content increases and consequently as the BET surface (S_{BET}) increases, WO_3 tend to also increase because of its specific surface area been small. Further analysis as shown in Fig. 8b, indicates a −196 °C nitrogen isotherm for WO_3/Fe_3O_4, unsupported WO_3, and unmodified Fe_3O_4 catalyst. Using aqueous solutions of Na_2SO_4 and $Na_2WO_4.2H_2O$, the XRD pattern at a pH of 1.8 showed the presence of hexagonal nanoparticles of WO_3, at pH 0.0, monoclinic while at pH 0.4, orthorhombic $WO_3.0.33H_2O$ species were shown indicating that the mesoporous structure of the catalyst is preserved with improved structural parameter due to the presence of WO_3 within the catalyst.

3.4. Sol-gel method

The sol-gel process referred to sometimes as the chemical solution deposition process is a wet chemical method used for the synthesis of doped inorganic-organic nanoparticles (NP), functional materials such as supercapacitors, nonlinear optical materials, ferroelectrics, photocatalyst, and catalytic membranes. This process takes place through a series of steps which includes hydrolysis and polycondensation, gelation, aging, drying, densification, and crystallization in chronological order [143–146]. The sol-gel method was first demonstrated by Graham Thomas in 1864 [147]. This method is regarded as an efficient surface modification process of substances. The ability of the sol-gel method to create a large surface area with stable surfaces is considered the most important advantage of this method as the physical and chemical properties of the materials prepared through this method are associated with the applied experimental conditions during the process [148].

The first step in this process which is the hydrolysis step involves the formation of gel which depends on the quantity of water where for higher bridging oxygen to non -bridging ratio requires much uptake of water during the condensation to form polymerized branched structure [149]. The formation of the liquid phase-based porous structure is determined by the solvent viscosity while the pH and alkoxide precursor determines their cross-linking pattern and size in the colloidal particles [150]. Furthermore in this method, the calcination temperature influences the density and pore size of the material formed [151]. The sol-gel method is widely considered because of its advantages such as reduced production cost, lower operation temperatures, purity, and high yield of the final product [152,153].

WO_3 was used in a study to modify TiO_2 catalyst for the removal of

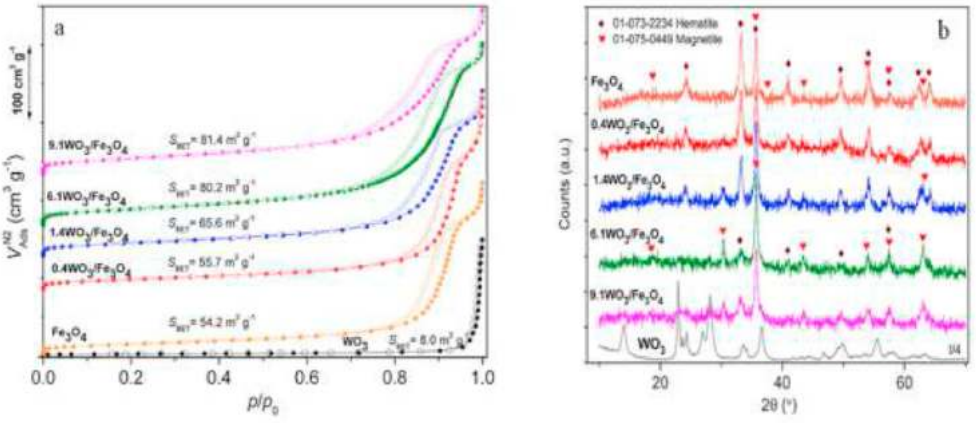

Fig. 8. (a). Nitrogen isotherms at −196 °C of unsupported WO_3, unmodified Fe_3O_4, and WO_3/$Fe3O_4$ catalysts (adsorption — filled symbols; desorption — empty symbols), (b). XRD pattern of unsupported WO_3, unmodified Fe_3O_4, and WO_3/Fe_3O_4 catalysts [142].

amoxicillin and to reduce the bandgap energy of TiO_2 for enhanced photocatalytic performance by the sol-gel method using ammonium p-tungstate (ApT), tetrabutyl orthotitanate (TBT), sec-butanol (SB), and glacial acetic acid (GAA) as precursors [154]. The effect of calcination temperature on the photocatalytic degradation performance of the photocatalyst in the solar spectrum was also investigated. For this purpose, the experimental cycles were carried out in a compound parabolic collector (CPC). The photocatalytic result of the degradation showed that the highest removal of amoxicillin was 64% with 100 ppm of amoxicillin concentration at 700 °C with $0.1gL^{-1}$ catalyst load. Though the degradation performance was considered low due to the small surface area of the photocatalyst and its particle size during the sintering process, however, it was observed that the bandgap energy of the photocatalyst reduced with respect to the bare TiO_2, and this was attributed to the modification of the TiO_2 crystalline structure due to the presence of WO_3. The presence of WO_3 added a localized state to the bandgap energy between the valence and the conduction band. Its presence as an electron acceptor also prevented the electron-hole recombination by increasing the energy density holes and vacancies.

In another study, WO_3/TiO_2–N catalyst was fabricated for the removal of diclofenac (DCF) sodium using the sol-gel method [155]. Tetrabutyl orthotitanate ($C_{16}H_{36}O_4Ti$), ammonium p-tungstate [$(NH_4)10H_2W_{12}O_{42}{\cdot}4H_2O$], and ammonium nitrate (NH_4NO_3) as the source of nitrogen were used in the process. The Transmission electron microscopy (TEM) images show the dispersion of tungsten atoms on the surface of TiO_2 asWO_3 as can be seen in Fig. 9. The TEM images also indicated that doping with the Nitrogen (N), resulted in smaller particles for the coupled oxide in comparison with the TiO_2 and TiO_2/WO_3. On the other hand, as can be seen from Fig. 9(a, b, and c), the XRD patterns for TiO_2, TiO_2/WO_3, and WO_3/TiO_2–N show that the focal diffraction peaks can be designated in all cases to anatase type structure. The diffraction peaks (Fig. 9d) associated with the existence of W and N were not seen and this is because of the little quantity of W or N in the sample. However, the pattern indicated that the peak was 25.20 at 2θ exhibiting a shift a little higher in value of 25.35 at 2θ (Fig. 9e) as the peak of {101} plane TiO_2/WO_3 and WO_3/TiO_2–N samples due to the heterojunction between TiO_2 and WO_3 with its intensity decreasing with increase in the amount of N showing a reduction in the crystalline size due to N doping. The study also indicated a reduction in the bandgap energy and an improvement in the photocatalytic activity of the modified photocatalyst in degradation of the diclofenac in which 92% degradation of the diclofenac was achieved with 100% chloride release while the TOC was above 80%. The reduction in the bandgap energy of the photocatalyst was attributed to the method of synthesis. Due to the simplicity and other advantages of the method, it has been an attractive synthesis method for the synthesis of various nanoparticles photocatalyst, simple oxides, and nanocomposites [156].

3.5. Green synthesis

Conventional approaches involving both chemical and physical methods for the synthesis of WO_3 based materials and photocatalysts have been considered over the years. Among these various methods, green synthesis or technique is largely regarded as fast, efficient, cost-effective, facile, and suitable to synthesize or produce new morphologies of the photocatalyst. Recently this technique has been developed to prepare metal oxides having varying morphologies via the use of various plant parts such as stem, starch, seeds, roots, flowers, leaves, and fruit juice as fuel [30]. Green synthesis is used to prevent the formation of unwanted and harmful side-products during preparation by adopting more sustainable, environmentally friendly, and dependable methods of synthesis [157].

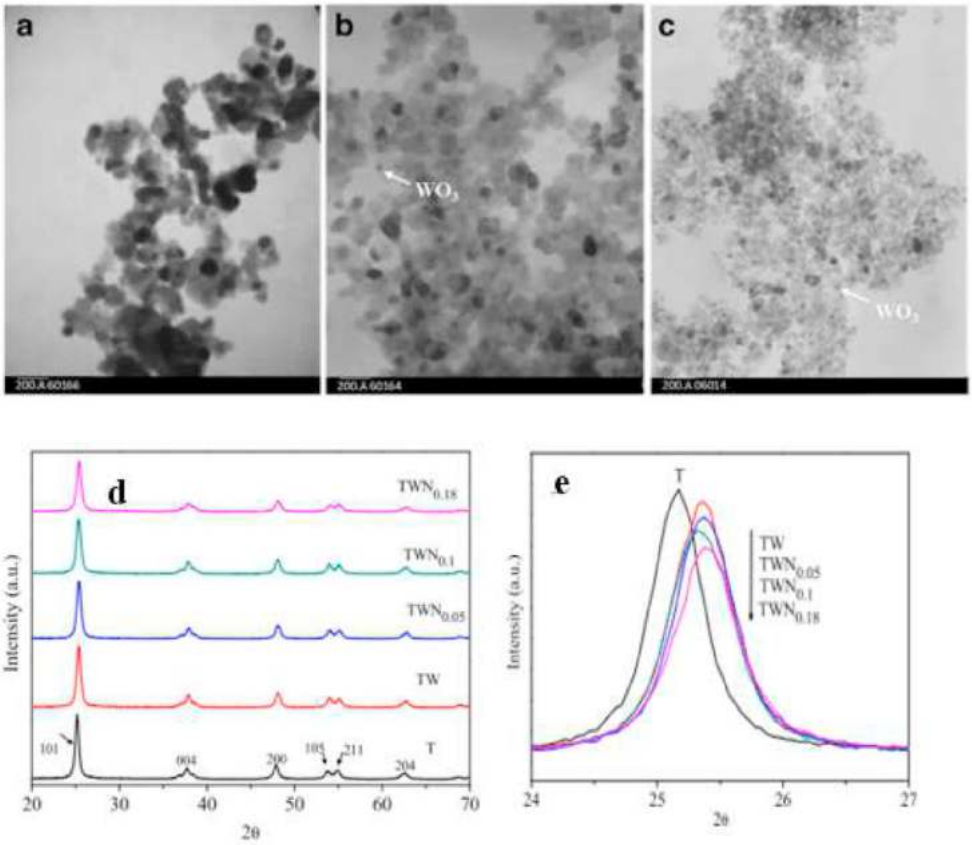

Fig. 9. Transmission electron microscopy images of (a) T, (b) TW and (c) $TWN_{0.18}$, (d). Diffraction patterns of T, TW, and TWN samples. (e). Enlarged XRD pattern showing the peak at 2θ = 25.35 [155].

In a study to fabricate SnO_2-WO_3 composite using solution combustion technique for methylene blue degradation, lemon juice was used as a reducing agent while stannous chloride and sodium tungstate were used as oxidizers [158]. The result shows an effective photocatalytic performance of SnO_2-WO_3 composites under visible light for dye mineralization. The photocatalytic removal of dye was carried out varying the catalyst dosage from 20 to 80 mg and keeping the dye concentration (5 ppm) constant. It was deduced from the result that with an increase in the catalyst dosage, there was a corresponding increase in the dye removal. It was also observed that there was an increase in the active sites on the surface of the catalyst with a corresponding increase in hydroxyl and holes resulting in fast degradation.

3.6. Template assisted synthesis

This method is one of the most important techniques for the controlled and optimized synthesis of various nanostructured materials. This technique directs the formation of nanomaterials into forms that would otherwise be difficult to produce using a pre-existing guide with desired nanoscale properties. This technique is capable of producing nanostructures with unique characteristics, morphologies, and structures [159].

Mokhtarifar et al. [160] synthesized a Pt:TiO_2/WO_3 photocatalyst by the hydrogenated glucose template method for round-the-clock decomposition of methanol. This process involves; the templated synthesis of TiO_2/WO_3, H_2 treatment of TiO_2/WO_3 to obtain a defective structure (H_2–TiO_2/WO_3) and finally loading of Pt on H_2–TiO_2/WO_3. They reported that the photocatalytic material synthesized can be charged under light illumination after which it can continue its photocatalytic activity in the absence of illumination or the dark for over 6h. They also reported that the photocatalyst had a higher surface area and was photoactive in the visible light spectrum which they attributed to the presence of oxygen vacancies in the WO_3 matrix as a result of the surface modification strategy used to synthesize the photocatalyst.

In another related study, Mokhtarifar et al. [161] fabricated a dual-phase TiO_2/WO_3 photocatalyst having post-illumination photocatalytic memory using the template method to investigate their round the clock photocatalytic performance for the degradation of methanol under light illumination and in the dark. They fabricated the TiO_2/WO_3 composite photocatalyst from their precursor via the glucose-template assisted method by varying the WO_3 concentration. They reported that the fabricated photocatalyst exhibited photo absorption in the visible light due to the incorporation of the WO_3 which was also confirmed using other methods such as impedance response of the systems and photocurrent measurements method. The fabricated photocatalyst exhibited round-the-clock photocatalysis for the degradation of methanol attributing this to the incorporation of the WO_3 which resulted in the formation of new energy levels in the TiO_2 structure as well as the

Table 2
Summary of preparation methods for WO_3-based photocatalysts.

Methods	Photocatalyst	Shape	Pollutant	Degradation efficiency (%)	Time (min)	Radiation	Precursor WO_3	Reference
Hydrothermal	WO_3	Flower-like, nanorods, nanowires	RhB	95.3	100	Solar	Tungstic acid	[163]
	$BiFeWO_6$/WO_3	Small sphere with dense particle	RhB	83	60	Vis	Tungstic acid	[164]
	WO_3	Nanoflake and hollow sphere	RhB	93	100	Vis	Sodium tungstate dehydrate	[165]
	$CuBi_2O_4$/WO_3	Sphere with flower-flake nanosheets	Tetracycline	60	120	Solar	Sodium tungstate dehydrate	[166]
	WI_8O_{49}	Polycrystalline	MB	97	8	Solar	Tungsten hexachloride	[126]
	S-doped WO_3	Nanoscale block	MB	79	120	Vis	Sodium tungstate dehydrate	[167]
	WO_3–$SnCl_4.5H_2O$	Rods	RhB	87	160	Vis	Sodium tungstate dehydrate	[168]
Solvothermal	WO_3	Urchin-like	MB	93	60	Vis	ATP	[169]
	TiO_2-WO_3	TiO_2 spherical WO_3sheet like	MB	80	60	Solar light	Tungstic acid	[129]
	La-WO_3/$SrTiO_2$	Layer structure and sheet-stacks	MO	100	75	Vis	Sodium tungstate dehydrate	[135]
Co-precipitation	WO_3/TiO_2/carbon fiber	Spherical	Orange II	UV (70) Sunlight (85)	180	UV Sunlight	Sodium tungstate dehydrate	[170]
	2D WC/WO_3	Flower-like	RhB, MB, MO, phenol	RhB: 89, MB: 96, MO: 80, Phenol: 40	240	Vis	Tungsten chloride	[171]
	WO_3-GO	Nanosphere	MB indigo carmine (IC)	MB (97) IC (95)	MB (180) IC (120)	Sunlight	Tungsten hexachloride	[172]
	$CuWO_4$/WO_3	Spherical-like	Sulfur	85	120	Vis	ATP	[173]
	Ni-WO_3	Nanoplates	Methyl red	96	120	Vis	Sodium tungstate dehydrate	[174]
	WO_3/Fe_3O_4	Irregular	Thiacloprid	66	120	UV	Sodium tungstate dehydrate	[142]
Sol-gel	Pt/WO_3-GO	Mesoporous	MB	94	70	Vis	Tungstic acid	[175]
	Zn & Cu co-doped WO_3	Irregular	Gentamicin antibiotic	UV: 90 Vis: 70	30	UV Vis	AMT	[176]
	WO_3	Spherical	RhB	79	200	UV	Tungstic acid	[177]
	WO_3	Polyhedral	Cr (VI)	50	120	Vis	Tungsten (V) ethoxide	[178]
Green synthesis	Citrus lemon SnO_2-WO_3	Tetragonal	MB	75	180	Vis	Citrus Limon (lemon juice), Sodium tungstate	[158]
Template assisted synthesis	Pt:TiO_2/WO_3	Near spherical	Methanol	61	120	Vis	Hexachloride Tungstate	[160]
	TiO_2/WO_3	Spherical	Methanol	-	-	Vis	Hexachloride Tungstate	[161]

induced oxygen vacancies formed near the valence band of TiO_2.

All the synthesis methods discussed above are aimed at developing a good photocatalyst having great characteristics in terms of light-harvesting, rate of diffusion of reactive molecules, the range at which it can respond to light, excellent charge carrier migration and separation, crystallinity, and specific surface area. However, each photocatalyst has varying physiochemical properties making it have varying morphologies interfacial properties, surface state, and exposed facets which should all be present for their material synthesis [162]. The various preparation or synthesis route discussed above are summarized in Table 2. This table also shows how the various methods or synthesis route affects the degradation time, efficiency, shape of the photocatalyst, type and rate of light absorption, choice of precursor, and type of pollutant to be degraded.

It was therefore observed and concluded from the survey of literature and publications on the synthesis of WO_3-based photocatalysts that hydrothermal methods are widely used by researchers for the synthesis of WO_3- based photocatalysts and this can be attributed to the fact that though other synthesis methods just like hydrothermal synthesis methods can produce photocatalyst with good photocatalytic activity, high particle purity, high crystallinity, Hydrothermal synthesis can boast of having the advantage of using water as the solvent which is not the same in the case of solvothermal and other methods which uses ethanol and as a result makes hydrothermal synthesis cost-effective.

Another important advantage of the hydrothermal method over the other methods is its inexpensive instrumentation in comparison to other methods which require slightly expensive instrumentation for the synthesis process. The hydrothermal method in most cases involves one-step synthesis with good dispersion in solvent (water) which makes it easy, environmentally friendly, with production feasibility which however in the case of other methods, the synthesis involves more than one step, and most times involve series of complex reactions.

4. WO_3-based coatings/deposition techniques

WO_3 is a versatile material having numerous advantages which include having low fabrication cost and being abundantly available. It is suitable to be produced in the form of thin films or coatings which makes it much more attractive for various applications [65]. Thin films are layers of materials deposited on a bulk substrate to impart or introduce properties that cannot be attained (or not easily attained) by the parent or base material. The coating is done on a new surface or an already deposited or coated layer. The application of WO_3-based thin films has the advantage of changing the interaction of the parent material to a newly formed material or flatform preventing it from exhibiting the properties of the bulk or base materials but to the properties that are desired for a particular application. WO_3- based materials in powder form are limited due to difficulty in controlling the coating process, high startup cost, and color changes over time. WO_3 -based thin films have important applications in the degradation of pollutants, in health care as antimicrobial material, photoanodes for water splitting, and CO_2 reduction.

4.1. Electrochemical deposition

Electrochemical deposition is an attractive deposition technique due to its numerous advantages which includes the ability to coat large area, low cost, and ability to control the coating thickness. The deposition technique set up includes an electrochemical cell filled with an electrolyte which contains the metal species to be deposited with two or three electrodes: the anode (in general Pt), the cathode, as a conducting substrate upon which the film grows, and a reference electrode in the case of a three-electrode arrangement.

With the supply of a direct current (DC) to the circuit, the metal species from the solution are migrated or driven to the cathode where they are reduced and eventually electrodeposited forming the film [173]. By tailoring the electrolyte composition and the process parameters, the resulting or obtained film microstructure can be precisely controlled and modified. Numerous works have been done to study electrodeposition of WO_3 films after the work of Yamanaka which was the first article publication [180]. Another study was then conducted 10 years later to study the mechanism of WO_3 electrodeposition from peroxytungstate solution [181]. Another study was reported to investigate the influence of the deposition time and that of the peroxotungstic acid on the photoelectrochemical and structural properties ofWO_3 films. The result shows nanoflake array films electrodeposited on fluorine-doped tin oxide (FTO) coated with a seed layer having improved and enhanced electrochromic and sensing to H_2S properties [176,177].

In another related study to investigate the formation of nanoparticulate films as a function of the pulses characteristics variation in a pulsed electrodeposition process, it was reported that they showed improved and enhanced photoactivity in comparison to the coating obtained through continuous electrodeposition. Habazaki et al. [178], studied the effect of annealing temperature on the crystallinity of WO_3 film which they fabricated by electrodeposition after which the film was used as anodes in the electrochemical decomposition of phenol present in wastewater.

4.2. Anodization

The anodization process of W involves the growing of a WO_3 layer via the passage of a DC through an electrolyte solution. The release of hydrogen takes place at the cathode (e.g., wire, mesh, or platinum foil) while oxygen is produced at the anode (metallic tungsten) consequently the formation of a tungsten oxide layer. Cristino et al. [178], in their study proposed and reported that the oxidation in this process occurs through multiple reactions which first involve the formation of oxides with mixed stoichiometries (W_2O_5 and WO_2), then by WO_3 when the applied voltage exceeds 2V only.

Because of definite growth control conditions, flexibility, availability of electrolytes, and low cost of equipment set-up, much more work, and attention has been put into studying WO_3 formation having varying 2D and 3D structures. Vergé et al. [180], in a related study investigated the formation of anodically grown oxide in 0.1 M H_2SO_4 + 0.4 M Na_2SO_4 electrolyte on both sputter and bulk deposited W films using rotating and stationary disk electrodes. Numerous analytical techniques have been investigated in getting detailed information about the dissolution/growth of oxides [187]. In a similar study, the photoelectrochemical anodization of a W foil was investigated for several hours in a two-electrode setup at 50V under illumination. The process led to the formation of nanoporous WO_3 with a thickness of 2.6 μm having enhanced and improved photocurrent response. Ou et al. [183], in a related work via anodizing sputter technique deposited W films in an electrolyte containing NH_4F and ethyl glycol, obtained 3D nanoporous WO_3 layers as can be seen in Fig. 10. The WO_3 films they obtained gave remarkable electrochromic properties which were attributed to its high surface area in addition to crystallinity.

A similar study of the galvanostatic anodization of W in oxalic acid showed porous structures formation [189]. Tsuchiya et al. [185], in another work studied the formation of self-organized WO_3 nano-tubes for achieving regular pore diameter and arrangement in various concentrations of NaF electrolyte. Several works to investigate W- nanowires formation when exposed to various electrolytes from directionally solidified NiAl–W eutectic alloys to create W-based nanostructures or nano-sized filters for varying applications have also been investigated [186–189].

4.3. Thermal evaporation

Thermal evaporation is a physical vapor deposition (PVD) technique used for coating deposition purposes. The precursor or source of material which is a metal oxide or metal is vacuum heated, and upon

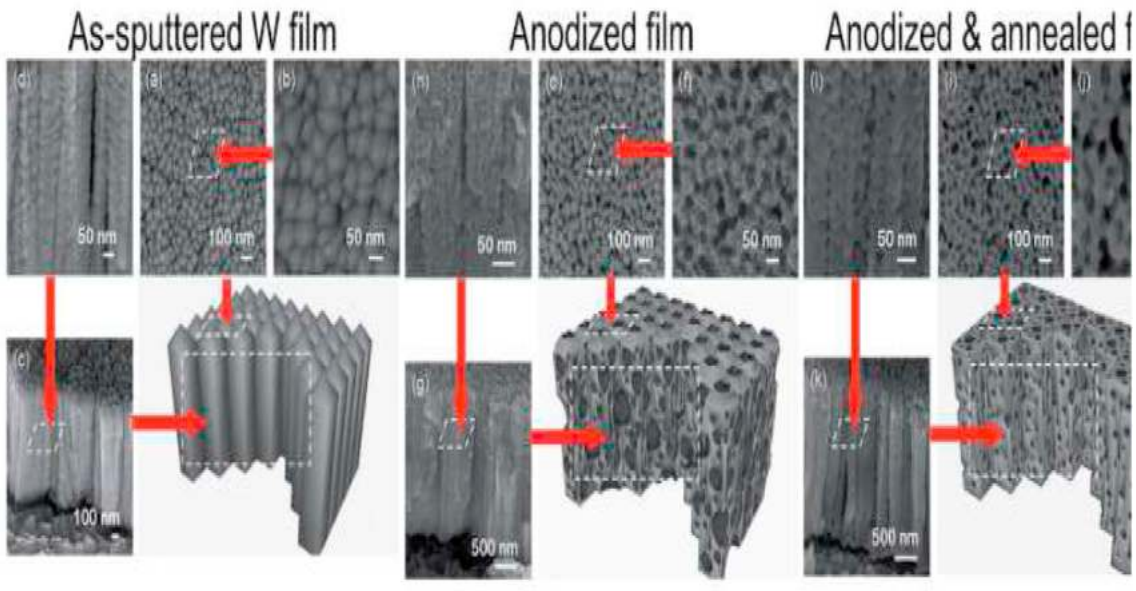

Fig. 10. SEM images of the surface and cross-section of a sputter-deposited W film, followed by anodization and subsequent annealing at 450 °C [188].

receiving enough or adequate thermal energy, the material sublimes or evaporate. The substrate accepts or collects the atoms of the heated source as they are directionally released onto it [190]. The source of material in pellets or powder form can either be metallic WO_3 or W to obtain tungsten oxide films. The resulting coating will be metallic when metallic tungsten is used as an evaporation source. To obtain the tungsten oxide, it is further required that post-deposition annealing in an oxygen-containing environment is available and as well tungsten trioxide can be directly used as the evaporation source. During the vacuum heating process, tungsten trioxide sublimates, however, there is the release of some oxygen because of the thermal energy supplied which consequently forms substoichiometric tungsten oxide species. The equation for this process can be represented as seen in Eqn. (1)

$$WO_3(s) \xrightarrow{sublimate} WO_{3-x}(g) + \frac{x}{2}O_2(g) \rightarrow WO_{3-x}(s) \quad (1)$$

Accordingly, the coating formed can have varying stoichiometries (x = 2–3) as a function of deposition parameters and in addition, oxide films are generally amorphous because of the lower energy of the species in the thermal evaporation process. It is required that annealing takes place at a temperature exceeding or above 400 °C for stoichiometric and crystalline WO_3 to be achieved [196]. For sensing application, rough-surfaced evaporated WO_3 films is most suitable for this application [197]. Thermally evaporated WO_3 was reported to have been used to fabricate smart glass windows having excellent electrochromic properties and energy storage [193].

4.4. Sputtering

Sputtering is also a PVD technique used to prepare thick and thin films. It has wide application in the industry because of its large-scale coating ability and versatility. The coating process is done under a pressure range of 10^{-1} to 10 Pa in a vacuum chamber achieved via the introduction of sputtering gas (Xe, Ar, He, etc.) [190]. The process involves the bombardment of the source material (the target) with energetic ions from the sputtering gas (e.g., Ar^+) which results in the ejection of the target atoms and consequently their deposition or coating on the substrate. The source or precursor material can either be metallic WO_3 or W in the radio frequency (RF) or DC configuration like the thermal evaporation process. Reactive processes are possible in the sputtering technique via the introduction of O_2 in varying proportions with the sputtering gas. Therefore, tungsten oxide coatings can be obtained directly with controlled stoichiometry from both oxide and metallic targets during the deposition process. Heat treatments during or after deposition can be used to obtain stoichiometric films in fully crystalline form.

Numerous features such as coating quality, crystallinity, stoichiometry can be controlled by changing, adjusting, or varying the sputtering parameters like substrate temperature, power density, oxygen content, and pressure [199,200].

4.5. Pulse laser deposition

Pulsed laser deposition (PLD) is considered an appropriate or suitable coating technique in the study of the fundamental properties of materials [190]. Because of its versatility in turning materials from amorphous to crystalline structures and its ability to reliably reproduce the target stoichiometry from films, PLD has also been used for WO_3 deposition. PLD principle is hinged on cutting off a ceramic target surface using an excimer laser, leading to plasma generation. The substrate placed in front of the plasma plum containing molten material droplet and atom cluster receives the film as it is deposited onto it. WO_3 films in either crystalline or amorphous form as well as varying substoichiometric oxides can be obtained as a function of oxygen content and substrate temperature during the process [196]. By changing the energy and laser fluence, turning the structure of the coating can be done from continuous film to nanowires (Fig. 11). The formation of varying polymorphs such as orthorhombic stabilization of WO_3 and monoclinic came with the change [202].

5. Visible light enhancement strategies for WO_3-based photocatalysts

Addressing current environmental pollution and global energy demand requires advanced photocatalytic materials such as visible-light-driven semiconductor photocatalyst. WO_3 appears promising due to some of its outstanding properties that have been studied which include its tunable bandgap, excellent optical properties, having deep valence band, its high ability to absorb visible light up to 480 nm, and high oxidative-power holes which are advantageous for visible-light-driven pollutant degradation. However, even with the excellent properties of WO_3 mentioned above, its low conduction band level (thus low electron

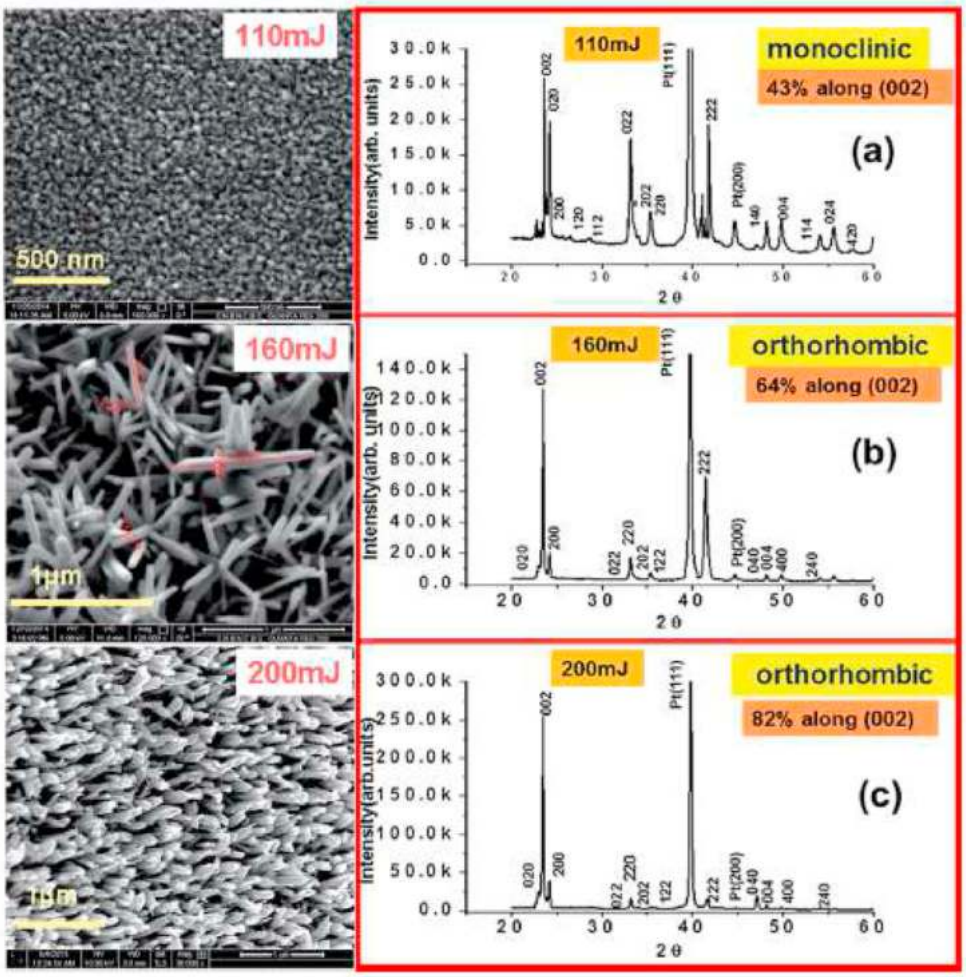

Fig. 11. SEM images of different morphology obtained for WO_3 coatings deposited by PLD using various laser energy values and the change of crystalline structure corresponding to these morphologies as evidenced by XRD patterns [188].

reduction potential), as well as its visible light absorption performance, is greatly hindered mainly by the rapid and fast recombination rate of photogenerated electrons and holes constituting a major drawback in its ability to efficiently convert light energy [88,92]. As a result, various approaches have been adopted to minimize this phenomenon and to improve its photocatalytic efficiency and performance in the visible light range.

Thus, enhancing the photocatalytic activity of WO_3 especially in the visible light region is significantly important to fully utilize its numerous excellent properties for environmental and other applications. The need to address this drawback has received tremendous attention over the years in which numerous enhancement and improvement strategies have been employed and reported. This section discusses various visible light enhancement and improvement strategies for WO_3-based photocatalyst which includes active facet and morphology control, elemental doping, controls in the crystal phase, loading of noble metal NPs, hybridization with carbon materials, and stoichiometry/oxygen-vacancy, constructing heterojunctions and coupling with other semiconductors.

5.1. Doping/noble metal loading

Loading of noble metal NPs such as Ag, Au, and Pt, have attracted increasing interest for improving and enhancing the photocatalytic effectiveness and efficiency of WO_X [203–205]. WO_3 was considered unstable and not suitable to be used in efficient and effective oxidative degradation and decomposition of organic pollutants and thought to be limited for a reaction involving strong electron acceptors because its negative CB is not negative enough for single-electron oxygen reduction [206]. The presence of metal ions in the crystal lattice of semiconductor materials is believed to alter their electronic structure. These metal ions are believed to create centers in the photocatalyst crystal lattice where the trapping of photogenerated electron occurs and therefore extending the lifetime of the photo-generated charge carrier [207,208]. A lot of work has reported that metal doping can significantly improve the photocatalytic activity and performance of WO_3.

Mehta et al. [209], reported loading Ru metal into WO_3 crystal structure in their work and that there was a considerable improvement in the photocatalytic activity of the photocatalyst which they attributed to the presence of the loaded noble metal which acts to minimize charge carrier recombination. In a similar study, Dhanalakshmi et al. [210] reported Ir noble metal loading into the WO_3 structure and found that there was a significant improvement in the photocatalytic degradation of methyl blue and crystal blue of which this improvement was attributed to the efficient separation of electron-hole pair ability of the loaded noble metal. In another study by Mohite et al. [211] where they doped WO_3 film with Yb found out that the WO_3 exhibited excellent photoelectrocatalytic performance in comparison with the pristine WO_3 film in which they observed that a considerable difference was noticed in the mitigation of chemical oxygen demand (COD) from the treated contaminated water with the undoped and doped photoanode.

Abe et al. [206] in their work in which Pt nanoparticles was loaded onto WO_3, found out that O_2 could be reduced by the photogenerated

electrons present in Pt/WO_3 via multi-electron reduction ways (e.g., $O_2 + 2H^+ + 2e^- = H_2O_2$ (aq), +0.682 V vs. NHE). Pt works in this process as an electron pool where photogenerated electrons from WO_3 are accepted by the Pt and it as well acts as a cocatalyst to facilitate the O_2 multi-electron reduction producing H_2O_2. In another related study, it was reported that the in situ reductive decomposition of H_2O_2 as a result of O_2 reduction upon the surface of Pt/WO_3 could be considered a significant path for OH radical generation which is considered a key active specie for organic pollutants and compounds degradation [205]. Au/WO_3 and Ag/WO_3 composites have also demonstrated enhanced photocatalytic activity via this mechanism which involves electron-hole separation and transfer as shown in Fig. 12a [212,213].

A key factor contributing to enhancement in photocatalytic activity or efficiency of WO_3- based noble metal composite photocatalyst is the effect induced by the noble metal NPs via a strong localized surface plasma resonance (LSPR). The excited surface conduction electrons are a result of electromagnetic radiation due to coherent oscillation of the surface plasma resonance (SPR) and much smaller particles interact with the incident wavelength in the LSPR [214]. The noble metal NPs proximity to other nanoparticles, size, and shape are related to their plasmon frequency. A decrease in the size of the particle could lead to plasmon frequency reduction which means a redshift in the absorption rate of the plasmon resonance [215].

A study by Gondal et al. [216] in which Ag was used to doping WO_3, discovered that the presence of the noble metal promoted carrier charge generation which was as a result of the inducement of the surface plasmon resonance and as well enhanced efficient photogenerated electron pair separation. The result shows an increase of three-fold in photoactivity of WO_3 in the degradation of atrazine herbicide with just 1% of the noble metal loading. Choi et al. [204] in their work discovered that the addition of Au to the crystal lattice of WO_3 minimized the hole and electron recombination rate and created a redshift in the absorption edge of the photocatalyst to a longer wavelength with an improvement in the photocatalytic degradation of the pollutant by about 50%. The redshift is a result of the noble metals' ability to enhance excitation by lowering the photocatalyst photons energy like visible light [217].

Generally smaller noble metal NPs less than 10 nm loaded on the surface of WO_3 absorbed in the NIR and visible region corresponds to plasmon resonance absorption in that region. The LSPR tend to disappear when the NPs size of the noble metal reduces to about 2 nm or less as the band structure breaks down into discrete energy level and becomes discontinuous [215]. In plasmonic photocatalysis enhancement, two mechanisms have mostly been studied; a local electric field and charge transfer enhancement. Tian & Tatsuma [218], were the first to study and propose the charge transfer mechanism of Ag–TiO_2 and Au–TiO_2 systems. In this proposed mechanism, electrons present in the noble metal NPs, are excited by the plasmon resonance after which they are transferred to the CB of their adjacent semiconductor, meaning that the NPs of the noble metal acts as electron donors as can be seen in Fig. 12b.

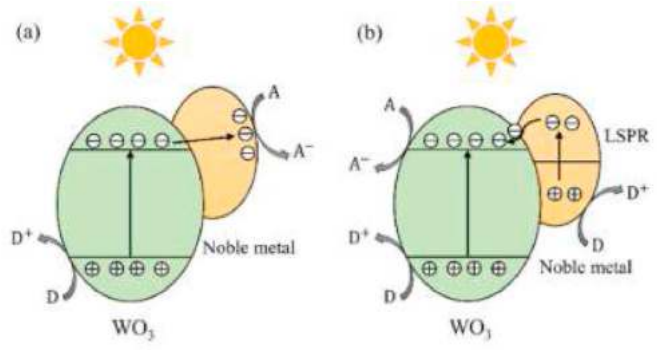

Fig. 12. Schematic illustration of electron-hole transfer and separation in a noble metal loaded WO_3 photocatalyst: (a) the noble metal act as an electron pool (b) the LSPR effect dominates [65].

Some researchers and authors have accepted and adopted the charge transfer mechanism to explain and attribute the noble metal-WO_3 based photocatalytic activity enhancement behavior of the photocatalysts to this mechanism [219]. In the case of the local electric field enhancement mechanism, it has been revealed that irradiating the NPs close to their plasmon resonance frequency, could generate an intense local electric field close to or near the noble metal surface. Studies have also shown that the local plasmonic "hot spot" electric field intensity can reach or get to as much as 1000 times the value of the incident electric field as revealed from studies by electromagnetic simulations using the finite-difference time-domain (FDTD) method [220]. As stated above, since the rate of electron-hole pair generation in the "hot spot" could be as much as 1000 times in comparison to the incident electromagnetic field, this means that due to the enhancement as a result of the local field plasmonic NPs, there will be an increase in the amount of photoinduced charge locally generated in the photocatalyst. Thus, the mechanism of the local electric field has also been adopted to explain and justify the photocatalytic activity enhancement of their developed WO_3 noble metal-based photocatalyst.

It is desired that there should be a uniform distribution of noble metal NPs on WO_3 surface for better photocatalytic activity. Any loading above the optimal level could lead to the noble metal NPs agglomeration, resulting in deteriorating and inhibiting efficient photocatalytic performance [219]. Various factors are responsible for the optimal loading amount of the noble metal NPs for even the same noble metal. This optimal loading value may vary considerably with the morphology of the WO_3 [88,221]. However, from the literature, the noble metal NPs optimal loading value on the surface of WO_3 has mostly been reported not to be up to 5 wt %. Several other metals/noble metals like Cu [176], Co [222], Fe [223], Mn [224], Eu [176], Bi [225], Zn [176], Ce [226], Gd [227], etc have been studied as addition or dopants in a bit to improve and enhance the photocatalytic efficiency of WO_3 for degradation and other purposes.

5.2. Hybridization with carbon materials

The coupling of WO_3 with carbon materials to obtain highly efficient and effective composite photocatalysts has received tremendous attention over the years. Several carbon-based materials having unique structures have been considered and studied for this purpose. These carbon materials include graphene and its oxide as well as reduced graphene oxide (RGO), carbon fiber, multi-walled carbon nanotube (MWCNT), carbon nanodot, and carbon nanotube (CNT) [87,228–231].

Some of the excellent characteristics of the carbon material include its exceptional electron mobility exceeding ~15,000 $m^2\ V^{-1}\ s^{-1}$, outstanding mechanical strength, and excellent thermal and chemical stability which makes it a superior and excellent supporting matrix for photocatalysts. The photogenerated electrons generated or produced in WO_3 in a WO_3/carbon hybrid upon absorption of light irradiation could be quickly transferred to the carbon material via the interface, leaving behind photogenerated holes in WO_3. The photogenerated electrons in the WO_3 undergo a redox reaction on the surface of the carbon material with the adsorbed electron-acceptors which leads to efficient and effective charge separation.

Amongst the numerous carbon materials, RGO and graphene have drawn much attention because of their multilayer or a single layer of sp^2 bonded carbon atoms and their honeycomb-like lattice structure, flexible feature, ultralight-weight, and ultra-large specific surface area (~2600 $m^2\ g^{-1}$). RGO is normally prepared from the reduction of graphene oxide (GO), which itself is prepared by the modified Hummers' method of which graphite is used as the precursor or starting material which is oxidized strongly during a grinding process [232,233]. The oxidation process of the graphite introduces numerous oxygen-containing functional groups, like carbonyl, epoxy, carboxyl,

and hydroxyl groups onto the basal plane of the carbon atom making the prepared GO easy to stably disperse in water and hydrophilic. These oxygen-containing functional groups on the GO surface act as active sites for the deposition and growth of the WO_3 catalyst. The preparation of WO_3/RGO composites can be classified into two categories or routes based on the loading or deposition mechanism of WO_3 onto the GO surface. These routes involve; (i), the addition of GO into the precursor used for the WO_3 synthesis which makes the WO_3 grow and nucleates onto the GO surface during the synthesis process (e.g. hydrothermal treatment process) [234]. The second route involves first synthesizing the WO_3 after which it is mixed in solution with the GO and then the solution undergoes a specific treatment that allows WO_3 to be deposited onto the GO surface. The reduction of GO to RGO in the as-prepared WO_3/GO composite then occurs via a specific reduction or thermal decomposition process (e.g., as seen in chemical reduction using hydrazine vapor at 90 °C for 24 h) [235].

Sajjad et al. [236] in their work modified WO_3 using GO and the result showed that the photocatalytic activity of the obtained photocatalyst in the visible light region was significantly enhanced. WO_3/GO composite had a favorable lower energy band. In another related work by Smrithi et al. [237] in which a monoclinic tungsten oxide (m-WO_3) was modified with carbon nanodots (g-CDs) prepared by the green synthesis via the hydrothermal method for the degradation of crystal violet, they reported a 95% efficiency for the photocatalytic degradation of the pollutant. The work also reported that even after four cycles, the photocatalytic system had good performance and reusability.

Truong et al. [238] in their study to investigated under visible light the photocatalytic degradation performance of C_3N_4-WO_3 composite nanosheet (nsCW21) for the degradation of natural organic matter (NOM). They compared the degradation performance of the nsCW21 photocatalyst to the pure WO_3 and found out that the nsCW21 had a better photocatalytic degradation performance and when H_2O_2 was added as a co-catalyst a 71% degradation rate was achieved after 5h of irradiation. The nsCW21 photocatalyst was also reported to have exhibited good stability even after five cycles of degradation.

In a study by Song et al. [239] to investigate the influence of the addition of carbon nanodots to WO_3 on the photocatalytic performance of the composite and its photoelectrochemical properties, they reported that the composite exhibited a considerable reduction in resistance to charge transfer with enhanced and improved photocurrent intensity in comparison to the pure WO_3. The study also reported an almost 7.7 times better pollutant degradation of some selected pollutants as compared to pure WO_3. The study concluded that this performance was because of efficient electron-hole pair separation which resulted in improved absorption of light due to the presence of the carbon nanodots.

In another study reported by Zhu et al. [233] in which they prepared a nanocomposite of RGO/WO_3 for the visible light degradation of Sulfamethoxazole, they reported from the study that the nanocomposite exhibited high photocatalytic activity in comparison with pristine WO_3 and found out that the nanocomposite also showed enhanced optical absorption capacity, lower value of bandgap energy and minimal electron-hole recombination.

A separate study by Hossain et al. [240] and Prabhu et al. [241] reported the enhanced photoelectrochemical and photocatalytic performance of the GO/WO_3 thin film and RGO/WO_3 nanostructure respectively for the degradation of organic contaminants. They attributed this enhancement to the presence of the carbon material incorporated into the WO_3 lattice. In a similar study, Zheng et al. [242], synthesize a carbon-doped $WO_3{\cdot}0.33H_2O$ hierarchical photocatalyst which exhibited improved photoactivity. The doping by the carbon resulted in changing the band structure giving rise to defect in the lattice of WO_3 which influenced the improved photoactivity of the photocatalyst.

Shahzad et al. [243], investigated the incorporation of activated carbon into the structure of WO_3 and reported that this incorporation resulted in WO_3 bandgap reduction with enhanced light sensitivity. The as-prepared photocatalyst showed a 40% higher photocatalytic degradation of paracetamol compared to the undoped WO_3. Similarly, Isari et al. [244] and Zhu et al. [231] in their separate study reported that modification of WO_3 with carbon nanotubes resulted in improvement in the photocatalytic degradation capacity of the obtained photocatalyst for the degradation of tetracycline and sulfamethoxazole respectively in water. They both concluded that enhanced photocatalytic activity was attributed to the presence of the carbon nanotube which inhibited the charge carrier recombination. It can be concluded that the properties of carbon material such as its high adsorption capacity and excellent conductivity has made researchers to adopt its use as a dopant to WO_3 for enhanced photocatalytic performance of the semiconductor.

5.3. Doping/addition of non-metals

The influence of various non-metals like P, I, S, and N have been studied to investigate how they can enhance the photocatalytic activity of WO_3 semiconductors. They have at various times been used to modify the optical and electronic properties of the semiconductor to enhance performance. Their positive influence in enhancing the photocatalytic efficiency of WO_3 is similar to that of carbon materials. Huang et al. [245] in their work studied the effect of doping nitrogen to WO_3 and they found out by both theoretical and experimental analysis that the doped photocatalyst exhibited the excellent capacity to absorb light and superior separation of the photogenerated electron-hole carrier which resulted in narrowing the bandgap of the semiconductor as can be seen from Fig. 13. They compared the reaction rate constant of the N-doped WO_3 and that of the undoped WO_3 for phenol degradation and discovered that the reaction rate constant of the N-doped was 4.6 times higher than that of the undoped WO_3.

In a related and separate work by both Chen et al. [246] and Han et al. [247], where they doped WO_3 with Sulfur (S) for enhanced visible-light degradation of dye and other organic pollutants, reported that the photocatalytic degradation capacity and light absorption ability of the WO_3 was significantly enhanced due to the doping of the WO_3 with sulfur (S). Rettie et al. [248] in a similar study doped the WO_3 crystal lattice with iron (I) and S for improved and enhanced visible light harvesting by WO_3. The result of the characterization from the work indicates that oxygen (O) in the metal oxide was substituted by both non-metals, though other routes such as cation substitution and interstitial incorporation were thought possible for I. It was also discovered that a relatively shallow impure state was created by the S doping resulting in higher visible light harvesting and absorption by the WO_3 without having any negative effect on its crystal lattice. It was also discovered on the other hand that at all concentrations of I doping, a deep impurity band was created in the WO_3 crystal lattice which negatively impacted its photocatalytic performance.

Another study by Sun et al. [249] in which they doped WO_3 with P found out that this doping resulted in the reduction in the bandgap energy of the photocatalyst from 2.40 to 2.33eV and enhanced photocatalytic degradation of methyl blue by 96% within 120 min. However, it is obvious that much work needs to be done in investigating the effect of non-metal doping onto WO_3 so has to gain more insight into its influence in enhancing the photocatalytic performance of WO_3.

5.4. Heterojunction formation with other semiconductors

Numerous research works and studies have reported on the advantages of adopting the technique of formation of heterojunction by semiconductors in addressing the limitation of a single photocatalyst in harnessing light especially visible light and utilizing it for efficient photocatalytic activity [250–252]. Heterojunction(s) formation by coupling two or more semiconductors has been observed to a large extent to minimize charge carrier recombination and extend the light absorption capacity of the resulting photocatalyst to the visible light region [253,254]. An interface existing between two semiconductors

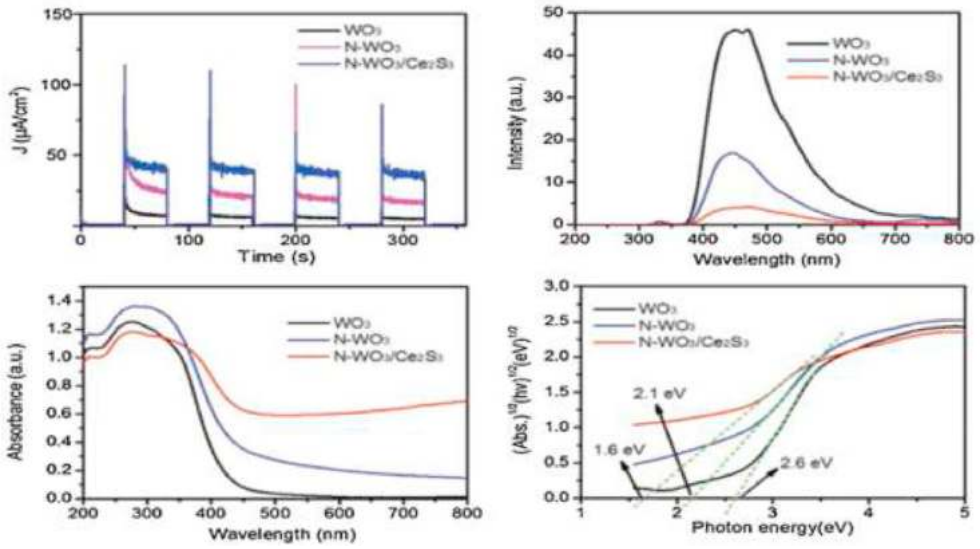

Fig. 13. Plot showing the effects of nitrogen doping on electron-hole recombination rate, optical properties, and photoelectrochemical response, of WO_3 [245].

having an unequal bandgap resulting in bang gap alignment is referred to as heterojunction [255]. One advantage of this alignment is that it aids charge carrier movement within the heterostructured catalyst thereby extending the lifetime and long-term existence of photoexcited electrons and holes [256]. It is possible to have a p-p (i.e heterojunction between p-type and another p-type semiconductor), n-n (i.e heterojunction between n-type and another n-type semiconductor), and p-n (i.e heterojunction between p-type and an n-type semiconductor) formation which depends on the type of semiconductor coupled. Double heterojunction formation involving coupling three semiconductors together is also possible and has attracted some attention. Another categorization of heterojunction is based on the coupled semiconductor (SC) bandgap structure alignment namely, Straddling gap (Type 1), Staggered gap (Type II), and Broken gap (Type III) (Fig. 14a) [257].

In Type I, the valence band of SC-A is more positive than that of SC-B while the conduction band of SC-A is more negative than that of SC-B. In Type II, the valence band of SC-A is less positive than that of SC-B while the conduction band of SC-A is more negative than that of SC-B and finally in Type III, both the valence and conduction bands of SC-A are higher than that of SC-B. It is believed that holes and electrons migrate to the less positive valence band and less negative conduction band respectively in a semiconductor/semiconductor heterojunction. In a

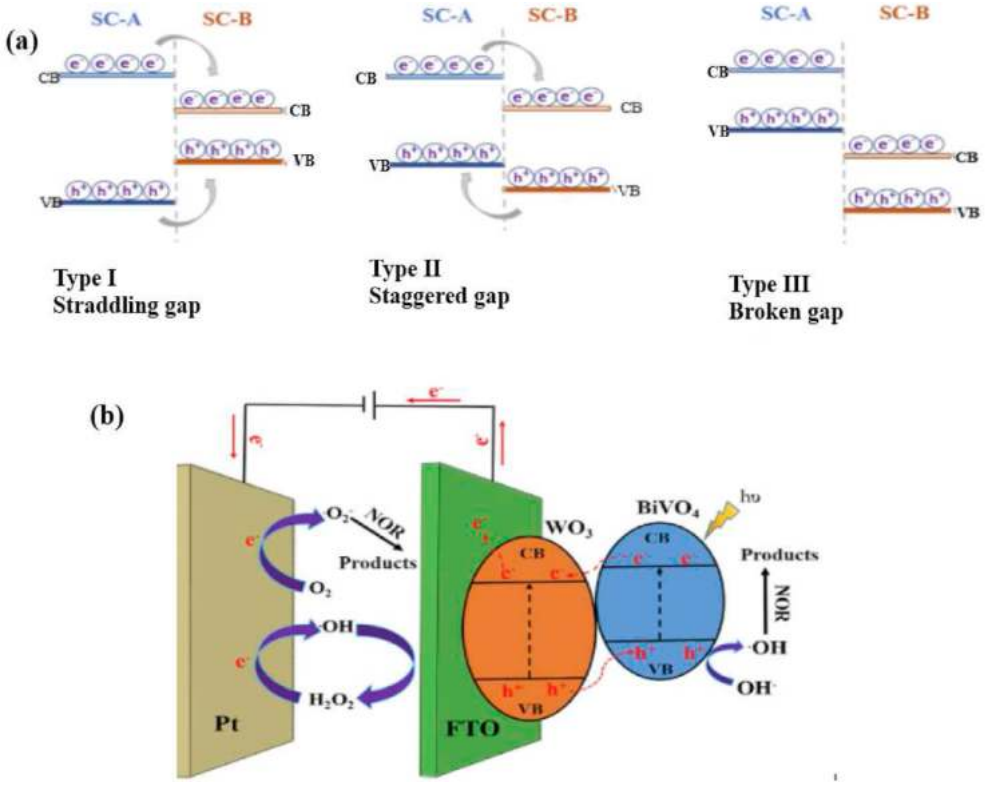

Fig. 14. (a) Various types of band alignment in semiconductor heterojunction [258], (b) Formation of heterojunction between $BiVO_4$ and WO_3 for norfloxacin degradation [259].

Type, I alignment, holes and electrons tend to end up accumulating in the semiconductor having the smallest bandgap which is the SC-B in this case. As a result, there is the likelihood of recombination which could lead to non-improvement in photocatalytic performance. In the case of Type II alignment, holes and electrons will be separated in the two semiconductors which means there will be better charge carrier separation. However, in the case of Type III alignment, there is no heterojunction formation between the semiconductors, and as such both holes and electrons present in one semiconductor are not able to migrate to the other. Here the semiconductors are treated as individual semiconductors. Fig. 14b, gives an illustration of heterojunction formation between two semiconductors $BiVO_4$ and WO_3.

Tahmasebi et al. [260], in their work, prepared p-n heterojunction Bi_2WO_6/BiOCl composite via the hydrothermal method to investigate its photocatalytic performance under LED lamp irradiation and/or simulated/natural solar light irradiation for photocatalytic degradation of Methyl orange (MO), Malachite green (MG) and Rhodamine B (RhB). They reported an enhanced photocatalytic performance of the heterojunction photocatalyst under light source with nearly 100% degradation of RhB molecules after 80 min in comparison to that of BiOCl and Bi_2WO_6 which was 20% and 91% respectively under the same condition. They attributed the enhanced photocatalytic performance of the heterojunction photocatalyst to the strong interaction between BiOCl and Bi_2WO_6 which effectively and efficiently inhibits and impedes the photogenerated electron-hole pairs recombination at the two semiconductors interface.

A related study by Du et al. [259], prepared $BiVO_4/WO_3$ composite film through the hydrothermal route and successive ionic layer adsorption and reaction (SILAR) to investigate its photoelectrocatalytic (PEC) degradation performance under visible light for norfloxacin (NOR) degradation. They reported that the $BiVO_4/WO_3$ composite film exhibited improved and enhanced PEC performance under visible light irradiation with the degradation rate constant for NOR degradation estimated to be 2.68×10^{-3} min^{-1}, which was found to be 2.39 and 3.52 times higher than that of $BiVO_4$ film and WO_3 respectively. They attributed the superior performance of the PEC to the n-n heterojunction formation between the two semiconductors which facilitated interfacial separation rate and charge transfer leading to enhanced and improved light absorption and harvesting capacity.

Wei et al. [261] prepared a series of TiO_2/WO_3 hierarchical hollow spheres via a simple one-pot method to investigate the photocatalytic performance of the prepared heterojunction photocatalyst for the visible light degradation of malachite green (MG). They reported an improved and enhanced visible-light performance of the as-prepared TiO_2/WO_3 microspheres with a 99% photocatalytic degradation of MG after just 60 min in comparison to that of TiO_2 and WO_3 which were 58% and 92% respectively after 180 min under visible light irradiation. They attributed this enhanced performance and highly effective utilization of visible light to the efficient and effective charge separation across the interface of TiO_2/WO_3 heterostructure.

Lei et al. [262] in a related work reported the synthesis of ZnO nanoparticles which they deposited onto WO_3 nanosheets arrays (NSAs) via hydrothermal and impregnation technique followed by thermal treatment for photodegradation under the sunlight of nonbiodegradable methyl blue and azo dye. They reported that the as-prepared WO_3/ZnO heterojunction photocatalyst demonstrated good stability and as well displayed superior and enhanced photocatalytic activities in the degradation of MB in comparison with WO_3 NSAs. They suggested that the enhanced and improved photocatalytic performance should be attributed to the strong light-absorption capacity, quick and fast photogenerated electron-hole pairs separation as well as a favorable band structure of the heterostructured photocatalyst.

In another work, Fukumura et al. [263] reported the synthesis of a visible light CeO_2/WO_2 thin layer photocatalyst and investigated its visible light photodegradation for volatile organic compound (VOC). They reported an improved and enhanced photocatalytic performance of WO_3/CeO_2 photocatalyst for the photodegradation of the VOC under visible light irradiation at room temperature and attributed this superior performance to the CeO_2 electron scavenging property which aided the charge carrier separation. As a result, WO_3/CeO_2 exhibited excellent photocatalytic activity for volatile organic compound decomposition under visible light at room temperature. Other visible light-sensitive semiconductors which have been reported to have been coupled with WO_3 to form heterojunction in an attempt to enhance its visible light performance capacity includes, Fe_3O_4, Ag_3PO_4, g-C_3N_4, $BiVO_4$, etc [142, 264–266].

5.5. Z-scheme systems

Despite type II heterojunctions' better charge separation and transport efficiencies, the system's redox capacity is compromised during the process because photogenerated electrons and holes are respectively moved to CB and VB, which have lower reduction and oxidation potentials [253,254,256,267–269]. To solve this problem, Bard devised the Z-scheme mechanism in 1979, which mimicked the natural photosynthetic process [270]. Over the last 30 years, three generations of Z-scheme photocatalyst systems have been developed: the mediated Z-scheme [271], the all-solid-state Z-scheme (ASS) [272], and the direct Z-scheme [273]. The mediated Z-scheme is made up of two photocatalytic semiconductors coupled together with a liquid redox mediator like Fe^{2+}/Fe^{3+} or IO_3^-/I^- [274]. The linked materials are not physically in contact in this system, but the redox pair acts as a link between them. Each photocatalyst with the highest reduction or oxidation potential undergoes reduction or oxidation processes, and the redox pair functions as a donor or an acceptor depending on the photosystem. Because of the high positive potential of its VB (2.83–3.22 V), WO_3 is commonly used as an oxidation photosystem (OPS) [275,276]. Numerous studies have reported significantly enhanced and improved visible light absorption capacity and photocatalytic activity of numerous photocatalysts in the visible light region using this method [256].

There have been reports of enhanced visible light absorption capacity of WO_3- based photocatalyst developed via the Z-scheme such as in the construction of combined Pt-WO_3 and Pt–$SrTiO_3$ (Cr–Ta-doped) photocatalyst and IO_3^-/I^- as a mediator for the production of hydrogen gas (H_2) under visible light via water splitting [277], $Ag/AgPO_4/WO_3$ nanocomposite for rhodamine B degradation under visible light [272], $AgCO_3/Ag/WO_3$ photocatalyst for efficient degradation of organic pollutants under visible light [267], WO_3 nanoplates decorated with Ag/β-Ag_2WO_4 for the photodegradation of methyl orange (MO), methylene blue (MB) and rhodamine B (RhB) under visible light [278].

5.6. Defect formation via vacancy creation

Lately, defect engineering of semiconductor photocatalysts has been regarded as one of the most advanced and comprehensive approaches to overcoming semiconductor material limitations. As a result, defect engineering is a realistic way to understand the electrical, geometric, and chemical properties of semiconductor photocatalysts, as well as their synergistic interactions, to improve their photocatalytic activity [279]. To create efficient photocatalysts, defect engineering is a critical strategy. In photocatalysts, defects are typically classed based on their atomic structure or their effective position. A semiconductor photocatalyst can be induced with (i) 0D point defects such as vacancy generation and heteroatom doping, (ii) 1D line defects such as screw and edge modulations, (iii) 2D planar defects such as grain and twin boundaries, and (iv) volume defects which involves void generation or disorder in the lattice depending on dimensionality. Photocatalytic water decontamination [280], energy storage devices, organic synthesis, and electrocatalysis are among the many applications of defect rich photocatalysts (such as graphene oxide, metal chalcogenides, carbon nitride, metal oxides, and graphene among others) [281]. Various studies have reported enhancement in visible light absorption capacity

of WO_3-based photocatalyst fabricated via defect formation such as in the fabrication of WO_3 nanosheets for enhanced photoelectrochemical performance and electrochromism [282], WO_3 nanosheets for improved photoreduction of hexavalent uranium (U(VI)) [283], Pt/WO_3 nanosheet for improved oxidation of gaseous toluene [284], defect engineered Z-scheme WO_{3-x}/g-C_3N_4 heterostructure for improved photocatalytic CO_2 reduction [285].

5.7. Morphology control

It has been widely accepted by many researchers that controlling the morphology of a photocatalyst has a far-reaching effect and influence on the enhancement of the photocatalytic efficiency and effectiveness of the photocatalyst. Morphology control for enhancing the photocatalytic performance of a photocatalyst is considered promising because basically, reactions are surface-based processes which means that a photocatalyst performance depends mainly on the relationship between the morphology and microstructure of the photocatalyst, [286]. Surface to volume ratio increase is considered one of the efficient ways of enhancing the photocatalytic efficiency and performance of a visible-light-driven semiconductor photocatalyst. Because of this reason, numerous 1D nanostructured WO_3 such as nanofibers, nanorods, and nanotubes have been prepared and fabricated for various applications. Among several others, 1D-tungsten oxides have been widely explored because of their optical properties for enhanced photocatalytic performance and their lower dimensionality. WO_3 nanowires and nanorods are mostly prepared or fabricated by the simple solvothermal method.

In a study by Choi et al. [110], they fabricated via the simple solvothermal technique several nanoparticles of WO_3 having varying morphologies which include nanorods, nanosheets, and nanowires. Tungsten hexachloride used as the raw material or precursor material was treated with various solvent such as water, mixed solvents, and ethanol at 200 °C for 10 h. They reported that they obtained morphologies of tungsten oxide which includes hexagonal WO_3 platelets, monoclinic $W_{18}O_{49}$, and monoclinic WO_3 nanosheets by just changing solvent compositions as can be seen from Fig. 15.

Another thing they observed was that, for determining the final phases, oxygen in water played a vital role. The monoclinic $W_{18}O_{49}$ nanorods changed into nanowires with a decrease in the raw material concentration (WCl_6). By this fabrication method, it is possible to control the crystalline phases and morphologies of the nano WO_3 photocatalytic system. It has been reported lately that tungsten oxide nanorod and nanowire were prepared by the wet chemical reaction method and results obtained show that the method could be used to control the shape, particle size, improve the visible light absorption capacity of the photocatalytic semiconductor as well provide an opportunity for the likelihood of large scale production [287,288]. Nanofibers WO_3 has shown to be more desired among the various 1D Nanomaterials because of its outstanding mechanical property and electrospinning is regarded as the most adopted technique for its fabrication because it allows large-scale production and helps improve its elastic property by altering some basic technical parameters. Ofori et al. [289] used citric acid, tungstic acid, and polyvinyl pyrrolidone (PVP) as precursors to fabricate WO_3 nanofibers by the electrospinning technique in which they found the nanofibers average diameter to be between 80 and 100 nm and gradually increase with the increase in the concentration of PVP. They discovered that the structure of WO_3 nanofibers was transformed from amorphous to orthorhombic and the diameter of a nanofiber of WO_3 was noticed to have reduced after sintering at 500 °C for 2 h. They also found out that for the photodegradation of methyl blue in the visible light, the WO_3 nanofiber exhibited an enhanced photocatalytic degradation performance of about 2 times higher in comparison with the pure WO_3.

In a related study by Zhao and Miyauchi [88] where they fabricated nanoporous-walled WO_3 nanotubes as can be seen in Fig. 16a, using an economical and simple technique which they developed for the fabrication of the WO_3 nanotubes. They found out that the as-prepared nanotubes were monodispersed varying approximately between 2 and 20 mm in length and 300 and 1000 nm in diameter. They also found out that the nanotubes had a specific WO_3 nanoparticles linear arrangement like building blocks. It was confirmed that the as-prepared nanotube absorbed visible light at a wavelength above 400 nm as indicated by the UV/Vis spectrum and a 2.6eV estimated energy band gap value. Upon loading Pt, WO_3 nanoparticles exhibited more enhanced and improved photocatalytic degradation performance in comparison with pure WO_3 and nitrogen-doped-TiO_2 for the photodegradation of gas-phase

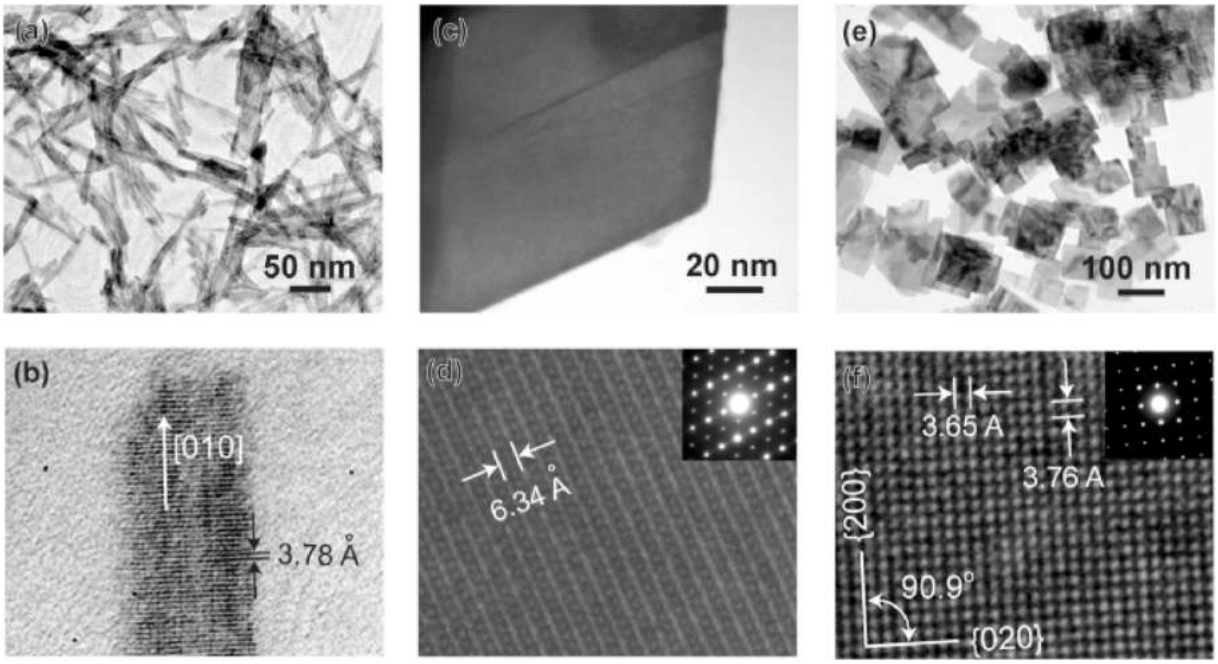

Fig. 15. TEM images (top) and corresponding high-resolution atomic images (bottom) of tungsten oxide particles: (a), (b) sample ES, monoclinic $W_{18}O_{49}$; (c), (d) sample MS, hexagonal WO_3; and (e), (f) sample WS, monoclinic WO_3 [110].

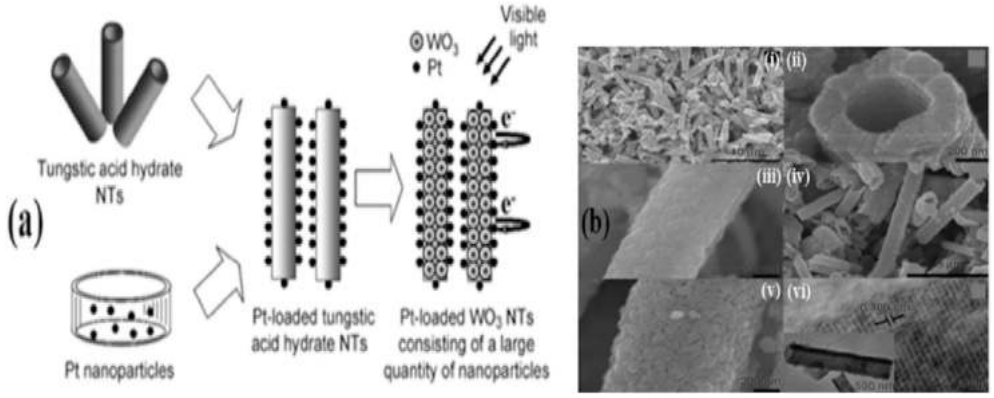

Fig. 16. (a) Fabrication of Pt-doped WO_3 nanotubes, (b) SEM images of WO_3 nanotubes before (i–iii) and after annealing (iv, v), (vi) TEM image. The inset in (vi) displays a TEM image of a single nanotube after annealing [88].

acetaldehyde. They attributed the enhancement in photocatalytic activity to the annealing temperature which after annealing altered the specific area and pore size resulting in enhanced photoactivity, the distinctive tubular morphology or structure of the as-prepared photocatalyst which provided a platform for increased photon adsorption, quick and advanced migration of charge carriers as well as effective and large surface area as can be seen from Fig. 16b.

In another work by Rong and Wang [290] which they fabricated via the hydrothermal method hollow nest-like WO_3 nanostructure photocatalyst for tetracycline degradation under visible light. They found out that the hollow nest-like WO_3 nanostructured photocatalyst exhibited better stability, improved visible light absorption as well excellent photocatalytic degradation of tetracycline better than pure WO_3 with a degradation rate of 94.3% and 52% respectively under visible light after 60 min of photodegradation. They attributed the excellent photocatalytic performance of the hollow nest-like WO_3 nanostructured photocatalyst to its ability to quickly generate enough charge carriers after absorbing more light energy, available large surface area which provided more active sites for the photoreaction to take place, its hollow cavity and perfect crystal structure as can be seen from Fig. 17.

6. Heterogeneous photocatalysis

Heterogeneous photocatalysis is a complex chemical process whereby a photocatalyst absorbs photons energy (hv) greater than its bandgap energy (Eg) upon light irradiation falling on it to generate electron-hole pairs, which then migrate to the surface of the catalyst to start or initiate redox reactions [291–293]. The photocatalytic process involves three steps: (i) photoexcitation of semiconductors to create electron-hole pairs, (ii) separation of electron-hole pairs, and (iii) surface redox reaction [294]. The excited carriers can undergo redox reactions with a variety of substances, such as CO_2, N_2, H_2O, and O_2 which makes its application widely used in solar fuel production [295], CO_2 reduction [296], organic pollutant removal [297], water and environmental purification [291,298–300]. Heterogeneous photocatalysis has gained tremendous attention now that environmental pollution is increasing considerably because simple aerial oxidation and self-purification processes are no longer efficient and sufficient to tackle this problem. The photocatalysis process has the overall reaction equation (Eqn. (2)) thus;

$$Organic\ \ pollutant + O_2 \xrightarrow[UV/Vis]{semiconductor} CO_2 + H_2 + mineralacids \quad (2)$$

The photodegradation process mechanism is as shown in Fig. 18 is represented by Eqn. (3) – (7). From Equations (4) and (6), the reaction of e^- and h^+ with O_2 and H_2O respectively result in the formation of highly

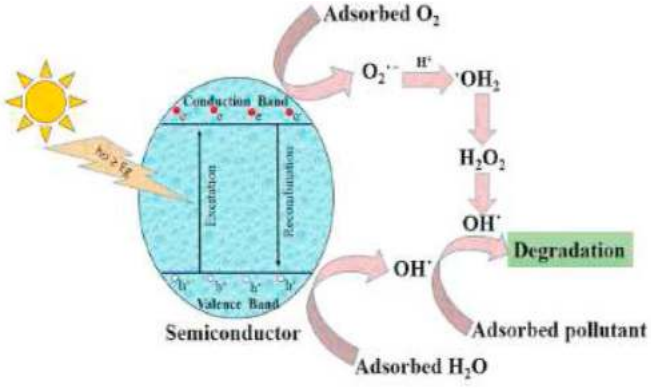

Fig. 18. Mechanism of the semiconductor-based photocatalytic process [291].

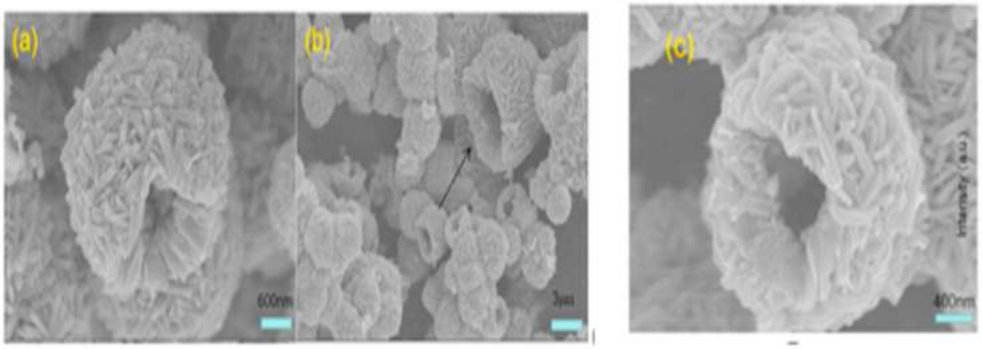

Fig. 17. (a, b and c) SEM images of the as-synthesized HNWMs [290].

reactive radical species, $*OH$ and O_2^-. Equation (5), shows the reaction of these radical species with the organic pollutants leading to the degradation of these pollutants.

$$\text{Catalyst} + h_V \rightarrow e_{CB}^- + h_{VB}^+ \quad (3)$$

$$e_{CB}^- + O_2 \rightarrow O_2^- \quad (4)$$

$$O_2^- + e_{CB}^- + 2H^+ \rightarrow *OH + OH^- \quad (5)$$

$$h_{VB}^+ + H_2O \rightarrow H^+ + *OH \quad (6)$$

$$Pollutants + *OH \rightarrow Degradationproducts\left(CO_2, H_2O, etc\right) \quad (7)$$

Photocatalysis has the advantage of low cost, ease of handling and application, non-generation of toxic waste or sludge in most cases, efficient, low energy requirement, high pollutant removal rate, and environmentally friendly in comparison to other pollutant removal methods which do not completely remove pollutants, has high energy requirement and generate toxic sludge or waste in most cases [294,301]. Photocatalysis requires a continuous photo-assistance to perform or undergo redox reaction, which greatly limits its wide applications particularly in the absence of light, in the dark, or at night [302]. Once there is no light source, the generation of carriers (electron-hole pairs) within the semiconductor will cease or stop, which immediately results in loss of their catalytic activity. As a result of this limitation, there is currently a paradigm shift in this field from photocatalysis to round the clock photocatalytic systems (RTCPS) or memory catalysis (MC) by researchers with interest in how to maintain the catalytic activity under dark conditions [303,304]. Just like how the reaction system of RTCPS is diverse, so also the corresponding reaction mechanism.

Apart from the basic requirements for photocatalysis, the process involves an additional component which is the energy storage substance (ESS), required to initiate or take off the catalytic reaction in the dark or the absence of a light source [305]. Here photo-generated carriers generated by the photocatalyst under light irradiations can be stored and released in the absence of light based on carrier storage mechanism been a common reaction system. Electrons are briefly excited from the valence band (VB) to the conduction band (CB) under light illumination and some of the electrons move or migrate to the surface of the catalyst to participate in the catalytic reactions while the excess carriers are stored in the ESS. Then, these stored carriers can be released or discharged to electrolyte solution to maintain or keep up the catalytic activity through anodic or cathodic reactions in the absence of light or the dark. This RTCPS can be achieved by combining (i) an ESS and (ii) a semiconductor (SC). The performance of this RTCPS normally depends on the kinetics of the carrier processes at the interface between the ESS and SC and the relative energy levels of the SC. Some basic principles or process to construct or develop an efficient and effective RTCPS includes the following: (i) The CB of the SC should be above the CB edge or Fermi level of the ESS for efficient electron transfer from SC to ESS, (ii) For efficient and effective electron transfer, good contact is needed or required in SC-EES inter-face; (iii) ESS should possess the property and characteristic of slowly releasing electrons in the absence of light source or the dark; (iv) The Fermi or CB level position of the ESS should equate or match the redox potential of the specific reaction conditions. Additionally, it is worthy of note that this is not the only way to achieve RTCP reactions. Other material systems based on peroxidase mimic mechanism [306] and fluorescence-assisted mechanisms have also been studied and reported [307–311]. Metal oxides like WO_3 having high valency can mainly store electrons because of their abundant varying valence metal ion (e.g W^{+5}, $W^{+6,}$ etc.).

Most WO_3-based memory photocatalysts reported have good stability and reusability. Yang et al. [312], reported that the Bi_2WO_6 memory photocatalyst they fabricated exhibited continuous performance in cycling H_2O_2 yield which did not deteriorate even in the dark indicating that the photocatalyst had good stability and reusability. Zhao et al. [313], also reported stability in the MgZnO/WO_3 QDs/GO composite they prepared which maintained high memory and photocatalytic stability and reusability for more than 40 days indicating that the composite is stable and reusable. Other memory WO_3-based photocatalyst reported to have relative stability and reusability includes; rGO/-TiO_2/WO_3 [314],$Bi_4TaO_8Cl/W_{18}O_{49}$ [315],WO_3/g-C_3N_4 [316], Pt: TiO_2/WO_3 [160], dual-phase TiO_2/WO_3 [161],

6.1. Mechanism of RTCPS: memory catalysis

Solar light-driven semiconductor photocatalysis has over the years attracted increasing interest and attention in energy and environmental applications [317]. However, a crucial problem that has been a limitation to its application is that for photocatalysis to take place continuously, it requires a continuous light source for the redox reaction. The capability and need to keep catalytic reaction activity to proceed even in the dark or in the absence of light has been the main goal for the wide application of photocatalysis [302]. Continued efforts have been put into developing photocatalysts that can support, and accomplish photocatalytic reactions under both dark and light conditions, which is so-referred to as RTCPS [318,319]. RTCPS with the capacity for energy storage can perform well both at night and daytime. These systems are widely used for organic pollutant degradation, heavy metal ion removal, hydrogen generation, disinfection, and many other photocatalytic applications using a round-the-clock photocatalyst (RTCPt) also called “all day active photocatalyst” [319].

The general principle and mechanism of RTCPS of a semiconductor-based photocatalyst also referred to as ‘memory catalysis’ (MC) involves hole storage (a reductive mechanism), multi-electron storage, and oxidative mechanism [319]. In memory catalysis, a catalytic material requires a semiconductor (SC) and a supporting material to accept/store electrons during light irradiation and release the stored electrons in the dark for photocatalytic activity. The "catalytic memory" is a phenomenon in which a part of photoinduced electrons stored in the material under light combines with water molecules or adsorbed oxygen to degrade pollutants in the dark at room pressure and temperature. This potential for RTCPS is important for the degradation of pollutants in air or wastewater which as well can be expanded toward material design with lower energy consumption and at a lower cost. It is worthy of note that the use of photocatalytic memory systems has emerged as a promising field for developing more effective photocatalytic materials for the breakdown of various harmful organic pollutants, anti-bacterial activity, hydrogen generation via water splitting, self-cleaning concrete and glasses, cancer treatment, bacterial disinfection, heavy metal ion detoxification and fuel conversion [319,320].

It has been found that the memory effect mechanism in a continuous photocatalytic system is finite which is detected via its remediation efficiency in the dark when the photo-charge catalyst is stored in the absence of illumination or the dark for varied periods [321]. The findings also show that the remediation efficiency of a continuous photocatalytic process in the dark is mostly dependent on the memory effect created during exposure to a light source before the dark condition rather than other interfering factors such as toxicity and adsorption. The rate of electron release from the energy storage material determines the dark storage time of this photo-charged catalyst [322].

6.2. WO_3-based RTCPt electron energy storage mechanism

As stated earlier, most RTCPS are electron storage-based mechanisms. This system consists of two types of materials, an ESS and a SC. Under light irradiation, photo-generated electrons are provided by the SC acting as the photocatalyst while ESS acting as the electron sink traps the electrons migrating from the SC. When light is removed or in the absence of light, the trapped electrons are released by the ESS to the appropriate electron acceptors like H^+ and O_2, etc. “Dark catalysis” is related to the electron storage capacity arising from the reaction activity

involving the released electron and the acceptance of electrons which has wide applications in the field of environment and energy, especially in pollutant removal and disinfection. A photocatalytic material system like TiO_2-WO_3 stores electrons ("reductive energy storage") via intermediate reversible product formation (Equations (Eqn. (8)– (12)) [305, 323–326] where the WO_3 act as an electron storage material and the TiO_2 functions as a light-absorbing or harvesting material.

$$TiO_2 + h_V \rightarrow TiO_2{}^*(e^- + h^+)(carrier\ generation) \quad (8)$$

$$e^-(TiO_2) \rightarrow e^-(WO_3)\ (interfacial\ electron\ transfer) \quad (9)$$

$$WO_3 + xe^- + xM^+ \rightarrow M_x\ WO_3\ (charging) \quad (10)$$

$$M_x\ WO_3 \rightarrow\ WO_3 + xe^- + xM^+\ (discharging) \quad (11)$$

$$e^- + O_2 \rightarrow {}^*O_2^-\ (dark\ reaction) \quad (12)$$

Electron-hole pairs are generated in TiO_2 upon light irradiation as can be seen from Eqn. (1). Two possibilities occur here, on one part, the holes remain on the TiO_2 surface reacting with an environmental medium like humid/adsorbed H_2O and another electrolyte. The other part involves the injection of excited electrons to the WO_3 CB where they are trapped via the intercalation of M^+ ions (M may represent Na+, Li^+, K^+, H^+, etc.) as can be seen from Eqns. (2) and (3). When in the dark or absence of a light source, the electrons that were trapped can be released as seen from Eqn. (4) and react with the electron acceptors like O_2 (Eqn. (5)). The mechanism of electron storage under light source in TiO_2-WO_3 and electron release in the dark is illustrated in Fig. 19a. It was found that the amount of stored charge depends on the radii of the M^+ ion [327]. As can be seen from Fig. 19b, as the ionic radii increase, there is a corresponding increase in the charge storage capacity. This relationship can be as well explained that larger ions stay longer in the structure because the movement of the M^+ ions is limited by the large ionic radii. Consequently, as the ionic radii increase from H^+ to K^+, the charge storage capacity is enhanced (Fig. 19c).

6.3. Round-the-clock electron energy storage ability of WO_3-based photocatalysts for environmental applications

Tatsuma et al. [305] were the first to develop the TiO_2-WO_3 RTCPS for anticorrosion application under both dark and light conditions. To date, a lot of research has been going on in investigating the various RTCPS by researchers. As a result, numerous areas of application of RTCPS have emerged including the field of energy and environmental applications. Some areas that have emerged as a result of numerous researches in this field include pollutant degradation, heavy metal removal from water, disinfection, etc.

6.3.1. Degradation of pollutants

In a study to investigate the degradation of methanol (MeOH) under visible light irradiation and in the dark, Mokhtarifar et al. [160] synthesized a Pt:TiO_2/WO_3 photocatalyst by the hydrogenated glucose template method. They reported that the H_2–Pt-G:TiO_2/WO_3 photocatalyst degraded around 61% and 33% of MeOH in light and dark conditions respectively in which they attributed its photocatalytic activity in the dark to the synergic interaction of the hybrid system (Pt, WO_3, TiO_2) which resulted in the extension of the absorption capacity of the photocatalyst into the visible light region thereby enhancing photocatalysis and electron stored discharge due to the incorporation of WO_3 and the presence of oxygen vacancies on the hybrid system.

In another related work, Mokhtarifar et al. [161] fabricated a dual-phase TiO_2/WO_3 photocatalyst for the degradation of methanol in both the presence of light illumination and also post illumination. They reported that the photocatalyst exhibited photocatalytic memory even in the dark for the methanol degradation. They attributed this to the electron storage ability of WO_3 which provided the stored electron for degradation of methanol under dark conditions.

Li et al. [328] fabricated WO_3/TiO_2 hollow microsphere composite photocatalyst to investigate its degradation capacity for the degradation of methyl orange (MO) in the presence of both light and dark conditions. They reported from their investigation that the WO_3/TiO_2 hollow microsphere composite photocatalyst apart from exhibiting excellent photodegradation of the MO in the presence of a light source was also

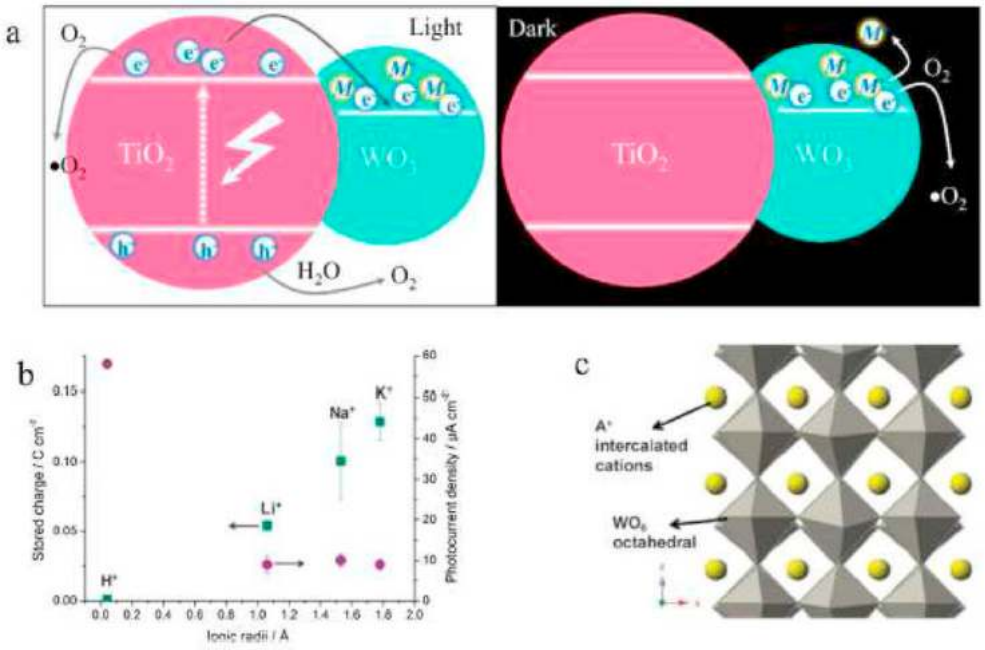

Fig. 19. Electron storage mechanism in TiO_2-WO_3 system. (b), The effect of ionic radii on the amount of stored charge and the photocurrent density generated after a 10 s off-on cycle from the respective alkali cations electrolyte. (c) Diagram showing the WO_3 crystal structure and intercalated alkali cations to illustrate the effect of ionic radii on the ability to store charges [327].

able to achieve an excellent degradation of 22% of the MO in the dark after exposure to visible for a period.

In another related work by Li et al. [329] fabricated a Pt-loaded and hydrogen treated WO_3 (Pt–H:WO_3) photocatalyst for the photodegradation of formaldehyde under full sunlight spectrum. They reported that the photocatalyst exhibited an excellent and strong absorption capacity for the absorption of sunlight having a superior long-lasting energy storage capacity for a period of more than 300 h to have the formaldehyde degraded in the dark. They reported a degradation rate of approximately 80%. They concluded that the hydrogen treated WO_3 simultaneously functioned as energy storage and light harvesting material and the Pt basically acted as a cocatalyst assisting to display the energy storage effect. Pt nanoparticles also aided in promoting the multielectron reduction of O_2 over Pt for the formaldehyde degradation. It can be seen from Fig. 20a, that the available oxygen vacancies present in the tungsten oxide were because of the hydrogen treatment which provided more trapping sites for light harvesting. Fig. 20b demonstrates Fermi level upshift due to induced defect band in the energy band gap. Fig. 20c (Process 1, 3 and 4) demonstrates transfer of excited electrons to the defect band or conduction band (CB) from the valence band (VB). The next process involves trapping of electrons to be stored by the trapping sites of the defect band inhibiting recombination of electrons and holes in the VB (process 2). The electron stored in the defect band are then released in the dark and consequently migrated to Pt (process 5). Multielectron reduction of O_2 is represented by the equations (e.g., $O_2 + 2H^+ + 2e^- = H_2O$ (aq), $+0.682\ V_{NHE}$; $O_2 + 4H^+ + 4e^- = 2H_2O$, $+\ 1.23V_{NHE}$) (process 6, Fig. 20c), thereby facilitating degradation of formaldehyde in the dark via formaldehyde oxidation.

In another work where the RTCP mechanism was investigated was in the work by Khan et al. [330] in which they reported the preparation of titania tungstated photocatalyst (TiO_2/WO_3) for the degradation of MB. The result of the work showed that the degradation involved adsorption and photolysis in which the hybrid photocatalyst $TW_{0.075}$ outperformed other samples in degradation of the pollutant (MB) with a degradation rate of 90% in 100 min under UV irradiation. They reported that the degradation process of 100 min took place as 30 min in the dark, 40 min with light, and 30 min in the dark demonstrating that the photocatalyst exhibited energy storage capacity for degradation even in the dark.

Khan et al. [331] reported the fabrication of a UV–Vis light photocatalyst with Pt as support over TiO_2/WO_3 for the photodegradation of MB under both UV and visible light. They reported a degradation rate of 78% and 56% for UV and visible light respectively after 120 min. Then with an additional 1 h of degradation in the absence of light irradiation to investigate the energy storage capacity of the photocatalyst, the degradation reached a rate of 98% and 77% under UV and visible light, respectively. With this performance, they suggest that the photocatalyst exhibits energy storage capability to be used for degradation even in the dark.

In another study, Xie et al. [332] prepared WO_3–ZnO composite with energy storage capability under UV–Vis light for methyl orange (MO) degradation. They investigated the photocatalytic performance of the composite photocatalyst in MO degradation in the presence of light and the dark. They reported a degradation rate of MO to reach 17.2% in the dark which suggests that the photocatalyst composites exhibit a form of energy storage capacity for MO degradation even in the dark.

6.3.2. Removal of heavy metals

In work to investigate the RTCP mechanism of WO_3-based photocatalyst energy storage, Zhao et al. [333] designed and prepared an embedded TiO_2-WO_3 nanohybrid material with WO_3 cluster acting as the electron storage sites for the system which they explored for the reduction, removal and treatment of poisonous heavy metals ions in water in the absence of light or the dark. They reported that the as-prepared photocatalyst could still store energy with the presence of O_2 where these stored electrons are released for heavy metal ion reduction in water.

6.3.3. Disinfection

Tatsuma et al. [334] investigated the effect of TiO_2-WO_3 composite photocatalyst film for its RTCP ability to disinfect bacteria in the presence and absence of light. They found that the film can be energy-charged inductively by UV light and that the photo charged film showed a moderate bactericidal effect on *E.coli* after 6 h exposure in the absence of light or in the dark. They reported that this moderate effect can stop bacterial from growing or multiplying during the night when there is no light with TiO_2 killing any bacteria that might have survived. They concluded that the composite photocatalyst exhibited a form of energy storage capability for the bacterial disinfection even in the dark. Table 3, gives a summary of the various areas of application of WO_3-based memory photocatalyst RTCP energy storage mechanism, showing the electron storage mechanism, various pollutants been degraded, photocatalytic activity under light source and in the dark and

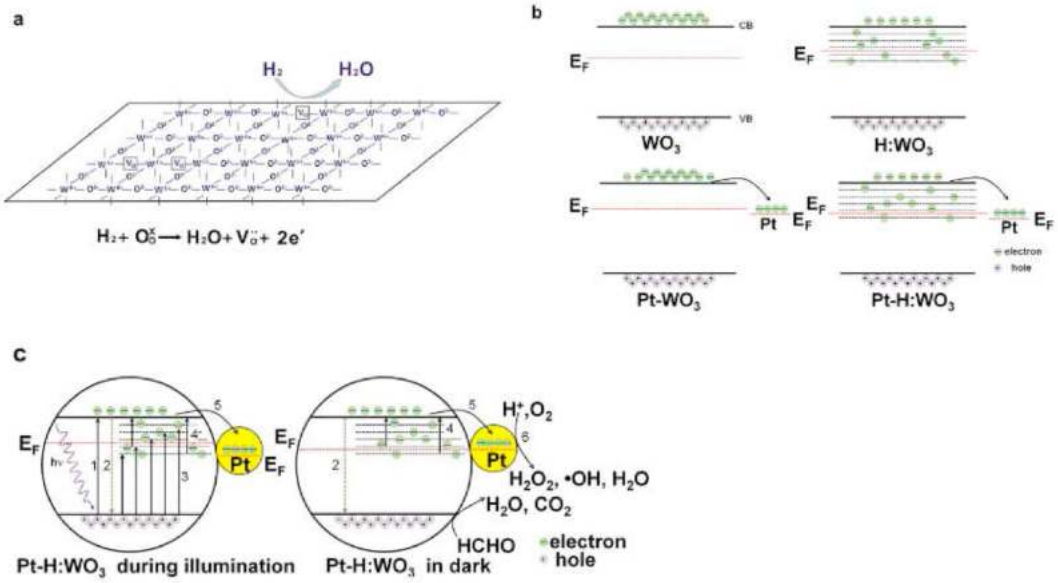

Fig. 20. Full sunlight spectrum broad absorption and long-persistent energy storage mechanism of Pt–H:WO_3. (a) Reaction model of hydrogen treatment. (b) Energy band structure of WO_3, H:WO_3, Pt-WO_3, Pt–H:WO_3. (c) Absorption of full-spectrum and mechanism of degradation of formaldehyde in the dark by Pt–H:WO_3 [329].

Table 3
Summary of the applications and mechanism of different round-the-clock photocatalytic memory of WO_3-based catalytic systems.

Photocatalyst (catalytic system)	RTCP mechanism	Pollutant	Activity under light source	Activity in the dark	Reference
WO_3/TiO_2 (Hollow microsphere)	Electron energy storage	Methyl Orange (MO) (20 mg/L)	Exhibited good photocatalytic efficiency in UV/Vis	Maximum degradation efficiency of 22%	[335]
WO_3/TiO_2	Electron energy storage	Methyl blue (MB) (6.0 mg/L)	Reached 90% degradation after 100 min (40 min in light)- UV	Degradation proceeded for 60 min in the dark	[330]
$Pt/TiO_2/WO_3$	Electron energy storage	MB (6.0 mg/L)	78% - UV light, 56%- Vis, degradation.	With an additional 1 h in the dark, degradation reached, 98%- UV, 77%- Visible light	[331]
$Pt–H:WO_3$	Electron energy storage	Formaldehyde (100 ppm)	80% degradation of formaldehyde under sunlight	Degrade formaldehyde in the dark with long-lasting energy storage for over 300 h.	[335]
WO_3–ZnO	Electron energy storage	MB (20 mg/L)	Almost complete degradation of MB within 180 min.	Degradation efficiency reached 17.2% in the dark after 60 min.	[332]
WO_3-rGO	Electron energy storage	MB (10 mg/L)	78% degradation of MB under visible light after 180 min.	Showed energy storage capacity of capacitance 577 Fg^{-1}.	[336].
TiO_2-WO_3	Electron energy storage	*Escherichia Coli (E.coli)*	Demonstrated bactericidal effect against *(E. coli)* with exposure to UV light	Demonstrated bactericidal effect against *(E.coli)* with exposure in dark for about 6 h	[334]
TiO_2-WO_3 nanohybrid	Electron energy storage	Poisonous heavy metals (Cr^{6+}, Hg^{2+}, and Ag^{+}).	Poisonous heavy metal reduction under UV light.	Achieved reduction treatment of the heavy metals in absence of light (dark)	[333]
MgZnO/WO_3 QDs/GO	Electron energy storage	Rhodamine B	96.1% degradation under visible light after 40 min.	Achieved degradation of Rhodamine B even under dark condition	[313]
g-C_3N_4/WO_3	Electron energy storage	Rhodamine B	97.46% removal of Rhodamine B under visible light	42.33% Rhodamine removal in the dark with nearly 8h memory photocatalytic activity	[316]
TiO_2/WO_3/rGO film	Electron energy storage	Chromium (Cr) (VI)	97% Cr (VI) reduction under UV light	17% more Cr (VI) reduction was achieved	[314]
$Bi_4TaO_8Cl/W_{18}O_{49}$	Electron energy storage	Carbon dioxide (CO_2)	87 times in CO_2 reduction was achieved under Visible	Exhibited long-lasting catalytic CO_2 reduction in the dark	[315]
Bi_2WO_6	Electron energy storage	*E. Coli*	A good disinfection ratio with a decrease in *E. Coli* survival ratio to 30% under simulated solar illumination.	*E.Coli* survival ratio was decreased to about 55% in the dark after 2h	[312]
Dual-phase TiO_2/WO_3	Electron energy storage	Methanol	High degradation of methanol under visible light	Achieved degradation of methanol even under dark condition	[161]
$Pt:TiO_2/WO_3$	Electron energy storage	Methanol	66% degradation of Methanol in 2h	33% degradation of Methanol and the photocatalytic process lasted for 6h in the dark	[160]

the percentage degradation in the absence of light demonstrating the potential of WO_3- based photocatalyst to store energy and utilize it for various environmental applications in the dark. It shows that with proper tailoring and synthesis of WO_3- based photocatalysts, it can be used in both the day and in the night for these purposes describing a continuous process of photocatalysis.

7. Concluding remarks

This review has demonstrated that WO_3 has attracted significant attention in recent years with respect to the visible light photoactivity of WO_3-based catalysts. It is evident from some carefully selected published articles (1976–2021) that WO_3 has numerous advantages which include narrow bandgap, low cost, stability, and non-toxic. This makes it an ideal candidate for photocatalysis and energy storage applications. We presented discussions on the electronic structure, synthesis methods, strategies for enhancing its photocatalytic activity, and its "round-the-clock photocatalytic" (RTCP) memory. The enhanced photocatalytic efficiency of WO_3-based photocatalysts is attributed to its considerable charge separation and transfer ability as well as large surface area which provides sufficient reaction sites for photocatalytic reaction as well as fast photogenerated charge transfer and separation.

In addition, composites formation through proper synthesis, coatings, deposition, and visible light enhancements strategies was found to be an effective means of enhancing and inducing photogenerated charge separation and transfer to improve photocatalytic performance. It was found that the green synthesis method for WO_3 based photocatalysts has recently been considered as been effective, environmentally friendly, cost-effective, fast, facile, and suitable for the synthesis of new morphologies, however, the hydrothermal method is widely used and from various research found to give photocatalyst with better photoactivity.

Another area considered was the RTCP storage ability of WO_3-based photocatalysts for various environmental applications in the absence of a light source. It was found that only a handful of studies have reported on this area. WO_3 based photocatalysts shows promising results in this area where there is an evolution in the combination of energy storage material (ESM) and visible-light-driven (VLD) performance during photocatalysis.

It was concluded that to achieve better ESS and VLD properties for WO_3-based photocatalysts, there is the need to prevent and inhibit disrupting the mechanism of the system by minimizing or eliminating recombination of charge carriers. It is expected that studies in the future devoted to or targeting other photocatalysts should implement both ESM and VLD for the photocatalyst been studied to develop a photocatalytic technology that is effective and efficient for various environmental applications.

Finally, this review has shown that a properly developed WO_3-based photocatalysts with high visible light absorption and excellent energy storage capacity will have better improved and outstanding prospective application for heat generation (Thermo/pyroelectricity, water evaporation, and near-infrared (NIR) shielding), hydrogen production, water oxidation, CO_2 production, medical-related applications, and energy-related applications (capacitors/Lithium-ion batteries, fuel cells and gas sensors). Therefore, researchers can explore the inherent advantages of WO_3-based catalysts for improved environmental applications.

Declaration of competing interest

The authors declare that they have no known competing financial interests or personal relationships that could have appeared to influence the work reported in this paper.

Acknowledgments

The authors gratefully acknowledge the financial support from the JICA Technical Cooperation Project for ASEAN University Network/ Southeast Asia Engineering Education Development Network (JICA Project for AUN/SEED-Net) via Alumni Support Program for Research (Project number: UTM ASP-R 2101/R.J130000.7309.4B651). The authors also would like to thank the Ministry of Higher Education Malaysia for the funding through the Higher Institution Centre of Excellence Scheme (Project Number: R.J090301.7809.4J430) and Universiti Teknologi Malaysia for the research grant namely the UTM High Impact Research (UTMHIR) (Project number: Q.J130000.2409.08G34) and Industry/International Incentive Grant (IIIG) (Project number: Q. J130000.3609.03M17). The authors would also like to thank the Research Management Centre, Universiti Teknologi Malaysia for technical support. The first author acknowledges the Tertiary Education Trust Fund (tetfund) Nigeria for the scholarship.

References

[1] B.P. Gumbi, B. Moodley, G. Birungi, P.G. Ndungu, Detection and quantification of acidic drug residues in South African surface water using gas chromatography-mass spectrometry, Chemosphere 168 (2017) 1042–1050, https://doi.org/10.1016/j.chemosphere.2016.10.105.

[2] T. Azuma, N. Arima, A. Tsukada, S. Hirami, R. Matsuoka, R. Moriwake, H. Ishiuchi, T. Inoyama, Y. Teranishi, M. Yamaoka, Y. Mino, T. Hayashi, Y. Fujita, M. Masada, Detection of pharmaceuticals and phytochemicals together with their metabolites in hospital effluents in Japan, and their contribution to sewage treatment plant influents, Sci. Total Environ. 548–549 (2016) 189–197, https://doi.org/10.1016/j.scitotenv.2015.12.157.

[3] L.M. Bexfield, P.L. Toccalino, K. Belitz, W.T. Foreman, E.T. Furlong, Hormones and pharmaceuticals in groundwater used as a source of drinking water across the United States, Environ. Sci. Technol. 53 (2019) 2950–2960, https://doi.org/10.1021/acs.est.8b05592.

[4] A.J. Ebele, T. Oluseyi, D.S. Drage, S. Harrad, M. Abou-Elwafa Abdallah, Occurrence, seasonal variation and human exposure to pharmaceuticals and personal care products in surface water, groundwater and drinking water in Lagos State, Nigeria, Emerg. Contam. 6 (2020) 124–132, https://doi.org/10.1016/j.emcon.2020.02.004.

[5] Z. Tousova, P. Oswald, J. Slobodnik, L. Blaha, M. Muz, M. Hu, W. Brack, M. Krauss, C. Di Paolo, Z. Tarcai, T.B. Seiler, H. Hollert, S. Koprivica, M. Ahel, J. E. Schollée, J. Hollender, M.J.F. Suter, A.O. Hidasi, K. Schirmer, M. Sonavane, S. Ait-Aissa, N. Creusot, F. Brion, J. Froment, A.C. Almeida, K. Thomas, K. E. Tollefsen, S. Tufi, X. Ouyang, P. Leonards, M. Lamoree, V.O. Torrens, A. Kolkman, M. Schriks, P. Spirhanzlova, A. Tindall, T. Schulze, European demonstration program on the effect-based and chemical identification and monitoring of organic pollutants in European surface waters, Sci. Total Environ. 601–602 (2017) 1849–1868, https://doi.org/10.1016/j.scitotenv.2017.06.032.

[6] K.H. Kim, E. Kabir, S.A. Jahan, Exposure to pesticides and the associated human health effects, Sci. Total Environ. 575 (2017) 525–535, https://doi.org/10.1016/j.scitotenv.2016.09.009.

[7] O. Mehrpour, P. Karrari, N. Zamani, A.M. Tsatsakis, M. Abdollahi, Occupational exposure to pesticides and consequences on male semen and fertility: a review, Toxicol. Lett. 230 (2014) 146–156, https://doi.org/10.1016/j.toxlet.2014.01.029.

[8] J. Rivero, O.P. Luzardo, L.A. Henríquez-Hernández, R.P. Machín, J. Pestano, M. Zumbado, L.D. Boada, M. Camacho, P.F. Valerón, In vitro evaluation of oestrogenic/androgenic activity of the serum organochlorine pesticide mixtures previously described in a breast cancer case-control study, Sci. Total Environ. 537 (2015) 197–202, https://doi.org/10.1016/j.scitotenv.2015.08.016.

[9] J. Wilker De Oliveira, A. Evald, A. Bezerra De Mira, A. Campos, F. Neto, E. Ferreira, Does calcined bone meal serve as phosphate for pastures in family farming? Farinha de ossos serve como fosfato para pastos na agricultura familiar? (2018) 171–179, https://doi.org/10.15361/1984-5529.2018v46n2p171-179.

[10] N. Zwart, S.L. Nio, C.J. Houtman, J. De Boer, J. Kool, T. Hamers, M.H. Lamoree, High-throughput effect-directed analysis using downscaled in vitro reporter gene assays to identify endocrine disruptors in surface water, Environ. Sci. Technol. 52 (2018) 4367–4377, https://doi.org/10.1021/acs.est.7b06604.

[11] J. Karpińska, U. Kotowska, Removal of organic pollution in the water environment, Water 11 (2019), https://doi.org/10.3390/w11102017, 2017.

[12] N.H. Tran, M. Reinhard, K.Y.H. Gin, Occurrence and fate of emerging contaminants in municipal wastewater treatment plants from different geographical regions-a review, Water Res. 133 (2018) 182–207, https://doi.org/10.1016/j.watres.2017.12.029.

[13] A. Butkovskyi, H. Bruning, S.A.E. Kools, H.H.M. Rijnaarts, A.P. Van Wezel, Organic pollutants in shale gas flowback and produced waters: identification, potential ecological Impact, and implications for treatment strategies, Environ. Sci. Technol. 51 (2017) 4740–4754, https://doi.org/10.1021/acs.est.6b05640.

[14] S. Garcia-Segura, E. Brillas, Applied photoelectrocatalysis on the degradation of organic pollutants in wastewaters, J. Photochem. Photobiol. C Photochem. Rev. 31 (2017) 1–35, https://doi.org/10.1016/j.jphotochemrev.2017.01.005.

[15] S. Jamil, P. Loganathan, J. Kandasamy, A. Listowski, J.A. McDonald, S.J. Khan, S. Vigneswaran, Removal of organic matter from wastewater reverse osmosis concentrate using granular activated carbon and anion exchange resin adsorbent columns in sequence, Chemosphere 261 (2020) 127549, https://doi.org/10.1016/j.chemosphere.2020.127549.

[16] S.J. Varjani, M. Chaithanya Sudha, in: S. Bhattacharya, A.B. Gupta, A. Gupta, A. Pandey (Eds.), Treatment Technologies for Emerging Organic Contaminants Removal from Wastewater BT - Water Remediation, Springer Singapore, Singapore, 2018, pp. 91–115, https://doi.org/10.1007/978-981-10-7551-3_6.

[17] J.H. Carey, J. Lawrence, H.M. Tosine, Photodechlorination of PCB's in the presence of titanium dioxide in aqueous suspensions, Bull. Environ. Contam. Toxicol. 16 (1976) 697–701, https://doi.org/10.1007/BF01685575.

[18] A. Fujishima, K. Honda, Electrochemical photolysis of water at a semiconductor electrode, Nature 238 (1972) 37–38, https://doi.org/10.1038/238037a0.

[19] K. Hashimoto, H. Irie, A. Fujishima, TiO 2 photocatalysis: a historical overview and future prospects, Japanese J. Appl. Physics, Part 1 Regul. Pap. Short Notes Rev. Pap. 44 (2005) 8269–8285, https://doi.org/10.1143/JJAP.44.8269.

[20] K. Okamoto, Y. Yamamoto, H. Tanaka, M. Tanaka, A. Itaya, Heterogeneous photocatalytic decomposition of phenol over TiO 2 powder, Bull. Chem. Soc. Jpn. 58 (1985) 2015–2022, https://doi.org/10.1246/bcsj.58.2015.

[21] B.G. Oliver, E.G. Cosgrove, J.H. Carey, Effect of suspended sediments on the photolysis of organics in water, Environ. Sci. Technol. 13 (1979) 1075–1077, https://doi.org/10.1021/es60157a011.

[22] S. Yamagata, R. Baba, A. Fujishima, Photocatalytic decomposition of 2-ethoxyethanol on titanium dioxide, Bull. Chem. Soc. Jpn. 62 (1989) 1004–1010, https://doi.org/10.1246/bcsj.62.1004.

[23] X. Chen, S.S. Mao, Titanium dioxide nanomaterials:synthesis ,properties , modifications ,and applications, Chem. Rev. 107 (2007) 2891–2959, https://doi.org/10.1021/cr0500535.

[24] C. Liu, L. Wang, Y. Tang, S. Luo, Y. Liu, S. Zhang, Y. Zeng, Y. Xu, Vertical single or few-layer MoS2 nanosheets rooting into TiO2 nanofibers for highly efficient photocatalytic hydrogen evolution, Appl. Catal. B Environ. 164 (2015) 1–9, https://doi.org/10.1016/j.apcatb.2014.08.046.

[25] C.T. Mehmood, Z. Zhong, H. Zhou, Y. Xiao, Constructing porous beads with modified polysulfone-alginate and TiO2 as a robust and recyclable photocatalyst for wastewater treatment, J. Water Process Eng. 38 (2020) 101601, https://doi.org/10.1016/j.jwpe.2020.101601.

[26] X.L. Yang, W.L. Dai, C. Guo, H. Chen, Y. Cao, H. Li, H. He, K. Fan, Synthesis of novel core-shell structured WO3/TiO2 spheroids and its application in the catalytic oxidation of cyclopentene to glutaraldehyde by aqueous H2O2, J. Catal. 234 (2005) 438–450, https://doi.org/10.1016/j.jcat.2005.06.035.

[27] M. Liu, H. Li, Y. Zeng, Facile preparation of efficient WOphotocatalysts based on surface modification, J. Nanomater. (2015), https://doi.org/10.1155/2015/502514, 2015.

[28] X. He, A. Wang, P. Wu, S. Tang, Y. Zhang, L. Li, P. Ding, Photocatalytic degradation of microcystin-LR by modified TiO2 photocatalysis: a review, Sci. Total Environ. 743 (2020), https://doi.org/10.1016/j.scitotenv.2020.140694.

[29] L. Yanyan, T.A. Kurniawan, Z. Ying, A.B. Albadarin, G. Walker, Enhanced photocatalytic degradation of acetaminophen from wastewater using WO3/TiO2/SiO2 composite under UV–VIS irradiation, J. Mol. Liq. 243 (2017) 761–770, https://doi.org/10.1016/j.molliq.2017.08.092.

[30] V. Dutta, S. Sharma, P. Raizada, V.K. Thakur, A.A.P. Khan, V. Saini, A.M. Asiri, P. Singh, An overview on WO3based photocatalyst for environmental remediation, J. Environ. Chem. Eng. 9 (2021) 105018, https://doi.org/10.1016/j.jece.2020.105018.

[31] M. Humayun, F. Raziq, A. Khan, W. Luo, Modification strategies of TiO2 for potential applications in photocatalysis: a critical review, Green Chem. Lett. Rev. Chem. Lett. Rev. 11 (2018) 86–102, https://doi.org/10.1080/17518253.2018.1440324.

[32] P. Mazierski, A. Mikolajczyk, B. Bajorowicz, A. Malankowska, A. Zaleska-Medynska, J. Nadolna, The role of lanthanides in TiO2-based photocatalysis: a review, Appl. Catal. B Environ. 233 (2018) 301–317, https://doi.org/10.1016/j.apcatb.2018.04.019.

[33] M. Miyauchi, H. Irie, M. Liu, X. Qiu, H. Yu, K. Sunada, K. Hashimoto, Visible-light-sensitive photocatalysts: nanocluster-grafted titanium dioxide for indoor environmental remediation, J. Phys. Chem. Lett. 7 (2016) 75–84, https://doi.org/10.1021/acs.jpclett.5b02041.

[34] A. Truppi, F. Petronella, T. Placido, M. Striccoli, A. Agostiano, M.L. Curri, R. Comparelli, Visible-light-active TiO2-based hybrid nanocatalysts for environmental applications, Catalysts 7 (2017), https://doi.org/10.3390/catal7040100.

[35] C. Liu, H. Lü, C. Yu, B. Ding, R. Ye, Y. Ji, B. Dai, W. Liu, Novel FeWO4/WO3nanoplate with p-n heterostructure and its enhanced mechanism for organic pollutants removal under visible-light illumination, J. Environ. Chem. Eng. 8 (2020) 104044, https://doi.org/10.1016/j.jece.2020.104044.

[36] Y. Yu, S. Wu, J. Gu, R. Liu, Z. Wang, H. Chen, F. Jiang, Visible-light photocatalytic degradation of bisphenol A using cobalt-to-oxygen doped graphitic carbon nitride

with nitrogen vacancies via metal-to-ligand charge transfer, J. Hazard Mater. 384 (2020) 121247, https://doi.org/10.1016/j.jhazmat.2019.121247.
[37] P. Gao, Z. Yin, L. Feng, Y. Liu, Z. Du, Z. Duan, L. Zhang, Solvothermal synthesis of multiwall carbon nanotubes/BiOI photocatalysts for the efficient degradation of antipyrine under visible light, Environ. Res. 185 (2020), https://doi.org/10.1016/j.envres.2020.109468, 109468.
[38] B.O. Orimolade, B.A. Koiki, B.N. Zwane, G.M. Peleyeju, N. Mabuba, O.A. Arotiba, Interrogating solar photoelectrocatalysis on an exfoliated graphite-BiVO4/ZnO composite electrode towards water treatment, RSC Adv. 9 (2019) 16586–16595, https://doi.org/10.1039/c9ra02366f.
[39] K.V.M.M. Naik, H.B. Naik, G. Nagaraju, M. Vinuth, H.R. Naika, Green synthesis of zinc ferrite nanoparticles in Limonia acidissima juice: characterization and their application as photocatalytic and antibacterial activities, Microchem. J. 146 (2019) 1227–1235.
[40] S. Mandal, S. Natarajan, A. Tamilselvi, S. Mayadevi, Photocatalytic and antimicrobial activities of zinc ferrite nanoparticles synthesized through soft chemical route: a magnetically recyclable catalyst for water/wastewater treatment, J. Environ. Chem. Eng. 4 (2016) 2706–2712, https://doi.org/10.1016/j.jece.2016.05.020.
[41] E. Skliri, J. Miao, J. Xie, G. Liu, T. Salim, B. Liu, Q. Zhang, G.S. Armatas, Assembly and photochemical properties of mesoporous networks of spinel ferrite nanoparticles for environmental photocatalytic remediation, Appl. Catal. B Environ. 227 (2018) 330–339, https://doi.org/10.1016/j.apcatb.2018.01.045.
[42] C. Regmi, Y.K. Kshetri, T.H. Kim, R.P. Pandey, S.W. Lee, Visible-light-induced Fe-doped BiVO4 photocatalyst for contaminated water treatment, Mol. Catal. 432 (2017) 220–231, https://doi.org/10.1016/j.mcat.2017.02.004.
[43] B.O. Orimolade, B.N. Zwane, B.A. Koiki, L. Tshwenya, G.M. Peleyeju, N. Mabuba, M. Zhou, O.A. Arotiba, Solar photoelectrocatalytic degradation of ciprofloxacin at a FTO/BiVO4/MnO2 anode: kinetics, intermediate products and degradation pathway studies, J. Environ. Chem. Eng. 8 (2020), https://doi.org/10.1016/j.jece.2019.103607.
[44] Y. Lu, Y. Zhao, J. Zhao, Y. Song, Z. Huang, F. Gao, N. Li, Y. Li, Photoactive β-Bi2O3 architectures prepared by a simple solution crystallization method, Ceram. Int. 40 (2014) 15057–15063, https://doi.org/10.1016/j.ceramint.2014.06.113.
[45] L. Zhang, Y. Shi, Z. Wang, C. Hu, B. Shi, X. Cao, Porous β-Bi2O3 with multiple vacancy associates on highly exposed active {220} facets for enhanced photocatalytic activity, Appl. Catal. B Environ. 265 (2020) 118563, https://doi.org/10.1016/j.apcatb.2019.118563.
[46] C. Yu, H. He, X. Liu, J. Zeng, Z. Liu, Novel SiO2 nanoparticle-decorated BiOCl nanosheets exhibiting high photocatalytic performances for the removal of organic pollutants, Chinese J. Catal. 40Yu, C. (2019) 1212–1221, https://doi.org/10.1016/S1872-2067(19)63359-0.
[47] Q. Zhang, H. Wang, Z. Li, C. Geng, J. Leng, Metal-free photocatalyst with visible-light-driven post-illumination catalytic memory, ACS Appl. Mater. Interfaces 9 (2017) 21738–21746, https://doi.org/10.1021/acsami.7b02473.
[48] B.A. Koiki, B.O. Orimolade, G.M. Peleyeju, O.A. Arotiba, Rapid and template-free synthesis of copper(I) oxide-graphitic carbon nitride heterojunction for photocatalytic degradation of orange II dye in water, Solid State Sci. 97 (2019) 105994, https://doi.org/10.1016/j.solidstatesciences.2019.105994.
[49] N.D. Khiavi, R. Katal, S.K. Eshkalak, S. Masudy-Panah, S. Ramakrishna, H. Jiangyong, Visible light driven heterojunction photocatalyst of cuo-cu2o thin films for photocatalytic degradation of organic pollutants, Nanomaterials 9 (2019), https://doi.org/10.3390/nano9071011.
[50] J. Di, J. Xia, M. Ji, B. Wang, S. Yin, Q. Zhang, Z. Chen, H. Li, Advanced photocatalytic performance of graphene-like BN modified BiOBr flower-like materials for the removal of pollutants and mechanism insight, Appl. Catal. B Environ. 183 (2016) 254–262, https://doi.org/10.1016/j.apcatb.2015.10.036.
[51] J. Xu, W. Meng, Y. Zhang, L. Li, C. Guo, Photocatalytic degradation of tetrabromobisphenol A by mesoporous BiOBr: efficacy, products and pathway, Appl. Catal. B Environ. 107 (2011) 355–362, https://doi.org/10.1016/j.apcatb.2011.07.036.
[52] G.M. Peleyeju, E.H. Umukoro, J.O. Babalola, O.A. Arotiba, Solar-light-responsive titanium-sheet-based carbon nanoparticles/B-BiVO4/WO3 photoanode for the photoelectrocatalytic degradation of orange II dye water pollutant, ACS Omega 5 (2020) 4743–4750, https://doi.org/10.1021/acsomega.9b02148.
[53] E.H. Umukoro, M.G. Peleyeju, J.C. Ngila, O.A. Arotiba, Towards wastewater treatment: photo-assisted electrochemical degradation of 2-nitrophenol and orange II dye at a tungsten trioxide-exfoliated graphite composite electrode, Chem. Eng. J. 317 (2017) 290–301, https://doi.org/10.1016/j.cej.2017.02.084.
[54] X. Li, K. Yang, C. Yu, K. Zhang, S. Yang, L. Zhu, H. Ji, W. Dai, Q. Fan, W. Huang, Broadband photocatalysis using a Z-scheme heterojunction of Au/NaYF4:Yb,Er/WO3·0.33H2O-W18O49via a synergetic strategy of upconversion function and plasmonic effect, Inorg. Chem. Front. 6 (2019) 3158–3167, https://doi.org/10.1039/C9QI00823C.
[55] C. Yu, F. Chen, D. Zeng, Y. Xie, W. Zhou, Z. Liu, L. Wei, K. Yang, D. Li, A facile phase transformation strategy for fabrication of novel Z-scheme ternary heterojunctions with efficient photocatalytic properties, Nanoscale 11 (2019) 7720–7733, https://doi.org/10.1039/C9NR00709A.
[56] D. Zeng, K. Yang, C. Yu, F. Chen, X.X. Li, Z. Wu, H. Liu, Phase transformation and microwave hydrothermal guided a novel double Z-scheme ternary vanadate heterojunction with highly efficient photocatalytic performance, Appl. Catal. B Environ. 237 (2018) 449–463, https://doi.org/10.1016/j.apcatb.2018.06.010.
[57] D. Zeng, C. Yu, Q. Fan, J. Zeng, L. Wei, Z. Li, K. Yang, H. Ji, Theoretical and experimental research of novel fluorine doped hierarchical Sn3O4 microspheres with excellent photocatalytic performance for removal of Cr(VI) and organic pollutants, Chem. Eng. J. 391 (2020) 123607, https://doi.org/10.1016/j.cej.2019.123607.
[58] J. Zhou, Y. Ding, S.Z. Deng, L. Gong, N.S. Xu, Z.L. Wang, Three-dimensional tungsten oxide nanowire networks, Adv. Mater. 17 (2005) 2107–2110, https://doi.org/10.1002/adma.200500885.
[59] D. Chen, L. Gao, A. Yasumori, K. Kuroda, Y. Sugahara, Size- and shape-controlled conversion of tungstate-based inorganic–organic hybrid belts to WO3 nanoplates with high specific surface areas, Small 4 (2008) 1813–1822, https://doi.org/10.1002/smll.200800205.
[60] G. Xi, Y. Yan, Q. Ma, J. Li, H. Yang, X. Lu, C. Wang, Synthesis of multiple-shell WO 3 hollow spheres by a binary carbonaceous template route and their applications in visible-light photocatalysis, Chem. Eur J. 18 (2012) 13949–13953, https://doi.org/10.1002/chem.201202312.
[61] A.G. Acedo-Mendoza, A. Infantes-Molina, D. Vargas-Hernández, C.A. Chávez-Sánchez, E. Rodríguez-Castellón, J.C. Tánori-Córdova, Photodegradation of methylene blue and methyl orange with CuO supported on ZnO photocatalysts: the effect of copper loading and reaction temperature, Mater. Sci. Semicond. Process. 119 (2020), https://doi.org/10.1016/j.mssp.2020.105257.
[62] P. Dong, G. Hou, X. Xi, R. Shao, F. Dong, WO3-based photocatalysts: morphology control, activity enhancement and multifunctional applications, Environ. Sci. Nano. 4 (2017) 539–557, https://doi.org/10.1039/C6EN00478D.
[63] J. Theerthagiri, S. Chandrasekaran, S. Salla, V. Elakkiya, R.A. Senthil, P. Nithyadharseni, T. Maiyalagan, K. Micheal, A. Ayeshamariam, M.V. Arasu, N. A. Al-Dhabi, H.S. Kim, Recent developments of metal oxide based heterostructures for photocatalytic applications towards environmental remediation, J. Solid State Chem. 267 (2018) 35–52, https://doi.org/10.1016/j.jssc.2018.08.006.
[64] C. Janáky, K. Rajeshwar, N.R. De Tacconi, W. Chanmanee, M.N. Huda, Tungsten-based oxide semiconductors for solar hydrogen generation, Catal. Today 199 (2013) 53–64, https://doi.org/10.1016/j.cattod.2012.07.020.
[65] H. Quan, Y. Gao, W. Wang, Tungsten oxide-based visible light-driven photocatalysts: crystal and electronic structures and strategies for photocatalytic efficiency enhancement, Inorg. Chem. Front. 7 (2020) 817–838, https://doi.org/10.1039/c9qi01516g.
[66] P.Q. Wang, Y. Bai, P.Y. Luo, J.Y. Liu, Graphene-WO3 nanobelt composite: elevated conduction band toward photocatalytic reduction of CO2 into hydrocarbon fuels, Catal. Commun. 38 (2013) 82–85, https://doi.org/10.1016/j.catcom.2013.04.020.
[67] Z. Zhu, W.R. Huang, C.Y. Chen, R.J. Wu, Preparation of Pd-Au/TiO2-WO3 to enhance photoreduction of CO2 to CH4 and CO, J. CO2 Util. 28 (2018) 247–254, https://doi.org/10.1016/j.jcou.2018.10.006.
[68] V. Lokhande, A. Lokhande, G. Namkoong, J.H. Kim, T. Ji, Charge storage in WO 3 polymorphs and their application as supercapacitor electrode material, Results Phys 12 (2019) 2012–2020, https://doi.org/10.1016/j.rinp.2019.02.012.
[69] S. Pokhrel, J. Birkenstock, A. Dianat, J. Zimmermann, M. Schowalter, A. Rosenauer, L.C. Ciacchi, L. Mädler, In situ high temperature X-ray diffraction, transmission electron microscopy and theoretical modeling for the formation of WO3 crystallites, CrystEngComm 17 (2015) 6985–6998, https://doi.org/10.1039/c5ce00526d.
[70] Y. Li, Z. Tang, J. Zhang, Z. Zhang, Defect engineering of air-treated WO3 and its enhanced visible-light-driven photocatalytic and electrochemical performance, J. Phys. Chem. C 120 (2016) 9750–9763, https://doi.org/10.1021/acs.jpcc.6b00457.
[71] S. Li, S. Hu, W. Jiang, J. Zhang, K. Xu, Z. Wang, In situ construction of WO3 nanoparticles decorated Bi2MoO6 microspheres for boosting photocatalytic degradation of refractory pollutants, J. Colloid Interface Sci. 556 (2019) 335–344, https://doi.org/10.1016/j.jcis.2019.08.077.
[72] J.Y. Zheng, G. Song, J. Hong, T.K. Van, A.U. Pawar, D.Y. Kim, C.W. Kim, Z. Haider, Y.S. Kang, Facile fabrication of WO3 nanoplates thin films with dominant crystal facet of (002) for water splitting, Cryst. Growth Des. 14 (2014) 6057–6066, https://doi.org/10.1021/cg5012154.
[73] D. Tanaka, Y. Oaki, H. Imai, Enhanced photocatalytic activity of quantum-confined tungsten trioxide nanoparticles in mesoporous silica, Chem. Commun. 46 (2010) 5286–5288, https://doi.org/10.1039/c0cc00540a.
[74] A.M. Smith, S. Nie, Semiconductor nanocrystals: structure, properties, and band gap engineering, Acc. Chem. Res. 43 (2010) 190–200, https://doi.org/10.1021/ar9001069.
[75] M. Rozman, B. Žener, L. Matoh, R.F. Godec, A. Mourtzikou, E. Stathatos, U. Bren, M. Lukšič, Flexible electrochromic tape using steel foil with WO3 thin film, Electrochim. Acta 330 (2020), https://doi.org/10.1016/j.electacta.2019.135329.
[76] Y. Zhao, G. Brocks, H. Genuit, R. Lavrijsen, M.A. Verheijen, A. Bieberle-Hütter, Boosting the performance of WO3/n-Si heterostructures for photoelectrochemical water splitting: from the role of Si to interface engineering, Adv. Energy Mater. 9 (2019) 1900940, https://doi.org/10.1002/aenm.201900940.
[77] S. Bhandari, A. Roy, A. Ghosh, T.K. Mallick, S. Sundaram, Performance of WO3-incorporated carbon electrodes for ambient mesoscopic perovskite solar cells, ACS Omega 5 (2020) 422–429, https://doi.org/10.1021/acsomega.9b02934.
[78] B. Ahmed, A.K. Ojha, A. Singh, F. Hirsch, I. Fischer, D. Patrice, A. Materny, Well-controlled in-situ growth of 2D WO3 rectangular sheets on reduced graphene oxide with strong photocatalytic and antibacterial properties, J. Hazard Mater. 347 (2018) 266–278, https://doi.org/10.1016/j.jhazmat.2017.12.069.
[79] C. Dong, R. Zhao, L. Yao, Y. Ran, X. Zhang, Y. Wang, A review on WO3 based gas sensors: morphology control and enhanced sensing properties, J. Alloys Compd. 820 (2020) 153194, https://doi.org/10.1016/j.jallcom.2019.153194.
[80] C. Xie, W. Chen, S. Du, D. Yan, Y. Zhang, J. Chen, B. Liu, S. Wang, In-situ phase transition of WO3 boosting electron and hydrogen transfer for enhancing

hydrogen evolution on Pt, Nanomater. Energy 71 (2020) 104653, https://doi.org/10.1016/j.nanoen.2020.104653.
[81] S. Adhikari, K. Sarath Chandra, D.H. Kim, G. Madras, D. Sarkar, Understanding the morphological effects of WO3 photocatalysts for the degradation of organic pollutants, Adv. Powder Technol. 29 (2018) 1591–1600, https://doi.org/10.1016/j.apt.2018.03.024.
[82] P.A. Shinde, S.C. Jun, Review on recent progress in the development of tungsten oxide based electrodes for electrochemical energy storage, ChemSusChem 13 (2020) 11–38, https://doi.org/10.1002/cssc.201902071.
[83] D.B. Migas, V.L. Shaposhnikov, V.N. Rodin, V.E. Borisenko, Tungsten oxides. I. Effects of oxygen vacancies and doping on electronic and optical properties of different phases of WO3, J. Appl. Phys. 108 (2010) 93713, https://doi.org/10.1063/1.3505688.
[84] C. Di Valentin, F. Wang, G. Pacchioni, Tungsten oxide in catalysis and photocatalysis: hints from DFT, Top. Catal. 56 (2013) 1404–1419, https://doi.org/10.1007/s11244-013-0147-6.
[85] F. Wang, C. Di Valentin, G. Pacchioni, Electronic and structural properties of WO3: a systematic hybrid DFT study, J. Phys. Chem. C 115 (2011) 8345–8353, https://doi.org/10.1021/jp201057m.
[86] M. Fakhari, M.J. Torkamany, S.N. Mirnia, S.M. Elahi, UV-visible light-induced antibacterial and photocatalytic activity of half harmonic generator WO3 nanoparticles synthesized by Pulsed Laser Ablation in water, Opt. Mater. 85 (2018) 491–499, https://doi.org/10.1016/j.optmat.2018.09.023.
[87] J. Zhang, Y. Ma, Y. Du, H. Jiang, D. Zhou, S. Dong, Carbon nanodots/WO3nanorods Z-scheme composites: remarkablyenhanced photocatalytic performance under broad spectrum, Appl. Catal., B 209 (2017) 253–264.
[88] Z.G. Zhao, M. Miyauchi, Nanoporous-walled tungsten oxide nanotubes as highly active visible-light-driven photocatalysts, Angew. Chem. Int. Ed. 47 (2008) 7051–7055, https://doi.org/10.1002/anie.200802207.
[89] Y.M. Hunge, Sunlight assisted photoelectrocatalytic degradation of benzoic acid using stratified WO3/TiO2 thin films, Ceram. Int. 43 (2017) 10089–10096, https://doi.org/10.1016/j.ceramint.2017.05.028.
[90] F. Riboni, D. Mv, P. Mc, E. Giamello, E. Selli, Photocatalytic activity of TiO2-WO3 mixed oxides in formic acid oxidation, Catal. Today 287 (2017) 176–181, https://doi.org/10.1016/j.cattod.2016.12.031.
[91] Z.-G.Z, M. Miyauchi, Nanoporous-Walled Tungsten Oxide Nanotubes as Highly Active, 2008, pp. 7051–7055, https://doi.org/10.1002/anie.200802207.
[92] B. Weng, J. Wu, N. Zhang, Y.-J. Xu, Observing the role of graphene in boosting the two-electron reduction of oxygen in graphene–WO3 nanorod photocatalysts, Langmuir 30 (2014) 5574–5584, https://doi.org/10.1021/la4048566.
[93] T. Nagyné-Kovács, I.E. Lukács, A. Szabó, K. Hernadi, T. Igricz, K. László, I. M. Szilágyi, G. Pokol, Effect of pH in the hydrothermal preparation of monoclinic tungsten oxide, J. Solid State Chem. 281 (2020) 1–7, https://doi.org/10.1016/j.jssc.2019.121044.
[94] T. Paik, M. Cargnello, T.R. Gordon, S. Zhang, H. Yun, J.D. Lee, H.Y. Woo, S.J. Oh, C.R. Kagan, P. Fornasiero, C.B. Murray, Photocatalytic hydrogen evolution from substoichiometric colloidal WO3–x nanowires, ACS Energy Lett 3 (2018) 1904–1910, https://doi.org/10.1021/acsenergylett.8b00925.
[95] G. Hai, J. Huang, L. Cao, Y. Jie, J. Li, X. Wang, G. Zhang, Influence of oxygen deficiency on the synthesis of tungsten oxide and the photocatalytic activity for the removal of organic dye, J. Alloys Compd. 690 (2017) 239–248, https://doi.org/10.1016/j.jallcom.2016.08.099.
[96] N. Zhang, C. Chen, Z. Mei, X. Liu, X. Qu, Y. Li, S. Li, W. Qi, Y. Zhang, J. Ye, V.A. L. Roy, R. Ma, Monoclinic tungsten oxide with {100} facet orientation and tuned electronic band structure for enhanced photocatalytic oxidations, ACS Appl. Mater. Interfaces 8 (2016) 10367–10374, https://doi.org/10.1021/acsami.6b02275.
[97] G. Zhang, K. Lu, X. Zhang, W. Yuan, M. Shi, H. Ning, R. Tao, X. Liu, R. Yao, J. Peng, Effects of annealing temperature on optical band gap of sol-gel tungsten trioxide films, Micromachines 9 (2018), https://doi.org/10.3390/mi9080377.
[98] S.S. Kaplan, M.S. Sonmez, Single step solution combustion synthesis of hexagonal WO3 powders as visible light photocatalysts, Mater. Chem. Phys. 240 (2020) 122152, https://doi.org/10.1016/j.matchemphys.2019.122152.
[99] S.S. Kalanur, I.H. Yoo, I.S. Cho, H. Seo, Niobium incorporated WO 3 nanotriangles: band edge insights and improved photoelectrochemical water splitting activity, Ceram. Int. 45 (2019) 8157–8165, https://doi.org/10.1016/j.ceramint.2019.01.117.
[100] M.B. Tahir, M. Sagir, M. Zubair, M. Rafique, I. Abbas, M. Shakil, I. Khan, S. Afsheen, A. Hasan, A. Ahmed, WO3 nanostructures-based photocatalyst approach towards degradation of RhB dye, J. Inorg. Organomet. Polym. Mater. 28 (2018) 1107–1113, https://doi.org/10.1007/s10904-017-0771-x.
[101] Y. Gu, Q. Zhuo, D. Wu, Large-mesopore hierarchical tungsten trioxide hydrate with exposed high energy facets: facile synthesis and enhanced photocatalysis, Mater. Sci. Semicond. Process. 53 (2016) 18–27, https://doi.org/10.1016/j.mssp.2016.05.016.
[102] T. Harada, E. Yagi, S. Ikeda, Synthesis of nano-sized tungsten oxide particles encapsulated in a hollow silica sphere and their photocatalytic properties for decomposition of acetic acid using Pt as a co-catalyst, RSC Adv. 10 (2020) 15360–15365, https://doi.org/10.1039/d0ra01988g.
[103] R. Wang, W. Zhang, W. Zhu, L. Yan, S. Li, K. Chen, N. Hu, Y. Suo, J. Wang, Enhanced visible-light-driven photocatalytic sterilization of tungsten trioxide by surface-engineering oxygen vacancy and carbon matrix, Chem. Eng. J. 348 (2018) 292–300, https://doi.org/10.1016/j.cej.2018.05.010.
[104] L.W. N, Z. Lu, Y. Zhang, B. Wang, L. Liu, K.L Guo, B.D.J. Huang, Direct evidence of IR-driven hot electron transfer in metal-free plasmonic W18O49/Carbon heterostructures for enhanced catalytic H2 production, Appl. Catal., B 233 (2018) 19–25.
[105] T. Zhu, M.N. Chong, E.S. Chan, Nanostructured tungsten trioxide thin films synthesized for photoelectrocatalytic water oxidation: a review, ChemSusChem 7 (2014) 2974–2997, https://doi.org/10.1002/cssc.201402089.
[106] W. Gu, W. Wang, G. Li, H. Xie, P.K. Wong, T. An, Microwave-assisted synthesis of defective tungsten trioxide for photocatalytic bacterial inactivation: role of the oxygen vacancy, Chin. J. Catal. 41 (2020) 1488–1497, https://doi.org/10.1016/S1872-2067(19)63409-1.
[107] K. Shahzad, M.B. Tahir, M. Ashraf, T. Nawaz, N.R. Khalid, M.R. Kabli, Interfacial growth of activated carbon on WO3 nanoplates for enhanced photocatalytic activity by surface plasmon resonance, Plasmonics 15 (2020) 1205–1212, https://doi.org/10.1007/s11468-020-01135-5.
[108] H. Zheng, J.Z. Ou, M.S. Strano, R.B. Kaner, A. Mitchell, K. Kalantar-Zadeh, Nanostructured tungsten oxide - properties, synthesis, and applications, Adv. Funct. Mater. 21 (2011) 2175–2196, https://doi.org/10.1002/adfm.201002477.
[109] M.A. Butler, R.D. Nasby, R.K. Quinn, Tungsten trioxide as an electrode for photoelectrolysis of water, Solid State Commun. 19 (1976) 1011–1014, https://doi.org/10.1016/0038-1098(76)90642-6.
[110] H.G. Choi, Y.H. Jung, D.K. Kim, Solvothermal synthesis of tungsten oxide nanorod/nanowire/nanosheet, J. Am. Ceram. Soc. 88 (2005) 1684–1686, https://doi.org/10.1111/j.1551-2916.2005.00341.x.
[111] N.A. Mohd Razali, W.N. Wan Salleh, F. Aziz, L.W. Jye, N. Yusof, A.F. Ismail, Review on tungsten trioxide as a photocatalysts for degradation of recalcitrant pollutants, J. Clean. Prod. 309 (2021) 127438, https://doi.org/10.1016/j.jclepro.2021.127438.
[112] J. Li, X. Liu, J. Cui, J. Sun, Hydrothermal synthesis of self-assembled hierarchical tungsten oxides hollow spheres and their gas sensing properties, ACS Appl. Mater. Interfaces 7 (2015) 10108–10114, https://doi.org/10.1021/am508121p.
[113] C.M. Wu, S. Naseem, M.H. Chou, J.H. Wang, Y.Q. Jian, Recent advances in tungsten-oxide-based materials and their applications, Front. Mater. 6 (2019) 1–17, https://doi.org/10.3389/fmats.2019.00049.
[114] J. Narang, C. Singhal, M. Khanuja, A. Mathur, A. Jain, C.S. Pundir, Hydrothermally synthesized zinc oxide nanorods incorporated on lab-on-paper device for electrochemical detection of recreational drug, Artif. Cells, Nanomedicine Biotechnol 46 (2018) 1586–1593, https://doi.org/10.1080/21691401.2017.1381614.
[115] C. Prasad, X. Yang, Q. Liu, H. Tang, A. Rammohan, S. Zulfiqar, G.V. Zyryanov, S. Shah, Recent advances in MXenes supported semiconductors based photocatalysts: properties, synthesis and photocatalytic applications, J. Ind. Eng. Chem. 85 (2020) 1–33, https://doi.org/10.1016/j.jiec.2019.12.003.
[116] S.A. Akbar, R. Zou, C.-M. Wu, S. Naseem, M.-H. Chou, J.-H. Wang, Y.-Q. Jian, Recent advances in tungsten-oxide-based materials and their applications, Front. Mater. 49 (2019), https://doi.org/10.3389/fmats.2019.00049. Www.Frontiersin.Org. 1.
[117] X. Wu, J. Wang, G. Zhang, K. ichi Katsumata, K. Yanagisawa, T. Sato, S. Yin, Series of MxWO3/ZnO (M = K, Rb, NH4) nanocomposites: combination of energy saving and environmental decontamination functions, Appl. Catal. B Environ. 201 (2017) 128–136, https://doi.org/10.1016/j.apcatb.2016.08.030.
[118] T. Okusako, T. Tokuyama, K. Mikami, Y. Nogami, N. Hanasaki, Thermoelectric effect in hexagonal tungsten oxides, J. Phys. Soc. Japan. 81 (2012) 2–5, https://doi.org/10.1143/JPSJS.81SB.SB028.
[119] H.F. Pang, X. Xiang, Z.J. Li, Y.Q. Fu, X.T. Zu, Hydrothermal synthesis and optical properties of hexagonal tungsten oxide nanocrystals assisted by ammonium tartrate, Phys. Status Solidi Appl. Mater. Sci. 209 (2012) 537–544, https://doi.org/10.1002/pssa.201127456.
[120] G. Li, J. Hou, W. Zhang, P. Li, G. Liu, Y. Wang, K. Wang, Graphene-bridged WO3/MoS2 Z-scheme photocatalyst for enhanced photodegradation under visible light irradiation, Mater. Chem. Phys. 246 (2020) 122827, https://doi.org/10.1016/j.matchemphys.2020.122827.
[121] X. Yao, X. Liu, One-pot synthesis of ternary Ag2CO3/Ag/AgCl photocatalyst in natural geothermal water with enhanced photocatalytic activity under visible light irradiation, J. Hazard Mater. 280 (2014) 260–268, https://doi.org/10.1016/j.jhazmat.2014.07.079.
[122] Y. Li, L. Fang, R. Jin, Y. Yang, X. Fang, Y. Xing, S. Song, Preparation and enhanced visible light photocatalytic activity of novel g-C3N4 nanosheets loaded with Ag2CO3 nanoparticles, Nanoscale 7 (2015) 758–764, https://doi.org/10.1039/c4nr06565d.
[123] M. Yan, Y. Wu, F. Zhu, Y. Hua, W. Shi, The fabrication of a novel Ag3VO4/WO3 heterojunction with enhanced visible light efficiency in the photocatalytic degradation of TC, Phys. Chem. Chem. Phys. 18 (2016) 3308–3315, https://doi.org/10.1039/C5CP05599G.
[124] M. Gao, L. You, L. Guo, T. Li, Fabrication of a novel polyhedron-like WO 3/Ag 2 CO 3 p-n junction photocatalyst with highly enhanced photocatalytic activity, J. Photochem. Photobiol. Chem. 374 (2019) 206–217, https://doi.org/10.1016/j.jphotochem.2019.01.022.
[125] P. Hu, Y. Chen, Y. Chen, Z. Lin, Z. Wang, Hydrothermal synthesis and photocatalytic properties of WO3 nanorods by using capping agent SnCl4·5H2O, Phys. E Low-Dimensional Syst. Nanostructures 92 (2017) 12–16, https://doi.org/10.1016/j.physe.2017.05.004.
[126] B. Bhuyan, B. Paul, S.S. Dhar, S. Vadivel, Facile hydrothermal synthesis of ultrasmall W18O49 nanoparticles and studies of their photocatalytic activity towards degradation of methylene blue, Mater. Chem. Phys. 188 (2017) 1–7, https://doi.org/10.1016/j.matchemphys.2016.12.035.
[127] J.X. Liu, X.L. Dong, X.W. Liu, F. Shi, S. Yin, T. Sato, Solvothermal synthesis and characterization of tungsten oxides with controllable morphology and crystal

phase, J. Alloys Compd. 509 (2011) 1482–1488, https://doi.org/10.1016/j.jallcom.2010.10.052.
[128] J. Wei, X. Wen, F. Zhu, Influence of surfactant on the morphology and photocatalytic activity of anatase TiO2 by solvothermal synthesis, J. Nanomater. (2018), https://doi.org/10.1155/2018/3086269, 2018.
[129] S. Prabhu, L. Cindrella, O.J. Kwon, K. Mohanraju, Photoelectrochemical and photocatalytic activity of TiO2-WO3 heterostructures boosted by mutual interaction, Mater. Sci. Semicond. Process. 88 (2018) 10–19, https://doi.org/10.1016/j.mssp.2018.07.028.
[130] K. Anandan, V. Rajendran, Morphological and size effects of NiO nanoparticles via solvothermal process and their optical properties, Mater. Sci. Semicond. Process. 14 (2011) 43–47, https://doi.org/10.1016/j.mssp.2011.01.001.
[131] G.S. Kamble, Y.C. Ling, Solvothermal synthesis of facet-dependent BiVO4 photocatalyst with enhanced visible-light-driven photocatalytic degradation of organic pollutant: assessment of toxicity by zebrafish embryo, Sci. Rep. 10 (2020) 1–11, https://doi.org/10.1038/s41598-020-69706-4.
[132] H. Li, Y. Chen, W. Zhou, H. Jiang, H. Liu, X. Chen, T. Guohui, WO3/BiVO4/BiOCl porous nanosheet composites from a biomass template for photocatalytic organic pollutant degradation, J. Alloys Compd. 802 (2019) 76–85, https://doi.org/10.1016/j.jallcom.2019.06.187.
[133] Y. Fan, X. Xi, Y. Liu, Z. Nie, Q. Zhang, L. Zhao, Growth mechanism of immobilized WO3 nanostructures in different solvents and their visible-light photocatalytic performance, J. Phys. Chem. Solid. 140 (2020) 109380, https://doi.org/10.1016/j.jpcs.2020.109380.
[134] Y. Xiao, Z. He, R. Wang, X. Tao, B. Li, Synthesis of WO3 nanofibers decorated with BiOCl nanosheets for photocatalytic degradation of organic pollutants under visible light, Colloids Surfaces A Physicochem. Eng. Asp. 580 (2019) 123752, https://doi.org/10.1016/j.colsurfa.2019.123752.
[135] Y. Wu, Y. Wei, Q. Guo, H. Xu, L. Gu, F. Huang, D. Luo, Y. Huang, L. Fan, J. Wu, Solvothermal fabrication of La-WO3/SrTiO3 heterojunction with high photocatalytic performance under visible light irradiation, Sol. Energy Mater. Sol. Cells 176 (2018) 230–238, https://doi.org/10.1016/j.solmat.2017.12.005.
[136] Katarzyna Siwińska-Stefańska, T. Jesionowski, Advanced hybrid materials based on titanium dioxide for environmental and electrochemical applications, in: Magdal. Janus, IntechOpen, 2017. https://www.intechopen.com/books/advanced-biometric-technologies/liveness-detection-in-biometrics.
[137] A. Rani, R. Reddy, U. Sharma, P. Mukherjee, P. Mishra, A. Kuila, L.C. Sim, P. Saravanan, A Review on the Progress of Nanostructure Materials for Energy Harnessing and Environmental Remediation, Springer Berlin Heidelberg, 2018, https://doi.org/10.1007/s40097-018-0278-1.
[138] J.I. Velasco, M. Ardanuy, M. Antunes, Layered double hydroxides (LDHs) as functional fillers in polymer nanocomposites, in: Adv. Polym. Nanocomposites Types Appl., Elsevier Inc., 2012, pp. 91–130, https://doi.org/10.1533/9780857096241.1.91.
[139] L. Anju Chanu, W. Joychandra Singh, K. Jugeshwar Singh, K. Nomita Devi, Effect of operational parameters on the photocatalytic degradation of Methylene blue dye solution using manganese doped ZnO nanoparticles, Results Phys 12 (2019) 1230–1237, https://doi.org/10.1016/j.rinp.2018.12.089.
[140] K. Talukdar, B.M. Jun, Y. Yoon, Y. Kim, A. Fayyaz, C.M. Park, Novel Z-scheme Ag3PO4/Fe3O4-activated biochar photocatalyst with enhanced visible-light catalytic performance toward degradation of bisphenol A, J. Hazard Mater. 398 (2020) 123025, https://doi.org/10.1016/j.jhazmat.2020.123025.
[141] N.G. Yadav, L.S. Chaudhary, P.A. Sakhare, T.D. Dongale, P.S. Patil, A.D. Sheikh, Impact of collected sunlight on ZnFe2O4 nanoparticles for photocatalytic application, J. Colloid Interface Sci. 527 (2018) 289–297, https://doi.org/10.1016/j.jcis.2018.05.051.
[142] N.D. Banić, B.F. Abramović, J.B. Krstić, D.V. Šojić Merkulov, N.L. Finčur, M. N. Mitrić, Novel WO3/Fe3O4 magnetic photocatalysts: preparation, characterization and thiacloprid photodegradation, J. Ind. Eng. Chem. 70 (2019) 264–275, https://doi.org/10.1016/j.jiec.2018.10.025.
[143] A. Mitra, G. De, Sol-gel synthesis of metal nanoparticle incorporated oxide films on glass, in: Glas. Nanocomposites Synth. Prop. Appl., Elsevier Inc., 2016, pp. 145–163, https://doi.org/10.1016/B978-0-323-39309-6.00006-7.
[144] I.A. Neacşu, A.I. Nicoară, O.R. Vasile, B.Ş. Vasile, Inorganic micro- and nanostructured implants for tissue engineering, in: Nanobiomaterials Hard Tissue Eng. Appl. Nanobiomaterials, Elsevier Inc., 2016, pp. 271–295, https://doi.org/10.1016/B978-0-323-42862-0.00009-2.
[145] S. Sakka, Sol-gel process and applications, in: Handb. Adv. Ceram. Mater. Appl. Process. Prop, second ed., second ed., Elsevier, 2013, pp. 883–910, https://doi.org/10.1016/B978-0-12-385469-8.00048-4.
[146] H. Zhao, G. Xiong, G.V. Baron, Pore-wall modified metal/ceramic catalytic membranes prepared by the sol-gel method, in: Stud. Surf. Sci. Catal., Elsevier Masson SAS, 1998, pp. 717–724, https://doi.org/10.1016/s0167-2991(98)80239-5.
[147] T. Graham, —on the properties of silicic acid and other analogous colloidal substances, J. Chem. Soc. 17 (1864) 318–327, https://doi.org/10.1039/JS8641700318. XXXV.
[148] E. Yilmaz, M. Soylak, Functionalized nanomaterials for sample preparation methods, in: Handb. Nanomater. Anal. Chem. Mod. Trends Anal., Elsevier, 2019, pp. 375–413, https://doi.org/10.1016/B978-0-12-816699-4.00015-3.
[149] B.E. Yoldas, Monolithic glass formation by chemical polymerization, J. Mater. Sci. 14 (1979) 1843–1849, https://doi.org/10.1007/BF00551023.
[150] C. De Coelho Escobar, J.H.Z. Dos Santos, Effect of the sol-gel route on the textural characteristics of silica imprinted with Rhodamine B, J. Separ. Sci. 37 (2014) 868–875, https://doi.org/10.1002/jssc.201301143.
[151] M. Parashar, V.K. Shukla, R. Singh, Metal oxides nanoparticles via sol–gel method: a review on synthesis, characterization and applications, J. Mater. Sci. Mater. Electron. 31 (2020) 3729–3749, https://doi.org/10.1007/s10854-020-02994-8.
[152] S. Esposito, "Traditional" sol-gel chemistry as a powerful tool for the preparation of supported metal and metal oxide catalysts, Materials 12 (2019) 1–25, https://doi.org/10.3390/ma12040668.
[153] R. Nisticò, D. Scalarone, G. Magnacca, Sol-gel chemistry, templating and spin-coating deposition: a combined approach to control in a simple way the porosity of inorganic thin films/coatings, Microporous Mesoporous Mater. 248 (2017) 18–29, https://doi.org/10.1016/j.micromeso.2017.04.017.
[154] A. Arce-Sarria, F. Machuca-Martínez, C. Bustillo-Lecompte, A. Hernández-Ramírez, J. Colina-Márquez, Degradation and loss of antibacterial activity of commercial amoxicillin with TiO2/WO3-assisted solar photocatalysis, Catalysts 8 (2018) 1–14, https://doi.org/10.3390/catal8060222.
[155] A. Cordero-García, G. Turnes Palomino, L. Hinojosa-Reyes, J.L. Guzmán-Mar, L. Maya-Teviño, A. Hernández-Ramírez, Photocatalytic behaviour of WO3/TiO2-N for diclofenac degradation using simulated solar radiation as an activation source, Environ. Sci. Pollut. Res. 24 (2017) 4613–4624, https://doi.org/10.1007/s11356-016-8157-0.
[156] M. Ismael, A review on graphitic carbon nitride (g-C3N4) based nanocomposites: synthesis, categories, and their application in photocatalysis, J. Alloys Compd. 846 (2020) 156446, https://doi.org/10.1016/j.jallcom.2020.156446.
[157] J. Singh, T. Dutta, K.H. Kim, M. Rawat, P. Samddar, P. Kumar, "Green" synthesis of metals and their oxide nanoparticles: applications for environmental remediation, J. Nanobiotechnol. 16 (2018) 1–24, https://doi.org/10.1186/s12951-018-0408-4.
[158] A.S. Manjunatha, N.S. Pavithra, M. Shivanna, G. Nagaraju, C.R. Ravikumar, Synthesis of Citrus Limon mediated SnO2-WO3nanocomposite: applications to photocatalytic activity and electrochemical sensor, J. Environ. Chem. Eng. 8 (2020) 104500, https://doi.org/10.1016/j.jece.2020.104500.
[159] Y. Liu, J. Goebl, Y. Yin, Templated synthesis of nanostructured materials, Chem. Soc. Rev. 42 (2013) 2610–2653, https://doi.org/10.1039/c2cs35369e.
[160] M. Mokhtarifar, D.T. Nguyen, M. Sakar, M.P. Pedeferri, M. Asa, R. Kaveh, M. V. Diamanti, T.O. Do, Mechanistic insights into photogenerated electrons store-and-discharge in hydrogenated glucose template synthesized Pt: TiO2/WO3 photocatalyst for the round-the-clock decomposition of methanol, Mater. Res. Bull. 137 (2021) 111203, https://doi.org/10.1016/j.materresbull.2020.111203.
[161] M. Mokhtarifar, D.T. Nguyen, M.V. Diamanti, R. Kaveh, M. Asa, M. Sakar, M. P. Pedeferri, T.O. Do, Fabrication of dual-phase TiO2/WO3with post-illumination photocatalytic memory, New J. Chem. 44 (2020) 20375–20386, https://doi.org/10.1039/d0nj04694a.
[162] Q. Xu, L. Zhang, J. Yu, S. Wageh, A.A. Al-Ghamdi, M. Jaroniec, Direct Z-scheme photocatalysts: principles, synthesis, and applications, Mater. Today 21 (2018) 1042–1063, https://doi.org/10.1016/j.mattod.2018.04.008.
[163] Z. Li, J. Ma, B. Zhang, C. Song, D. Wang, Crystal phase- and morphology-controlled synthesis of MoO3 materials, CrystEngComm 19 (2017) 1479–1485, https://doi.org/10.1039/C6CE02437H.
[164] A. Priya, P. Arunachalam, A. Selvi, J. Madhavan, A.M. Al-Mayouf, Synthesis of BiFeWO6/WO3 nanocomposite and its enhanced photocatalytic activity towards degradation of dye under irradiation of light, Colloids Surfaces A Physicochem. Eng. Asp. 559 (2018) 83–91, https://doi.org/10.1016/j.colsurfa.2018.09.031.
[165] G. Palanisamy, K. Bhuvaneswari, T. Pazhanivel, G. Bharathi, Enriched photocatalytic activity of Rhodamine B dye from aqueous solution using hollow sphere tungsten trioxide nanoparticles, Optik 204 (2020) 164171, https://doi.org/10.1016/j.ijleo.2020.164171.
[166] L. Wang, T. Huang, G. Yang, C. Lu, F. Dong, Y. Li, W. Guan, The precursor-guided hydrothermal synthesis of CuBi2O4/WO3 heterostructure with enhanced photoactivity under simulated solar light irradiation and mechanism insight, J. Hazard Mater. 381 (2020) 120956, https://doi.org/10.1016/j.jhazmat.2019.120956.
[167] G. Chen, Q. Wang, Z. Zhao, L. Gao, X. Li, Synthesis and photocatalytic activity study of S-doped WO3 under visible light irradiation, Environ. Sci. Pollut. Res. 27 (2020) 15103–15112, https://doi.org/10.1007/s11356-020-07827-z.
[168] P. Hu, Y. Chen, Y. Chen, Z. Lin, Z. Wang, Hydrothermal synthesis and photocatalytic properties of WO3 nanorods by using capping agent SnCl4·5H2O, Phys. E Low-Dimensional Syst. Nanostructures 92 (2017) 12–16, https://doi.org/10.1016/j.physe.2017.05.004.
[169] Y. Fan, X. Xi, Y. Liu, Z. Nie, Q. Zhang, L. Zhao, Growth mechanism of immobilized WO3 nanostructures in different solvents and their visible-light photocatalytic performance, J. Phys. Chem. Solid. 140 (2020) 109380, https://doi.org/10.1016/j.jpcs.2020.109380.
[170] Z. Balta, E. Bilgin Simsek, D. Berek, Solvothermal synthesis of WO3/TiO2/carbon fiber composite photocatalysts for enhanced performance under sunlight illumination, Photochem. Photobiol. 95 (2019) 1331–1338, https://doi.org/10.1111/php.13117.
[171] B. Wang, C. Chen, H. Liu, B. Xia, Y. Fan, T. Chen, WO3/TiO2 superhydrophilic and underwater superoleophobic membrane for effective separation of oil-in-water emulsions, Thin Solid Films 665 (2018) 9–16, https://doi.org/10.1016/j.tsf.2018.08.039.
[172] G. Jeevitha, R. Abhinayaa, D. Mangalaraj, N. Ponpandian, Tungsten oxide-graphene oxide (WO3-GO) nanocomposite as an efficient photocatalyst, antibacterial and anticancer agent, J. Phys. Chem. Solid. 116 (2018) 137–147, https://doi.org/10.1016/j.jpcs.2018.01.021.
[173] M. Kang, X. Wang, J. Zhang, Y. Lu, X. Chen, L. Yang, F. Wang, Boosting the photocatalytic oxidative desulfurization of dibenzothiophene by decoration of

MWO4 (M=Cu, Zn, Ni) on WO3, J. Environ. Chem. Eng. 7 (2019) 102809, https://doi.org/10.1016/j.jece.2018.11.053.
[174] F. Mehmood, J. Iqbal, M. Ismail, A. Mehmood, Ni doped WO3 nanoplates: an excellent photocatalyst and novel nanomaterial for enhanced anticancer activities, J. Alloys Compd. 746 (2018) 729–738, https://doi.org/10.1016/j.jallcom.2018.01.409.
[175] A.A. Ismail, M. Faisal, A. Al-Haddad, Mesoporous WO3-graphene photocatalyst for photocatalytic degradation of Methylene Blue dye under visible light illumination, J. Environ. Sci. (China) 66 (2018) 328–337, https://doi.org/10.1016/j.jes.2017.05.001.
[176] S. Mohammadi, M. Sohrabi, A.N. Golikand, A. Fakhri, Preparation and characterization of zinc and copper co-doped WO3 nanoparticles: application in photocatalysis and photobiology, J. Photochem. Photobiol. B Biol. 161 (2016) 217–221, https://doi.org/10.1016/j.jphotobiol.2016.05.020.
[177] B. Mirtaheri, M. Shokouhimehr, A. Beitollahi, Synthesis of mesoporous tungsten oxide by template-assisted sol–gel method and its photocatalytic degradation activity, J. Sol. Gel Sci. Technol. 82 (2017) 148–156, https://doi.org/10.1007/s10971-016-4289-4.
[178] R. Nagarjuna, S. Challagulla, P. Sahu, S. Roy, R. Ganesan, Polymerizable sol–gel synthesis of nano-crystalline WO3 and its photocatalytic Cr(VI) reduction under visible light, Adv. Powder Technol. 28 (2017) 3265–3273, https://doi.org/10.1016/j.apt.2017.09.030.
[180] K. Yamanaka, Electrodeposited films from aqueous tungstic acid-hydrogen peroxide solutions for electrochromic display devices, Jpn. J. Appl. Phys. 26 (1987) 1884–1890, https://doi.org/10.1143/jjap.26.1884.
[181] E.A. Meulenkamp, Mechanism of WO3Electrodeposition from peroxy-tungstate solution, J. Electrochem. Soc. 144 (1997) 1664–1671, https://doi.org/10.1149/1.1837657.
[183] P.M.S. Poongodi, P.S. Kumar, D. Mangalaraj, N. Ponpandian, C.L.Y. Masuda, Electrodeposition of WO3 nanostructured thin films for electrochromic and H2S gas sensor applications, J. Alloys Compd. 719 (2017).
[185] V. Cristino, S. Caramori, R. Argazzi, L. Meda, G.L. Marra, C.A. Bignozzi, Efficient photoelectrochemical water splitting by anodically grown WO3 electrodes, Langmuir 27 (2011) 7276–7284, https://doi.org/10.1021/la200595x.
[186] M.G. Vergé, C.O.A. Olsson, D. Landolt, Anodic oxide growth on tungsten studied by EQCM, EIS and AES, Corrosion Sci. 46 (2004) 2583–2600, https://doi.org/10.1016/j.corsci.2004.02.005.
[187] M. Krebsz, J.P. Kollender, A.W. Hassel, In situ monitoring of the electrochemical dissolution of tungsten, Phys. Status Solidi 214 (2017) 1600803, https://doi.org/10.1002/pssa.201600803.
[188] J.Z. Ou, S. Balendhran, M.R. Field, D.G. McCulloch, A.S. Zoolfakar, R.A. Rani, S. Zhuiykov, A.P. O'Mullane, K. Kalantar-Zadeh, The anodized crystalline WO3 nanoporous network with enhanced electrochromic properties, Nanoscale 4 (2012) 5980–5988, https://doi.org/10.1039/c2nr31203d.
[189] N. Mukherjee, M. Paulose, O.K. Varghese, G.K. Mor, C.A. Grimes, Fabrication of nanoporous tungsten oxide by galvanostatic anodization, J. Mater. Res. 18 (2003) 2296–2299, https://doi.org/10.1557/JMR.2003.0321.
[190] H. Tsuchiya, J.M. Macak, I. Sieber, L. Taveira, A. Ghicov, K. Sirotna, P. Schmuki, Self-organized porous WO3 formed in NaF electrolytes, Electrochem. Commun. 7 (2005) 295–298, https://doi.org/10.1016/j.elecom.2005.01.003.
[193] A.W. Hassel, S. Milenkovic, A.J. Smith, Large scale synthesis of single crystalline tungsten nanowires with extreme aspect ratios, Phys. Status Solidi Appl. Mater. Sci. 207 (2010) 858–863, https://doi.org/10.1002/pssa.200983319.
[196] C. Cantalini, H.T. Sun, M. Faccio, M. Pelino, S. Santucci, L. Lozzi, M. Passacantando, NO2 sensitivity of WO3 thin film obtained by high vacuum thermal evaporation, Sensor. Actuator. B Chem. 31 (1996) 81–87, https://doi.org/10.1016/0925-4005(96)80020-7.
[197] A. Ponzoni, E. Comini, M. Ferroni, G. Sberveglieri, Nanostructured WO3 deposited by modified thermal evaporation for gas-sensing applications, Thin Solid Films 490 (2005) 81–85, https://doi.org/10.1016/j.tsf.2005.04.031.
[199] B. Marsen, E.L. Miller, D. Paluselli, R.E. Rocheleau, Progress in sputtered tungsten trioxide for photoelectrode applications, Int. J. Hydrogen Energy 32 (2007) 1310–1315, https://doi.org/10.1016/j.ijhydene.2006.01.022.
[200] D.B.B. Lollman, C. Lemire, A. Al Mohammad, E. Gillet, K. Aguir, Reactive R.F. Magnetron sputtering deposition of WO3 thin films, Sensor. Actuator. B Chem. 84 (2002) 49–54, https://doi.org/10.1016/S0925-4005(01)01073-5.
[202] A. Ghatak, S. Roy Moulik, B. Ghosh, Pulsed laser assisted growth of aligned nanowires of WO3: role of interface with substrate, RSC Adv. 6 (2016) 31705–31716, https://doi.org/10.1039/C5RA27542C.
[203] J. Chen, Y. Ren, T. Hu, T. Xu, Q. Xu, Fabrication and application of substoichiometric tungsten oxide with tunable localized surface plasmon resonances, Appl. Surf. Sci. 465 (2019) 517–525, https://doi.org/10.1016/j.apsusc.2018.09.140.
[204] H.W. Choi, E.J. Kim, S.H. Hahn, Photocatalytic activity of Au-buffered WO3 thin films prepared by RF magnetron sputtering, Chem. Eng. J. 161 (2010) 285–288, https://doi.org/10.1016/j.cej.2010.01.050.
[205] J. Kim, C.W. Lee, W. Choi, Platinized WO3 as an environmental photocatalyst that generates OH radicals under visible light, Environ. Sci. Technol. 44 (2010) 6849–6854, https://doi.org/10.1021/es101981r.
[206] R. Abe, H. Takami, N. Murakami, B. Ohtani, Pristine simple oxides as visible light driven photocatalysts: highly efficient decomposition of organic compounds over platinum-loaded tungsten oxide, J. Am. Chem. Soc. 130 (2008) 7780–7781, https://doi.org/10.1021/ja800835q.
[207] J.Z. Bloh, R. Dillert, D.W. Bahnemann, Designing optimal metal-doped photocatalysts: correlation between photocatalytic activity, doping ratio, and particle size, J. Phys. Chem. C 116 (2012) 25558–25562, https://doi.org/10.1021/jp307313z.
[208] S. Mizutani, I. Karimata, L. An, T. Sato, Y. Kobori, H. Onishi, T. Tachikawa, Charge carrier dynamics in Sr-doped NaTaO3 photocatalysts revealed by deep ultraviolet single-particle microspectroscopy, J. Phys. Chem. C 123 (2019) 12592–12598, https://doi.org/10.1021/acs.jpcc.9b01929.
[209] S.S. Mehta, D.Y. Nadargi, M.S. Tamboli, L.S. Chaudhary, P.S. Patil, I.S. Mulla, S. S. Suryavanshi, Ru-Loaded mesoporous WO3 microflowers for dual applications: enhanced H2S sensing and sunlight-driven photocatalysis, Dalton Trans. 47 (2018) 16840–16845, https://doi.org/10.1039/C8DT03667E.
[210] M. Dhanalakshmi, S. Lakshmi Prabavathi, K. Saravanakumar, B. Filip Jones, V. Muthuraj, Iridium nanoparticles anchored WO3 nanocubes as an efficient photocatalyst for removal of refractory contaminants (crystal violet and methylene blue), Chem. Phys. Lett. 745 (2020) 137285, https://doi.org/10.1016/j.cplett.2020.137285.
[211] S.V. Mohite, V.V. Ganbavle, K.Y. Rajpure, Photoelectrocatalytic activity of immobilized Yb doped WO3 photocatalyst for degradation of methyl orange dye, J. Energy Chem. 26 (2017) 440–447, https://doi.org/10.1016/j.jechem.2017.01.001.
[212] D.P. DePuccio, P. Botella, B. O'Rourke, C.C. Landry, Degradation of methylene blue using porous WO3, SiO2–WO3, and their Au-loaded analogs: adsorption and photocatalytic studies, ACS Appl. Mater. Interfaces 7 (2015) 1987–1996, https://doi.org/10.1021/am507806a.
[213] S. Sun, W. Wang, S. Zeng, M. Shang, L. Zhang, Preparation of ordered mesoporous Ag/WO3 and its highly efficient degradation of acetaldehyde under visible-light irradiation, J. Hazard Mater. 178 (2010) 427–433, https://doi.org/10.1016/j.jhazmat.2010.01.098.
[214] K.A. Willets, R.P. Van Duyne, Localized surface plasmon resonance spectroscopy and sensing, Annu. Rev. Phys. Chem. 58 (2007) 267–297, https://doi.org/10.1146/annurev.physchem.58.032806.104607.
[215] W. Hou, S.B. Cronin, A review of surface plasmon resonance-enhanced photocatalysis, Adv. Funct. Mater. 23 (2013) 1612–1619, https://doi.org/10.1002/adfm.201202148.
[216] M.A. Gondal, M.A. Suliman, M.A. Dastageer, G.K. Chuah, C. Basheer, D. Yang, A. Suwaiyan, Visible light photocatalytic degradation of herbicide (Atrazine) using surface plasmon resonance induced in mesoporous Ag-WO3/SBA-15 composite, J. Mol. Catal. Chem. 425 (2016) 208–216, https://doi.org/10.1016/j.molcata.2016.10.015.
[217] H. Song, Y. Li, Z. Lou, M. Xiao, L. Hu, Z. Ye, L. Zhu, Synthesis of Fe-doped WO3 nanostructures with high visible-light-driven photocatalytic activities, Appl. Catal. B Environ. 166–167 (2015) 112–120, https://doi.org/10.1016/j.apcatb.2014.11.020.
[218] Y. Tian, T. Tatsuma, Plasmon-induced photoelectrochemistry at metal nanoparticles supported on nanoporous TiO2, Chem. Commun. (2004) 1810–1811, https://doi.org/10.1039/b405061d.
[219] J. Ding, L. Zhang, Q. Liu, W.L. Dai, G. Guan, Synergistic effects of electronic structure of WO3 nanorods with the dominant {001} exposed facets combined with silver size-dependent on the visible-light photocatalytic activity, Appl. Catal. B Environ. 203 (2017) 335–342, https://doi.org/10.1016/j.apcatb.2016.10.028.
[220] F. Le, D.W. Brandl, Y.A. Urzhumov, H. Wang, J. Kundu, N.J. Halas, J. Aizpurua, P. Nordlander, Metallic nanoparticle arrays: a common substrate for both surface-enhanced Raman scattering and surface-enhanced infrared absorption, ACS Nano 2 (2008) 707–718, https://doi.org/10.1021/nn800047e.
[221] H. Widiyandari, A. Purwanto, R. Balgis, T. Ogi, K. Okuyama, CuO/WO 3 and Pt/WO 3 nanocatalysts for efficient pollutant degradation using visible light irradiation, Chem. Eng. J. 180 (2012) 323–329, https://doi.org/10.1016/j.cej.2011.10.095.
[222] F. Mehmood, J. Iqbal, T. Jan, A. Gul, Q. Mansoor, R. Faryal, Structural, photoluminescence, electrical, anti cancer and visible light driven photocatalytic characteristics of Co doped WO3 nanoplates, Vib. Spectrosc. 93 (2017) 78–89, https://doi.org/10.1016/j.vibspec.2017.09.005.
[223] F. Mehmood, J. Iqbal, T. Jan, Q. Mansoor, Structural, Raman and photoluminescence properties of Fe doped WO3 nanoplates with anti cancer and visible light driven photocatalytic activities, J. Alloys Compd. 728 (2017) 1329–1337, https://doi.org/10.1016/j.jallcom.2017.08.234.
[224] M.H. Sayed Abhudhahir, J. Kandasamy, Photocatalytic effect of manganese doped WO3 and the effect of dopants on degradation of methylene blue, J. Mater. Sci. Mater. Electron. 26 (2015) 8307–8314, https://doi.org/10.1007/s10854-015-3496-z.
[225] Y. Deng, Y. Tan, H. Tang, Y. Xiang, J. Zhu, W. Wu, Y. Xu, H. Zou, Y. Zhou, Hydrothermal synthesis of Bi-doped WO3·0.5H2O material with tetragonal pyramid-like structure and its enhanced photocatalytic activity, Chemistry 5 (2020) 3917–3922, https://doi.org/10.1002/slct.202000597.
[226] M. Saleem, J. Iqbal, A. Nawaz, B. Islam, I. Hussain, Synthesis, characterization, and performance evaluation of pristine and cerium-doped WO3 nanoparticles for photodegradation of methylene blue via solar irradiation, Int. J. Appl. Ceram. Technol. 17 (2020) 1918–1929, https://doi.org/10.1111/ijac.13496.
[227] M.S.M.B. Tahir, Carbon nanodots and rare metals (RM= La, Gd, Er) doped tungsten oxide nanostructures for photocatalytic dyes degradation and hydrogen production, Separ. Purif. Technol. 209 (2019) 94–102.
[228] Y. Lu, X. Zhang, Y. Chu, H. Yu, M. Huo, J. Qu, J.C. Crittenden, H. Huo, X. Yuan, Cu2O nanocrystals/TiO2 microspheres film on a rotating disk containing long-afterglow phosphor for enhanced round-the-clock photocatalysis, Appl. Catal. B Environ. 224 (2018) 239–248, https://doi.org/10.1016/j.apcatb.2017.10.054.

[229] T.A. Saleh, V.K. Gupta, Functionalization of tungsten oxide into MWCNT and its application for sunlightinduced degradation of rhodamine B, J. Colloid Interface Sci. 362 (2011) 337–344.
[230] L. Tie, C. Yu, Y. Zhao, H. Chen, S. Yang, J. Sun, S. Dong, J. Sun, Fabrication of WO3 nanorods on reduced graphene oxide sheets with augmented visible light photocatalytic activity for efficient mineralization of dye, J. Alloys Compd. 769 (2018) 83–91, https://doi.org/10.1016/j.jallcom.2018.07.176.
[231] W. Zhu, Z. Li, C. He, S. Faqian, Y. Zhou, Enhanced photodegradation of sulfamethoxazole by a novel WO3-CNT composite under visible light irradiation, J. Alloys Compd. 754 (2018) 153–162, https://doi.org/10.1016/j.jallcom.2018.04.286.
[232] O.J.K, K.M.S. Prabhu, L. Cindrella, Green synthesis of rGO-WO3 composite and its efficient photoelectrochemical water splitting, Int. J. Hydrogen Energy 42 (2017) 29791–29796.
[233] W. Zhu, F. Sun, R. Goei, Y. Zhou, Facile fabrication of RGO-WO3 composites for effective visible light photocatalytic degradation of sulfamethoxazole, Appl. Catal. B Environ. 207 (2017) 93–102, https://doi.org/10.1016/j.apcatb.2017.02.012.
[234] L. Fu, T. Xia, Y. Zheng, J. Yang, A. Wang, Z. Wang, Preparation of WO3-reduced graphene oxide nanocomposites with enhanced photocatalytic property, Ceram. Int. 41 (2015) 5903–5908, https://doi.org/10.1016/j.ceramint.2015.01.022.
[235] X. Li, S. Yang, J. Sun, P. He, X. Xu, G. Ding, Tungsten oxide nanowire-reduced graphene oxide aerogel for high-efficiency visible light photocatalysis, Carbon N. Y. 78 (2014) 38–48, https://doi.org/10.1016/j.carbon.2014.06.034.
[236] S. Sajjad, M. Khan, S.A.K. Leghari, N.A. Ryma, S.A. Farooqi, Potential visible WO3/GO composite photocatalyst, Int. J. Appl. Ceram. Technol. 16 (2019) 1218–1227, https://doi.org/10.1111/ijac.13124.
[237] S.P. Smrithi, N. Kottam, V. Arpitha, A. Narula, A. G N, K.R.V. Subramanian, Tungsten oxide modified with carbon nanodots: integrating adsorptive and photocatalytic functionalities for water remediation, J. Sci. Adv. Mater. Devices. 5 (2020) 73–83, https://doi.org/10.1016/j.jsamd.2020.02.005.
[238] H.B. Truong, B.T. Huy, S.K. Ray, Y.I. Lee, J. Cho, J. Hur, H2O2-assisted photocatalysis for removal of natural organic matter using nanosheet C3N4-WO3 composite under visible light and the hybrid system with ultrafiltration, Chem. Eng. J. 399 (2020) 125733, https://doi.org/10.1016/j.cej.2020.125733.
[239] B. Song, T. Wang, H. Sun, Q. Shao, J. Zhao, K. Song, L. Hao, L. Wang, Z. Guo, Two-step hydrothermally synthesized carbon nanodots/WO3 photocatalysts with enhanced photocatalytic performance, Dalton Trans. 46 (2017) 15769–15777, https://doi.org/10.1039/C7DT03003G.
[240] S. Hossain, W.S. Chu, C.S. Lee, S.H. Ahn, D.M. Chun, Photocatalytic performance of few-layer Graphene/WO 3 thin films prepared by a nano-particle deposition system, Mater. Chem. Phys. 226 (2019) 141–150, https://doi.org/10.1016/j.matchemphys.2019.01.026.
[241] S. Prabhu, S. Manikumar, L. Cindrella, O.J. Kwon, Charge transfer and intrinsic electronic properties of rGO-WO3 nanostructures for efficient photoelectrochemical and photocatalytic applications, Mater. Sci. Semicond. Process. 74 (2018) 136–146, https://doi.org/10.1016/j.mssp.2017.10.041.
[242] Y. Zheng, G. Chen, Y. Yu, Y. Zhou, F. He, Synthesis of carbon doped WO 3 ·0.33H 2 O hierarchical photocatalyst with improved photocatalytic activity, Appl. Surf. Sci. 362 (2016) 182–190, https://doi.org/10.1016/j.apsusc.2015.11.115.
[243] M.R.K.K. Shahzad, M. Tahir, M. Ashraf, T. Nawaz, N. Khalid, Interfacial growth of activated carbon on WO 3 nanoplates for enhanced photocatalytic activity by surface plasmon resonance, Plasmonics, Plasmonics (2020) 1–8.
[244] A.A. Isari, M. Mehregan, S. Mehregan, F. Hayati, R. Rezaei Kalantary, B. Kakavandi, Sono-photocatalytic degradation of tetracycline and pharmaceutical wastewater using WO3/CNT heterojunction nanocomposite under US and visible light irradiations: a novel hybrid system, J. Hazard Mater. 390 (2020) 122050, https://doi.org/10.1016/j.jhazmat.2020.122050.
[245] Y. Huang, Z. Guo, H. Liu, S. Zhang, P. Wang, J. Lu, Y. Tong, Heterojunction architecture of N-doped WO3 nanobundles with Ce2S3 nanodots hybridized on a carbon textile enables a highly efficient flexible photocatalyst, Adv. Funct. Mater. 29 (2019) 1903490, https://doi.org/10.1002/adfm.201903490.
[246] X.L.G. Chen, Q. Wang, Z. Zhao, L. Gao, Synthesis and photocatalytic activity study of S-doped WO 3 under visible light irradiation, Environ. Sci. Pollut. Res. Int. (2020) 1–10.
[247] F. Han, H. Li, L. Fu, J. Yang, Z. Liu, Synthesis of S-doped WO3 nanowires with enhanced photocatalytic performance towards dye degradation, Chem. Phys. Lett. 651 (2016) 183–187, https://doi.org/10.1016/j.cplett.2016.03.017.
[248] A.J.E. Rettie, K.C. Klavetter, J.-F. Lin, A. Dolocan, H. Celio, A. Ishiekwene, H. L. Bolton, K.N. Pearson, N.T. Hahn, C.B. Mullins, Improved visible light harvesting of WO3 by incorporation of sulfur or iodine: a tale of two impurities, Chem. Mater. 26 (2014) 1670–1677, https://doi.org/10.1021/cm403969r.
[249] J. Sun, B. Li, Q. Wang, P. Zhang, Y. Zhang, L. Gao, X. Li, Preparation of phosphorus-doped tungsten trioxide nanomaterials and their photocatalytic performances, Environ. Technol. (2020) 1–11, https://doi.org/10.1080/09593330.2020.1745292.
[250] M.G. Peleyeju, O.A. Arotiba, Recent trend in visible-light photoelectrocatalytic systems for degradation of organic contaminants in water/wastewater, Environ. Sci. Water Res. Technol. 4 (2018) 1389–1411, https://doi.org/10.1039/C8EW00276B.
[251] X. Tang, Z. Wang, N. Wu, S. Liu, N. Liu, A novel visible-light-active B-Bi2O3/BiOBr heterojunction photocatalyst with remarkably enhanced photocatalytic activity, Catal. Commun. 119 (2019) 119–123, https://doi.org/10.1016/j.catcom.2018.10.025.
[252] J. Yang, R. Hu, W. Meng, Y. Du, A novel p-LaFeO3/n-Ag3PO4 heterojunction photocatalyst for phenol degradation under visible light irradiation, Chem. Commun. 52 (2016) 2620–2623, https://doi.org/10.1039/C5CC09222A.
[253] A. Kumar, P. Raizada, V. Kumar Thakur, V. Saini, A. Aslam Parwaz Khan, N. Singh, P. Singh, An overview on polymeric carbon nitride assisted photocatalytic CO2 reduction: strategically manoeuvring solar to fuel conversion efficiency, Chem. Eng. Sci. 230 (2021) 116219, https://doi.org/10.1016/j.ces.2020.116219.
[254] A. Sudhaik, P. Raizada, P. Singh, A. Hosseini-Bandegharaei, V.K. Thakur, V. H. Nguyen, Highly effective degradation of imidacloprid by H2O2/fullerene decorated P-doped g-C3N4photocatalyst, J. Environ. Chem. Eng. 8 (2020) 104483, https://doi.org/10.1016/j.jece.2020.104483.
[255] J. Low, J. Yu, M. Jaroniec, S. Wageh, A.A. Al-Ghamdi, Heterojunction photocatalysts, Adv. Mater. 29 (2017) 1601694, https://doi.org/10.1002/adma.201601694.
[256] A. Sudhaik, P. Raizada, S. Thakur, R.V. Saini, A.K. Saini, P. Singh, V. Kumar Thakur, V.H. Nguyen, A.A.P. Khan, A.M. Asiri, Synergistic photocatalytic mitigation of imidacloprid pesticide and antibacterial activity using carbon nanotube decorated phosphorus doped graphitic carbon nitride photocatalyst, J. Taiwan Inst. Chem. Eng. 113 (2020) 142–154, https://doi.org/10.1016/j.jtice.2020.08.003.
[257] L. Zhang, M. Jaroniec, Toward designing semiconductor-semiconductor heterojunctions for photocatalytic applications, Appl. Surf. Sci. 430 (2018) 2–17, https://doi.org/10.1016/j.apsusc.2017.07.192.
[258] O.A. Arotiba, B.O. Orimolade, B.A. Koiki, Visible light–driven photoelectrocatalytic semiconductor heterojunction anodes for water treatment applications, Curr. Opin. Electrochem. 22 (2020) 25–34, https://doi.org/10.1016/j.coelec.2020.03.018.
[259] H. Du, W. Pu, Y. Wang, K. Yan, J. Feng, J. Zhang, C. Yang, J. Gong, Synthesis of BiVO4/WO3 composite film for highly efficient visible light induced photoelectrocatalytic oxidation of norfloxacin, J. Alloys Compd. 787 (2019) 284–294, https://doi.org/10.1016/j.jallcom.2019.01.390.
[260] N. Tahmasebi, Z. Maleki, P. Farahnak, Enhanced photocatalytic activities of Bi2WO6/BiOCl composite synthesized by one-step hydrothermal method with the assistance of HCl, Mater. Sci. Semicond. Process. 89 (2019) 32–40, https://doi.org/10.1016/j.mssp.2018.08.026.
[261] Y. Wei, Y. Huang, Y. Fang, Y. Zhao, D. Luo, Q. Guo, L. Fan, J. Wu, Hollow mesoporous TiO2/WO3 sphere heterojunction with high visible-light-driven photocatalytic activity, Mater. Res. Bull. 119 (2019) 110571, https://doi.org/10.1016/j.materresbull.2019.110571.
[262] R. Lei, H. Zhang, H. Ni, R. Chen, H. Gu, B. Zhang, Novel ZnO nanoparticles modified WO 3 nanosheet arrays for enhanced photocatalytic properties under solar light illumination, Appl. Surf. Sci. 463 (2019) 363–373, https://doi.org/10.1016/j.apsusc.2018.08.218.
[263] T. Fukumura, E. Sambandan, H. Yamashita, Synthesis and VOC degradation ability of a CeO2/WO3 thin-layer visible-light photocatalyst, Mater. Res. Bull. 94 (2017) 493–499, https://doi.org/10.1016/j.materresbull.2017.07.003.
[264] J. Chen, X. Xiao, Y. Wang, Z. Ye, Ag nanoparticles decorated WO 3/g-C 3 N 4 2D/2D heterostructure with enhanced photocatalytic activity for organic pollutants degradation, Appl. Surf. Sci. 467–468 (2019) 1000–1010, https://doi.org/10.1016/j.apsusc.2018.10.236.
[265] W. Nareejun, C. Ponchio, Novel photoelectrocatalytic/solar cell improvement for organic dye degradation based on simple dip coating WO3/BiVO4 photoanode electrode, Sol. Energy Mater. Sol. Cells 212 (2020) 110556, https://doi.org/10.1016/j.solmat.2020.110556.
[266] J. Zhang, K. Yu, Y. Yu, L.L. Lou, Z. Yang, J. Yang, S. Liu, Highly effective and stable Ag3PO4/WO3 photocatalysts for visible light degradation of organic dyes, J. Mol. Catal. Chem. 391 (2014) 12–18, https://doi.org/10.1016/j.molcata.2014.04.010.
[267] X. Yuan, L. Jiang, X. Chen, L. Leng, H. Wang, Z. Wu, T. Xiong, J. Liang, G. Zeng, Highly efficient visible-light-induced photoactivity of Z-scheme Ag2CO3/Ag/WO3 photocatalysts for organic pollutant degradation, Environ. Sci. Nano. 4 (2017) 2175–2185, https://doi.org/10.1039/C7EN00713B.
[268] X. Zhang, R. Zhang, S. Niu, J. Zheng, C. Guo, Construction of core-shell structured WO3@SnS2 hetero-junction as a direct Z-scheme photo-catalyst, J. Colloid Interface Sci. 554 (2019) 229–238, https://doi.org/10.1016/j.jcis.2019.06.107.
[269] S.B. Rawal, H.J. Kang, D. Il Won, W.I. Lee, Novel ZnFe2O4/WO3, a highly efficient visible-light photocatalytic system operated by a Z-scheme mechanism, Appl. Catal. B Environ. 256 (2019) 117856, https://doi.org/10.1016/j.apcatb.2019.117856.
[270] A.J. Bard, Photoelectrochemistry and heterogeneous photo-catalysis at semiconductors, J. Photochem. 10 (1979) 59–75, https://doi.org/10.1016/0047-2670(79)80037-4.
[271] L. Jiang, X. Yuan, G. Zeng, J. Liang, X. Chen, H. Yu, H. Wang, Z. Wu, J. Zhang, T. Xiong, In-situ synthesis of direct solid-state dual Z-scheme WO3/g-C3N4/Bi2O3 photocatalyst for the degradation of refractory pollutant, Appl. Catal. B Environ. 227 (2018) 376–385, https://doi.org/10.1016/j.apcatb.2018.01.042.
[272] Q. Li, F. Wang, Y. Hua, Y. Luo, X. Liu, G. Duan, X. Yang, Deposition-precipitation preparation of Ag/Ag3PO4/WO3 nanocomposites for efficient Visible-light degradation of rhodamine B under strongly acidic/alkaline conditions, J. Colloid Interface Sci. 506 (2017) 207–216, https://doi.org/10.1016/j.jcis.2017.07.018.
[273] C. Shifu, J. Lei, T. Wenming, F. Xianliang, Fabrication, characterization and mechanism of a novel Z-scheme photocatalyst NaNbO3/WO3 with enhanced photocatalytic activity, J. Chem. Soc., Dalton Trans. 42 (2013) 10759–10768, https://doi.org/10.1039/c3dt50699a.

[274] L. Ye, Z. Wen, ZnIn2S4 nanosheets decorating WO3 nanorods core-shell hybrids for boosting visible-light photocatalysis hydrogen generation, Int. J. Hydrogen Energy 44 (2019) 3751–3759, https://doi.org/10.1016/j.ijhydene.2018.12.093.
[275] J. Zhang, J. Liu, X. Wang, J. Mai, W. Zhao, Z. Ding, Y. Fang, Construction of Z-scheme tungsten trioxide nanosheets-nitrogen-doped carbon dots composites for the enhanced photothermal synergistic catalytic oxidation of cyclohexane, Appl. Catal. B Environ. 259 (2019) 118063, https://doi.org/10.1016/j.apcatb.2019.118063.
[276] D. Liu, Y. Xu, M. Sun, Y. Huang, Y. Yu, B. Zhang, Photothermally assisted photocatalytic conversion of CO2–H2O into fuels over a WN–WO3 Z-scheme heterostructure, J. Mater. Chem. A. 8 (2020) 1077–1083, https://doi.org/10.1039/C9TA10629D.
[277] K. Sayama, K. Mukasa, R. Abe, Y. Abe, H. Arakawa, Stoichiometric water splitting into H2 and O2 using a mixture of two different photocatalysts and an IO3−/I− shuttle redox mediator under visible light irradiation, Chem. Commun. (2001) 2416–2417, https://doi.org/10.1039/B107673F.
[278] Q. Li, J. Yao, M. Arif, T. Huang, X. Liu, G. Duan, X. Yang, Facile fabrication and photocatalytic performance of WO3 nanoplates in situ decorated with Ag/β-Ag2WO4 nanoparticles, J. Environ. Chem. Eng. 6 (2018) 1969–1978, https://doi.org/10.1016/j.jece.2018.02.034.
[279] A. Kumar, P. Raizada, A. Hosseini-Bandegharaei, V.K. Thakur, V.H. Nguyen, P. Singh, C-, N-Vacancy defect engineered polymeric carbon nitride towards photocatalysis: viewpoints and challenges, Royal Society of Chemistry (2021), https://doi.org/10.1039/d0ta08384d.
[280] S. Sharma, V. Dutta, P. Raizada, A. Hosseini-Bandegharaei, P. Singh, V. H. Nguyen, Tailoring Cadmium Sulfide-Based Photocatalytic Nanomaterials for Water Decontamination: a Review, Springer International Publishing, 2021, https://doi.org/10.1007/s10311-020-01066-x.
[281] P. Raizada, V. Soni, A. Kumar, P. Singh, A.A. Parwaz Khan, A.M. Asiri, V. K. Thakur, V.H. Nguyen, Surface Defect Engineering of Metal Oxides Photocatalyst for Energy Application and Water Treatment, Elsevier Ltd, 2021, https://doi.org/10.1016/j.jmat.2020.10.009.
[282] X. Zhou, X. Zheng, B. Yan, T. Xu, Q. Xu, Defect engineering of two-dimensional WO 3 nanosheets for enhanced electrochromism and photoeletrochemical performance, Appl. Surf. Sci. 400 (2017) 57–63, https://doi.org/10.1016/j.apsusc.2016.12.072.
[283] J. Lei, H. Liu, C. Yuan, Q. Chen, J.A. Liu, F. Wen, X. Jiang, W. Deng, X. Cui, T. Duan, W. Zhu, R. He, Enhanced photoreduction of U(VI) on WO3 nanosheets by oxygen defect engineering, Chem. Eng. J. 416 (2021) 129164, https://doi.org/10.1016/j.cej.2021.129164.
[284] J.J. Li, M. Zhang, B. Weng, X. Chen, J. Chen, H.P. Jia, Oxygen vacancies mediated charge separation and collection in Pt/WO3 nanosheets for enhanced photocatalytic performance, Appl. Surf. Sci. 507 (2020) 145133, https://doi.org/10.1016/j.apsusc.2019.145133.
[285] S. Huang, Y. Long, S. Ruan, Y.-J. Zeng, Enhanced photocatalytic CO2 reduction in defect-engineered Z-scheme WO3–x/g-C3N4 heterostructures, ACS Omega 4 (2019) 15593–15599, https://doi.org/10.1021/acsomega.9b01969.
[286] Y. Qiu, G.L. Xu, Q. Kuang, S.G. Sun, S. Yang, Hierarchical WO3 flowers comprising porous single-crystalline nanoplates show enhanced lithium storage and photocatalysis, Nano Res 5 (2012) 826–832, https://doi.org/10.1007/s12274-012-0266-6.
[287] A. Tanaka, K. Hashimoto, H. Kominami, Visible-light-induced hydrogen and oxygen formation over Pt/Au/WO3 photocatalyst utilizing two types of photoabsorption due to surface plasmon resonance and band-gap excitation, J. Am. Chem. Soc. 136 (2014) 586–589, https://doi.org/10.1021/ja410230u.
[288] F. Wang, C. DiValentin, G. Pacchioni, Rational band gap engineering of WO3 photocatalyst for visible light water splitting, ChemCatChem 4 (2012) 476–478, https://doi.org/10.1002/cctc.201100446.
[289] F.A. Ofori, F.A. Sheikh, R. Appiah-Ntiamoah, X. Yang, H. Kim, A simple method of electrospun tungsten trioxide nanofibers with enhanced visible-light photocatalytic activity, Nano-Micro Lett. 7 (2015) 291–297, https://doi.org/10.1007/s40820-015-0042-8.
[290] R. Rong, L. Wang, Synthesis of hierarchical hollow nest-like WO3 micro/nanostructures with enhanced visible light-driven photocatalytic activity, J. Alloys Compd. 850 (2021) 156742, https://doi.org/10.1016/j.jallcom.2020.156742.
[291] P. Singh, P. Shandilya, P. Raizada, A. Sudhaik, A. Rahmani-Sani, A. Hosseini-Bandegharaei, Review on various strategies for enhancing photocatalytic activity of graphene based nanocomposites for water purification, Arab. J. Chem. 13 (2020) 3498–3520, https://doi.org/10.1016/j.arabjc.2018.12.001.
[292] A.L. Linsebigler, G. Lu, J.T. Yates, Photocatalysis on TiO2 surfaces: principles, mechanisms, and selected results, Chem. Rev. 95 (1995) 735–758, https://doi.org/10.1021/cr00035a013.
[293] J. Schneider, M. Matsuoka, M. Takeuchi, J. Zhang, Y. Horiuchi, M. Anpo, D. W. Bahnemann, Understanding TiO2 photocatalysis: mechanisms and materials, Chem. Rev. 114 (2014) 9919–9986, https://doi.org/10.1021/cr5001892.
[294] P. Raizada, A. Sudhaik, P. Singh, A. Hosseini-Bandegharaei, P. Thakur, Converting type II AgBr/VO into ternary Z scheme photocatalyst via coupling with phosphorus doped g-C3N4 for enhanced photocatalytic activity, Separ. Purif. Technol. 227 (2019) 115692, https://doi.org/10.1016/j.seppur.2019.115692.
[295] C. Xia, K.O. Kirlikovali, T.H.C. Nguyen, X.C. Nguyen, Q.B. Tran, M.K. Duong, M. T. Nguyen Dinh, D.L.T. Nguyen, P. Singh, P. Raizada, V.H. Nguyen, S.Y. Kim, L. Singh, C.C. Nguyen, M. Shokouhimehr, Q. Van Le, The emerging covalent organic frameworks (COFs) for solar-driven fuels production, Coord. Chem. Rev. 446 (2021) 214117, https://doi.org/10.1016/j.ccr.2021.214117.
[296] A. Kumar, V. Hasija, A. Sudhaik, P. Raizada, Q. Van Le, P. Singh, T.-H. Pham, T. Kim, S. Ghotekar, V.-H. Nguyen, Artificial leaf for light-driven CO2 reduction: basic concepts, advanced structures and selective solar-to-chemical products, Chem. Eng. J. 430 (2021) 133031, https://doi.org/10.1016/j.cej.2021.133031.
[297] V. Sonu, S. Dutta, P. Sharma, A. Raizada, Hosseini-Bandegharaei, V. Kumar Gupta, P. Singh, Review on augmentation in photocatalytic activity of CoFe2O4 via heterojunction formation for photocatalysis of organic pollutants in water, J. Saudi Chem. Soc. 23 (2019) 1119–1136, https://doi.org/10.1016/j.jscs.2019.07.003.
[298] T. Cai, Y. Liu, L. Wang, S. Zhang, Y. Zeng, J. Yuan, J. Ma, W. Dong, C. Liu, S. Luo, Silver phosphate-based Z-Scheme photocatalytic system with superior sunlight photocatalytic activities and anti-photocorrosion performance, Appl. Catal. B Environ. 208 (2017) 1–13, https://doi.org/10.1016/j.apcatb.2017.02.065.
[299] W. Dong, Y. Liu, G. Zeng, S. Zhang, T. Cai, J. Yuan, H. Chen, J. Gao, C. Liu, Regionalized and vectorial charges transferring of Cd1−xZnxS twin nanocrystal homojunctions for visible-light driven photocatalytic applications, J. Colloid Interface Sci. 518 (2018) 156–164, https://doi.org/10.1016/j.jcis.2018.02.018.
[300] J. Wang, L. Tang, G. Zeng, Y. Deng, Y. Liu, L. Wang, Y. Zhou, Z. Guo, J. Wang, C. Zhang, Atomic scale g-C3N4/Bi2WO6 2D/2D heterojunction with enhanced photocatalytic degradation of ibuprofen under visible light irradiation, Appl. Catal. B Environ. 209 (2017) 285–294, https://doi.org/10.1016/j.apcatb.2017.03.019.
[301] V. Hasija, A. Sudhaik, P. Raizada, A. Hosseini-Bandegharaei, P. Singh, Carbon quantum dots supported AgI/ZnO/phosphorus doped graphitic carbon nitride as Z-scheme photocatalyst for efficient photodegradation of 2, 4-dinitrophenol, J. Environ. Chem. Eng. 7 (2019) 103272, https://doi.org/10.1016/j.jece.2019.103272.
[302] Q. Zhou, F. Peng, Y. Ni, J. Kou, C. Lu, Z. Xu, Long afterglow phosphor driven round-the-clock g-C3N4 photocatalyst, J. Photochem. Photobiol. Chem. 328 (2016) 182–188, https://doi.org/10.1016/j.jphotochem.2016.06.002.
[303] V.W. hei Lau, D. Klose, H. Kasap, F. Podjaski, M.C. Pignié, E. Reisner, G. Jeschke, B.V. Lotsch, Dark photocatalysis: storage of solar energy in carbon nitride for time-delayed hydrogen generation, Angew. Chem. Int. Ed. 56 (2017) 510–514, https://doi.org/10.1002/anie.201608553.
[304] Q. Li, Y.W. Li, P. Wu, R. Xie, J.K. Shang, Palladium oxide nanoparticles on nitrogen-doped titanium oxide: accelerated photocatalytic disinfection and post-illumination catalytic “Memory, Adv. Mater. 20 (2008) 3717–3723, https://doi.org/10.1002/adma.200800685.
[305] T. Tatsuma, S. Saitoh, Y. Ohko, A. Fujishima, TiO2-WO3 photoelectrochemical anticorrosion system with an energy storage ability, Chem. Mater. 13 (2001) 2838–2842, https://doi.org/10.1021/cm010024k.
[306] Y.H. Chiu, Y.J. Hsu, Au@Cu7S4 yolk@shell nanocrystal-decorated TiO2 nanowires as an all-day-active photocatalyst for environmental purification, Nanomater. Energy 31 (2017) 286–295, https://doi.org/10.1016/j.nanoen.2016.11.036.
[307] F. Li, Z. Li, Y. Cai, M. Zhang, Y. Shen, W. Wang, Afterglow photocatalysis of Ag3PO4 through different afterglow coatings and photocatalysis mechanism, Mater. Lett. 208 (2017) 111–114, https://doi.org/10.1016/j.matlet.2017.04.106.
[308] H. Li, S. Yin, Y. Wang, T. Sato, Effect of phase structures of TiO 2-xN y on the photocatalytic activity of CaAl 2O 4:(Eu, Nd)-coupled TiO 2-xN y, J. Catal. 286 (2012) 273–278, https://doi.org/10.1016/j.jcat.2011.11.013.
[309] H. Li, S. Yin, Y. Wang, T. Sato, Blue fluorescence-assisted SrTi 1-xCr yO 3 for efficient persistent photocatalysis, RSC Adv. 2 (2012) 3234–3236, https://doi.org/10.1039/c2ra20278f.
[310] H. Li, S. Yin, Y. Wang, T. Sato, Persistent fluorescence-assisted TiO2-xNy-Based photocatalyst for gaseous acetaldehyde degradation, Environ. Sci. Technol. 46 (2012) 7741–7745, https://doi.org/10.1021/es300987s.
[311] H. Li, S. Yin, Y. Wang, T. Sato, Efficient persistent photocatalytic decomposition of nitrogen monoxide over a fluorescence-assisted CaAl2O4:(Eu, Nd)/(Ta, N)-codoped TiO2/Fe2O3, Appl. Catal. B Environ. 132–133 (2013) 487–492, https://doi.org/10.1016/j.apcatb.2012.12.026.
[312] W. Yang, Y. Chen, S. Gao, L. Sang, Post-illumination activity of Bi 2 WO 6 in the dark from the photocatalytic “ memory ” effect, J. Adv. Ceram. 10 (2021) 355–367.
[313] H. Zhao, Q. Fang, C. Chen, Z. Chao, Y. Tsang, Y. Wu, WO3 quantum dots decorated GO/Mg-doped ZnO composites for enhanced photocatalytic activity under nature sunlight, Appl. Organomet. Chem. 32 (2018) 1–10, https://doi.org/10.1002/aoc.4449.
[314] C. Wang, M. Long, B. Tan, L. Zheng, J. Cai, J. Fu, Facilitated photoinduced electron storage and two-electron reduction of oxygen by reduced graphene oxide in rGO/TiO2/WO3 composites, Electrochim. Acta 250 (2017) 108–116, https://doi.org/10.1016/j.electacta.2017.08.052.
[315] J. Yan, C. Wang, H. Ma, Y. Li, Y. Liu, N. Suzuki, C. Terashima, A. Fujishima, X. Zhang, Photothermal synergic enhancement of direct Z-scheme behavior of Bi4TaO8Cl/W18O49 heterostructure for CO2 reduction, Appl. Catal. B Environ. 268 (2020), https://doi.org/10.1016/j.apcatb.2019.118401.
[316] J. Du, Z. Wang, Y.H. Li, R.Q. Li, X.Y. Li, K.Y. Wang, Establishing WO 3/g-C 3 N 4 composite for “memory” photocatalytic activity and enhancement in photocatalytic degradation, Catal. Lett. 149 (2019) 1167–1173, https://doi.org/10.1007/s10562-019-02711-z.
[317] S. Bai, J. Jiang, Q. Zhang, Y. Xiong, Steering charge kinetics in photocatalysis: intersection of materials syntheses, characterization techniques and theoretical simulations, Chem. Soc. Rev. 44 (2015) 2893–2939, https://doi.org/10.1039/c5cs00064e.
[318] T. Cai, Y. Liu, L. Wang, W. Dong, G. Zeng, Recent advances in round-the-clock photocatalytic system: mechanisms, characterization techniques and applications,

J. Photochem. Photobiol. C Photochem. Rev. 39 (2019) 58–75, https://doi.org/10.1016/j.jphotochemrev.2019.03.002.
[319] M. Sakar, C.-C. Nguyen, M.-H. Vu, T.-O. Do, Materials and mechanisms of photo-assisted chemical reactions under light and dark conditions: can day–night photocatalysis Be achieved? ChemSusChem 11 (2018) 809–820, https://doi.org/10.1002/cssc.201702238.
[320] M. Mokhtarifar, M. Pedeferri, M.V. Diamanti, M. Sakar, T.-O. Do, in: M. Sakar, R. G. Balakrishna, T.-O. B, T.-P S, D. Do (Eds.), Chapter 13 - Round-The-Clock Photocatalytic Memory Systems: Phenomenon and Applications, Elsevier, 2021, pp. 359–384, https://doi.org/10.1016/B978-0-12-820532-7.00014-X.
[321] L. Liu, W. Sun, W. Yang, Q. Li, J.K. Shang, Post-illumination activity of SnO2 nanoparticle-decorated Cu2O nanocubes by H2O2 production in dark from photocatalytic "memory, Sci. Rep. 6 (2016) 1–11, https://doi.org/10.1038/srep20878.
[322] C. Zhang, Y. Li, M. Li, D. Shuai, X. Zhou, X. Xiong, C. Wang, Q. Hu, Continuous photocatalysis via photo-charging and dark-discharging for sustainable environmental remediation: performance, mechanism, and influencing factors, J. Hazard Mater. 420 (2021), https://doi.org/10.1016/j.jhazmat.2021.126607.
[323] Y.J. Li, K.M. Li, C.Y. Wang, C.I. Kuo, L.J. Chen, Low-temperature electrodeposited Co-doped ZnO nanorods with enhanced ethanol and CO sensing properties, Sensor. Actuator. B Chem. 161 (2012) 734–739, https://doi.org/10.1016/j.snb.2011.11.024.
[324] P. Ngaotrakanwiwat, T. Tatsuma, S. Saitoh, Y. Ohko, A. Fujishima, Charge–discharge behavior of TiO2–WO3 photocatalysis systems with energy storage ability, Phys. Chem. Chem. Phys. 5 (2003) 3234–3237, https://doi.org/10.1039/B304181F.
[325] P. Ngaotrakanwiwat, T. Tatsuma, Optimization of energy storage TiO2-WO3 photocatalysts and further modification with phosphotungstic acid, J. Electroanal. Chem. 573 (2004) 263–269, https://doi.org/10.1016/j.jelechem.2004.07.012.
[326] H. Park, A. Bak, T.H. Jeon, S. Kim, W. Choi, Photo-chargeable and dischargeable TiO 2 and WO 3 heterojunction electrodes, Appl. Catal. B Environ. 115–116 (2012) 74–80, https://doi.org/10.1016/j.apcatb.2011.12.006.
[327] C. Ng, Y.H. Ng, A. Iwase, R. Amal, Visible light-induced charge storage, on-demand release and self-photorechargeability of WO3 film, Phys. Chem. Chem. Phys. 13 (2011) 13421–13426, https://doi.org/10.1039/c1cp20412b.
[328] Y. Li, L. Chen, Y. Guo, X. Sun, Y. Wei, Preparation and characterization of WO 3/TiO 2 hollow microsphere composites with catalytic activity in dark, Chem. Eng. J. 181–182 (2012) 734–739, https://doi.org/10.1016/j.cej.2010.12.007.
[329] J. Li, Y. Liu, Z. Zhu, G. Zhang, T. Zou, Z. Zou, S. Zhang, D. Zeng, C. Xie, A full-sunlight-driven photocatalyst with super long-persistent energy storage ability, Sci. Rep. 3 (2013) 2409, https://doi.org/10.1038/srep02409.
[330] H. Khan, M.G. Rigamonti, G.S. Patience, D.C. Boffito, Spray dried TiO2/WO3 heterostructure for photocatalytic applications with residual activity in the dark, Appl. Catal. B Environ. 226 (2018) 311–323, https://doi.org/10.1016/j.apcatb.2017.12.049.
[331] H. Khan, M.G. Rigamonti, D.C. Boffito, Enhanced photocatalytic activity of Pt-TiO2/WO3 hybrid material with energy storage ability, Appl. Catal. B Environ. 252 (2019) 77–85, https://doi.org/10.1016/j.apcatb.2019.04.019.
[332] J. Xie, Z. Zhou, Y. Lian, Y. Hao, X. Liu, M. Li, Y. Wei, Simple preparation of WO3-ZnO composites with UV-Vis photocatalytic activity and energy storage ability, Ceram. Int. 40 (2014) 12519–12524, https://doi.org/10.1016/j.ceramint.2014.04.106.
[333] D. Zhao, C. Chen, C. Yu, W. Ma, J. Zhao, Photoinduced electron storage in WO3/TiO2 nanohybrid material in the presence of oxygen and postirradiated reduction of heavy metal ions, J. Phys. Chem. C 113 (2009) 13160–13165, https://doi.org/10.1021/jp9002774.
[334] T. Tatsuma, S. Takeda, S. Saitoh, Y. Ohko, A. Fujishima, Bactericidal effect of an energy storage TiO2-WO3 photocatalyst in dark, Electrochem. Commun. 5 (2003) 793–796, https://doi.org/10.1016/j.elecom.2003.07.003.
[335] Y.W.Y. Li, L. Chen, Y. Guo, X. Sun, Preparation and characterization of WO3/TiO2 hollow microsphere composites with catalytic activity in dark, Chem. Eng. J. 181–182 (2012) 734–739.
[336] Y.O. Ibrahim, M.A. Gondal, A. Alaswad, R.A. Moqbel, M. Hassan, E. Cevik, T. F. Qahtan, M.A. Dastageer, A. Bozkurt, Laser-induced anchoring of WO3 nanoparticles on reduced graphene oxide sheets for photocatalytic water decontamination and energy storage, Ceram. Int. 46 (2020) 444–451, https://doi.org/10.1016/j.ceramint.2019.08.281.